Function and dysfunction of Fibrinogen-like protein 2 in reproductive success and preeclampsia

Pascale Robineau-Charette

Department of Cellular and Molecular Medicine
Faculty of Medicine
University of Ottawa

This thesis is submitted to the University of Ottawa, in partial fulfillment of the requirements for the Doctorate in Philosophy (PhD) in Cellular and Molecular Medicine

Abstract

Fibrinogen-like protein 2 (FGL2) is a known immunomodulator and prothrombinase, expressed by several subsets of immune cells. This thesis explores its potential role during the establishment of pregnancy, in mice, as well as in trophoblast function and in an immune-mediated subtype of preeclampsia (PE), in humans. We first noticed a marked subfertility in *Fgl2* knockout (ko) and *Fgl2* overexpressing (tg) colonies, where litters were fewer and smaller. To explain this, we mapped spatiotemporal patterns of FGL2 expression in the female reproductive tract and through the estrous cycle. FGL2 is expressed in the ovarian stroma and theca cell layer, peaking shortly before ovulation. *Fgl2* ko and tg mice do not show a defect in natural or induced ovulation. FGL2 is expressed in secretory cells of the oviductal epithelium, and *Fgl2* ko mice have reduced fertilization efficiency. *Fgl2* tg pups are noticeably small, and we find that a reduced ratio of glycogen cells in the junctional zone of their placenta partly explains this. We next investigated the role of FGL2 in trophoblast function, using BeWo and HTR-8/SVneo cell lines. Inflammatory cytokines increase FGL2 expression in BeWo, and *FGL2* overexpression promotes syncytialization. We show that it therefore rescues the deleterious effect of inflammation on syncytium formation. In a large cohort of PE and non-PE human placentas, FGL2 is high in a subtype with immune activation, and low in a canonical, anti-angiogenic subtype. Its expression correlates with incidence of chronic inflammatory histopathological lesions, likely driven by immune rejection gene sets. High *FGL2* also associates with a high incidence of fibrin deposition in the placenta. Overall, we conclude that FGL2 is involved in several steps of maternal immune

adaptation, both before and after pregnancy. Its absence and excess both contribute to mouse subfertility. In the developing and mature placenta, FGL2 is increased by inflammation in the trophoblast and immune compartment of the mature placenta, as a physiological attempt to re-establish immune equilibrium and protect the ongoing pregnancy.

Table of Contents

Contributions

Published articles

- Robineau-Charette P, Grynspan D, Benton SJ, Gaudet J, Cox BJ, Vanderhyden BC & Bainbridge SA, FGL2-Associated Transcriptional and Histopathological Features of Immunological Preeclampsia, **Hypertension (2020)**, https://doi.org/10.1161/HYPERTENSIONAHA.120.14807

- Cook DP, Steed K, Read C, Baysarowich R, Redway T, Robineau-Charette P, & Carnegie J, Science Outreach: Six Examples of Programs that Enrich the Learning Environments of Students and Educators, **Human Anatomy and Physiology (HAPS) Educator (2020)**, https://doi.org/10.21692/haps.2020.107

- Al-Zahrani KN, Abou-Hamad J, Pryce BR, Cook DP, Hodgins JJ, Labrèche C, Robineau-Charette P, de Souza CT, Bell JC, Auer RC, Ardolino M, Vanderhyden BC & Sabourin LA, Loss of the Ste20-like kinase enhances tumorigenesis through AKT/Sox9-dependent Sox10 induction in HER2-positive breast cancers, **Oncogene (2020)**, https://doi.org/10.1038/s41388-020-1315-3

- Vuong NH, Cook DP, Forrest LA, Carter LE, Robineau-Charette P, Kofsky JM, Hodgkinson KM & Vanderhyden BC, Single-cell RNA-sequencing reveals transcription dynamics of estrogen-induced dysplasia in the ovarian surface epithelium, **PLoS Genetics (2018)**, Nov 12;14(11):e1007788.

Published abstracts

- Robineau-Charette P, Grynspan D, Vanderhyden BC & Bainbridge SA, FGL2-Associated Transcriptional and Histopathological Features of Immunological Preeclampsia, Abstracts from the International Federation of Placenta Associations 2019 annual meeting, **Placenta (2019)** 83:e106.

Contribution of undergraduate students under my supervision

- Lisa Oliviero: performed preliminary work on SNF2L and FGL2 leading to studies of ovarian function.
- Brendan Kelly: performed many experiments on luteal angiogenesis in *Fgl2*$^{wt/wt}$ and *Fgl2*$^{ko/ko}$ mice.

Contribution of colleagues and collaborators

- Dr. Ken Garson: provided technical expertise and protocols for cloning, lentivirus production and other molecular biology techniques.
- Elizabeth MacDonald: maintained mouse colonies and assisted in mouse manipulation training and experiments.
- Vincent Maranda: assisted in mouse manipulation and cell culture experiments.
- Jeremiah Gaudet: performed FGL2 western blots of cohort placenta samples.
- Dr. David Grynspan: performed semi-quantitative scoring of perivillous fibrin deposition in cohort placenta slides, and assisted in interpretation of histological findings.
- Dr. Brian Cox and lab members: performed computational analysis of microarray data, including initial clustering and characterization of molecular subclasses of preeclampsia.

Contribution of core facilities

- Louise Pelletier Histology Core Facility at the University of Ottawa: processed and embedded all tissues, and were very helpful and accommodating of special demands.
- Flow Cytometry and Virometry Core Facility at the University of Ottawa: performed cell sorting multiple times.
- Cell Biology and Image Acquisition Core Facility at the University of Ottawa: provided access to the Incucyte Zoom and its accompanying software, and provided expertise in analysis.
- Cell Sorting and Flow Cytometry Facility at the Ottawa Hospital Research Institute: performed cell sorting multiple times.

Funding sources

- CIHR Training Program in Reproduction, Early Development, and the Impact on Health Scholarship (2014-2015)
- PhD Ontario Graduate Scholarship (2017-2019)
- Preeclampsia Foundation Grant (2015-2016)

Thesis Advisory Committee members

- Dr. Jay Baltz
- Dr. Lakshmi Krishnan

List of Tables and Figures

List of Abbreviations

ANOVA – analysis of variance

BMDC – bone marrow-derived dentritic cell

BMI – body mass index

CAG – cytomegalovirus early enhancer/chicken β actin

COC – cumulus-oocyte complex

DAB – Diaminobenzidine

ddH_2O – double distilled water

DNA – desoxyribonucleic acid

eCG – equine chorionic gonadotropin

EGF – epidermal growth factor

ELISA – enzyme-linked immunosorbent assay

EVT – extravillous trophoblast

FACS – fluorescence-activated cell sorting

FGF – fibroblast growth factor

FGR – fetal growth restriction

FGL2 – fibrinogen-like protein 2, also called fibroleukin

GFP – green fluorescent protein

HEK293 – human embryonic kidney 293

H_2O_2 – hydrogen peroxide

H&E – hematoxylin and eosin

hCG – human chorionic gonadotropin

HELLP – hemolysis, elevated liver enzymes and low platelet syndrome

IGF – insulin growth factor

IHC – immunohistochemistry

HLA – human leukocyte antigen

IP – intra-peritoneal

KIR – killer immunoglobulin-like receptor

KO – knockout

LIF – leukemia inhibitory factor

MAP – mean arterial pressure

MHC – major histocompatibility complex

NBF – neutral buffered formalin

NK – natural killer

OVGP1 – Oviduct-specific glycoprotein 1

PBS – phosphate-buffered saline

PE – preeclampsia

PMSG – pregnant mare serum gonadotropin

PVDF – polyvinylidene difluoride

RNA – ribonucleic acid

SDS – sodium dodecyl sulfate

TBST – Tris-buffered saline with Tween 20

TGC – trophoblast giant cell

TGFβ - transforming growth factor beta

TSC – trophoblast stem cell

VEGF – vascular endothelial growth factor

Acknowledgments

A PhD is the most arduous, yet most rewarding adventure one can undertake.

To Andrée Gruslin who, through her evident passion and care, first sparked my interest in the placenta. To Shannon Bainbridge who, with down to earth and understanding support, stepped in at a much-needed time. To Barb Vanderhyden, who first took a chance on me, all those years ago, provided me with countless opportunities, and fostered my enthusiasm for all things reproductive biology. Thank you.

To my love Khalid, thank you for being my deep breath, my comfort, my home. Science and grad school bring countless frequent challenges, and being at each other's side through them all makes it all worth it.

À mes parents Danielle et Raymond, qui m'ont toujours fourni amour et soutien. Qui m'ont appris à fournir l'effort nécessaire à ce que j'entreprends. Qui m'ont transmis une curiosité sans bornes et les outils pour l'explorer. Qui m'ont aidée à naviguer un tourbillon sans fin d'études et d'activités, sans jamais douter de mes capacités, malgré mes projets parfois un peu ambitieux. À ma sœur Gabrielle, qui a bien souvent été la seule à comprendre et à partager mes états d'esprit.

À Fanny et Gabrielle, des perles rares d'amies avec qui naviguer l'âge adulte.

To Lauren and Dave, unwavering friends who never fail to be there in the face of great times and bad ones. I am grateful beyond what I can express for friends that are willing to take care of one another through scientific and personal challenges. For listening and challenging, and for constantly reinventing with me science and anything else we're passionate about.

To Tom, Val, Ced, Rose, Ben, and the other wonderful friends that formed our tight-knit grad student group, thank you, this spirit of community made all the difference. To past and present Biohazard players who let me bully you into playing ultimate, thank you for providing me with the amazingly effective outlet of sports and beers. The magnitude of a Biohazard losing record can only be this enjoyable with fantastic friends.

Who knew it would take so much time and effort to learn how much we still don't know?

Absolutely nothing about the process of a PhD has been easy, and yet, for the unnumerable lessons learned along the way, I wouldn't trade this experience for anything in the world. On to bigger and better science!

Merci.

CHAPTER 1: INTRODUCTION

1.1. Regulation of the establishment of pregnancy (pre-conception)

The establishment and success of a pregnancy depends on a multitude of events that are carefully coordinated and regulated. From estrous/menstrual cycling to production of gametes, to fertilization, implantation, and placentation, the endocrine and immune systems play a large part in regulating the process. Even before conception is achieved, there are key steps taken towards ensuring the success of the pregnancy, and these are described here.

1.1.1. Regulation of corpus luteum development and angiogenesis

Before the placenta is established, the corpus luteum (CL), the structure formed from the ruptured follicle that released an oocyte, is the main source of progesterone. This sustained progesterone is crucial for maintaining uterine receptivity and supporting early growth of the embryo and placenta, and lack of it leads to early pregnancy loss[1-3]. The CL develops remarkably fast, in terms of cellular growth. The developing follicle is avascular and therefore, massive angiogenesis is necessary to sustain the newly formed structure[4]. Before ovulation, vessels are only present within the theca cell layer of the follicle, as well as the ovarian stroma[5]. The luteinizing hormone (LH) surge, which induces ovulation, is also the initial signal that triggers a rise in fibroblast growth factor 2 (*FGF2*), fibronectin (*FN1*) and several pro-angiogenic and tissue remodeling genes[4,6,7]. Following ovulation, as cells at the apex of the follicle coordinate healing of the ovulatory wound, cells further within the follicle begin the process of luteinization. Both FGF2 and Vascular Endothelial Growth Factor A (VEGFA) promote branching

of the existing vasculature (within theca externa) towards the luteal cells, while VEGFA also promotes vascular permeability, necessary for leukocyte migration into the CL[5,8,9]. As in other tissues, hypoxia resulting from the lack of blood supply contributes to the upregulation of VEGFA, through HIF1[5,10]. As the vasculature branches and extends inwards in the CL, endothelial cells form junctions, and pericytes promote their migration and stabilization of newly formed vasculature[11,12].

Ovarian macrophages have been proposed as major regulators of luteal angiogenesis, as their depletion inhibited CL vasculature and progesterone production, leading to failure of embryo implantation[13-16]. Macrophages polarized to an M2, tolerant phenotype, promote the FGF2/VEGFA axis that leads to angiogenesis and progesterone production (luteal development branch), while the presence of M1 macrophages associates with high levels of Tumor Necrosis Factor α (TNFα) and Interferon γ (IFNγ), which promote luteal regression and ultimately, implantation failure (luteal regression branch)[13-16].

1.1.2. Initiation of immune tolerance in the oviduct

Following ovulation, the cumulus-oocyte complex (COC) transits through the oviduct, where it is available for possible fertilization. This represents the first interaction between the maternal immune system and paternal, non-self-antigens, and the first instance where immune adaptations have to be made to tolerate their presence.

The mammalian oviduct is composed of 3 main sections in which the landscape of the epithelium varies from distal to proximal sections: the infundibulum

(fimbria) is largely composed of ciliated cells, the ampulla presents a mix of ciliated and secretory cells, and the isthmus is mainly composed of secretory cells. Ciliated cells mainly contribute to fluid flow for oocyte/embryo transport, while secretory cells are responsible for oviductal fluid protein content[17-20]. Oviductal fluid contains plasma, extracellular vesicles and proteins, and its composition changes with stage of the estrous cycle, implying that it is steroid hormone responsive[21,22]. In addition to proteins involved directly in gamete interactions, such as Oviduct-specific glycoprotein 1 (OVGP1) and Albumin (ALB), several anti-inflammatory cytokines, such as Transforming Growth Factor β1 (TGFβ1) and Interleukin-10 (IL-10) are present in the fluid[23-25]. However, it is the presence of seminal plasma and secondarily, spermatozoa, that triggers the cascade leading to immune tolerance. Sperm selection in the female reproductive tract combines physical, biochemical (viscosity, pH) and molecular (protein-protein interactions with oviductal epithelium) challenges[26-29]. Initially, the presence of sperm induces inflammation, as macrophages and dendritic cells are recruited and IL-6, granulocyte-macrophage colony-stimulating factor (GM-CSF,) and other chemokines are secreted. TGFβ is also a key player, inducing IL-8 and prostaglandin E2 (PGE2)[30,31]. This inflammation leads to the activation of immune regulatory mechanisms, through T-cell priming and the recruitment and proliferation of regulatory T cells (Tregs)[32-34]. This initial response and its resolution are crucial, as they set the stage for long-term acceptance of fetal tissues.

It can therefore be concluded that even before placentation is initiated, several tolerogenic steps are taken in the female reproductive tract, as successful establishment of pregnancy depends on the regulation of this immune balance.

1.2. Hemochorial placentation

1.2.1. Early trophoblast differentiation (human)

By the time it reaches the uterus for implantation, the human blastocyst already includes cells that are committed to the trophoblast lineage, which will largely form the placenta. Following the implantation stages of apposition and adhesion, the trophoblast quickly differentiates into the cytotrophoblast. While these cytotrophoblast cells start migrating between maternal endometrial cells, they form a terminally differentiated, multinucleated unit called the syncytiotrophoblast (called the primitive syncytium, at this stage)[35,36]. Both the cytotrophoblast and syncytiotrophoblast populations remain throughout the pregnancy. The former is considered the progenitor cell type of the placenta, constantly proliferating and ensuring turnover of the syncytiotrophoblast, which eventually mediates maternal-fetal exchanges, as it is in direct contact with maternal blood when the placenta is mature.

At this early stage, the syncytiotrophoblast is only in contact with maternal blood and secretions through its erosion of uterine glands and small uterine venules. This is histiotrophic nutrition, which sustains the embryo through the first trimester of pregnancy[37,38]. The primary villi start forming around the third week of pregnancy, and contain only cytotrophoblast cells overlayed with a syncytiotrophoblast layer[39].

Fetal capillaries start growing when villi start containing stroma (secondary, or mesenchymal villi), and fetal circulation is mostly established by mid-first trimester[37]. Maternal blood, on the other hand, does not flow through the placenta until the end of the first trimester[40]. Until then, trophoblastic plugs block the spiral arteries, as EVT invasion and remodeling are not yet complete[37,41].

1.2.2. Trophoblast lineages (mouse)

Trophoblast lineages and pathways of differentiation present several differences, between the human and the mouse[42,43]. Perhaps the most notable morphological difference between human and mouse placenta is that the latter does not have a villous tree, but rather, a labyrinth. This is an intermingling of fetal and maternal vessels, separated by fetal endothelium, two layers of syncytiotrophoblast, and the sinusoidal trophoblast giant cells (TGCs) that line the maternal vessels[44]. The interface between fetal and maternal blood spaces, where exchanges are mediated, is therefore structurally different. Several populations of TGCs exist, named for their localization within the placenta: canal-associated, spiral artery-associated, sinusoidal and parietal. Between the labyrinth and the decidua is the junctional zone, formed of spongiotrophoblast (spT) and glycogen trophoblast cell (GlyT). GlyT and parietal TGCs are the invasive trophoblast types of the mouse placenta, with some found within the decidua, in the mature placenta[43,44]. Notably, trophoblast invasion is much shallower in the mouse, and the remodeling of uterine spiral arteries does not depend as much on depth and efficiency of invasion[36,45].

The mouse is therefore an effective model for several reproductive biology questions, but also has important limitations, especially around trophoblast invasion.

1.2.3. Extravillous trophoblast invasion

The cytotrophoblastic shell, which is at the interface with endometrial cells, at that stage, contains phenotypically distinct cytotrophoblast cells from which stems an important population, called the extravillous trophoblast (EVT)[39,41]. Later in development, when the villous part of the placenta is established, EVTs come from the cytotrophoblast columns at the tip of anchoring villi. These highly proliferative cytotrophoblast cells differentiate into interstitial EVTs (or interstitial cytotrophoblast), which migrate between endometrial stromal cells and invade the maternal spiral arteries). Interstitial EVTs eventually differentiate into endovascular EVTs, which migrate through the spiral arteries, cause endothelial cell apoptosis and replace that endothelium[36,39,46]. Cells originating in the cytotrophoblast cell columns progressively acquire migratory, then invasive abilities, changing their morphology and their expression of various integrins, cytokines and proteinases – matrix metalloproteinases (MMP) -2 and -9 are major players[39,47].

Their surrounding environment aids this transformation and the process of invasion. An oxygen concentration gradient is present, and EVTs participate in autocrine and paracrine action: they secrete several interleukins (Il-1, Il-6), for example, and express receptors for several more (Il-8, Il-12). Growth factors made by the EVTs themselves, by decidual stromal cells or by leukocytes exert promoting or limiting effects on invasion (EGF, FGF, IGFs, LIF, VEGFs, TGFβ, etc.)[39,48].

During the first trimester, uterine natural killer (uNK) cells represent the largest decidual leukocyte population of the thin decidua, and have a vital role to play in trophoblast invasion. At the start of invasion, interstitial EVTs invade through decidual stroma and encounter uNK cells and macrophages, which recruit them to the spiral arteries for remodelling[49-51]. Aside from recruitment, uNK show control over the trophoblast invasion process, limiting it through secretion of TNFα and IFNγ, among others. EVTs, but not the cytotrophoblast or the syncytiotrophoblast, express MHC class I antigens HLA-C, HLA-E and HLA-G, whose receptors, Killer Immunoglobulin-like Receptors (KIRs), are present on uNK cells. These interactions mediate the prevention of an adaptive immune response from the maternal immune system[50,52,53].

From the time of establishment of maternal circulation, most trophoblast populations are terminally differentiated, the exception being cytotrophoblast cells, which constantly proliferate to replenish and grow the syncytiotrophoblast as villi sprout and mature.

1.2.4. The maternal-fetal interface: the syncytiotrophoblast

The definitive syncytiotrophoblast arises from rapid proliferation and fusion of the villous cytotrophoblast, a process chiefly mediated by Syncytin-1 (*ERVW-1*)[54,55]. As soon as it becomes functional, the syncytiotrophoblast represents an important endocrine structure. The undifferentiated trophectoderm produces hCG starting only a few days into the pregnancy, which provides a feedback that ensures maintenance of the CL and its production of progesterone. This lasts until the syncytiotrophoblast,

around the eighth week, can take over progesterone production. Although levels are higher early on, production of hCG is important throughout pregnancy, as it is involved in maintenance of the syncytiotrophoblast layer through cytotrophoblast differentiation[55,56]. Beyond this endocrine function, the syncytiotrophoblast is also in direct contact with maternal blood, and as such, acts as a filtering barrier: it lets through gases and nutrients necessary to fetal nutrition, but does not allow most viruses and bacteria to attain fetal tissues.

The placenta is a highly dynamic structure that is constantly turned over, through cytotrophoblast fusion and shedding of syncytiotrophoblast nuclei (syncytial sprouts/knots)[57,58]. The fusion process involves cytotrophoblast proliferation, differentiation, and expression of adhesion factors. Main regulators of the process include ADAM12, syncytin1/2 and GCM1[59-62]. Several anomalies of syncytiotrophoblast structure or function have consequences on pregnancy outcomes and are visible in a pathological examination of the term placenta. Excessive syncytial nuclear aggregates, abnormal villous maturation or excessive fibrin deposition after syncytial injury, for example, are features often observed in cases of fetal growth restriction (FGR) or preeclampsia (PE)[57,58,63].

1.3. Placental dysfunctions and preeclampsia

1.3.1. Clinical presentation and intervention

Preeclampsia (PE) is a hypertensive disorder that affects 3 to 8% of all pregnancies and is the leading cause of maternal and fetal mortality and morbidity worldwide[64]. PE is diagnosed in the mother following new-onset hypertension after

20 weeks of gestation, when accompanied by signs of end organ damage: proteinuria, impaired liver function (usually as part of hemolysis, elevated liver enzymes levels and low platelets, or HELLP syndrome), or serious cerebral/visual symptoms[65-67].To date, there remains no effective therapeutic intervention to prevent or cure PE, aside from delivery of the placenta, which is considered to play a crucial role in disease pathology. In many cases, the condition of either mother or fetus warrants preterm delivery, which poses a high risk of iatrogenic co-morbidities for the newborn. However, the onset and severity of maternal symptoms, as well as fetal health outcomes, are highly variable across all PE cases[64,65,67].

1.3.2. Pathophysiology of PE

Decades of research have led to a widely accepted mechanism concerning the underlying placental pathology of PE. Early during placentation, an impairment in trophoblast differentiation and function causes improper invasion, leading to poorly remodelled uterine spiral arteries and insufficient blood flow to the placenta[46,67]. The resulting placental hypoxia, oxidative stress, and mechanical damage leads to the release of anti-angiogenic and pro-inflammatory factors, and placental debris into maternal circulation. These result in a maternal systemic response consistent with the clinical manifestations of the disease. Based on this paradigm, numerous factors, including soluble fms-like tyrosine kinase 1 (sFLT-1) and soluble endoglin (sENG), have been investigated as potential biomarkers of the disease[66,68,69].

Interestingly, predisposition to endothelial dysfunction is thought to play a part in the pathology of preeclampsia[68,70]. Anomalies of the placental vasculature result,

in part, from the failed remodelling of spiral arteries. Fibrin deposition in the maternal microcirculation and in the kidney glomerulus are commonly observed in PE, although not universal[71,72]. This is thought to be due to a pathological state of hypercoagulability in the mother, and how much placental hypoxia contributes to this phenotype is still unclear[70,73].

While this mechanism for the pathophysiology of PE and its associated biomarkers are likely representative of a large number of PE cases, there is increasing evidence that no one paradigm or predictive biomarker can accurately describe all cases of PE[65,74,75].

1.3.3. Prevention and biomarkers

The two-stage model for the pathophysiology of preeclampsia explains that the maternal symptoms, generally observed late during pregnancy, are rooted in defects in early placentation, that eventually result in a dysfunctional mature placenta[76,77]. This exposes the problem that clinical intervention, at the time of symptom appearance, cannot correct their underlying cause, as dysregulations happened much earlier in pregnancy. Identification of women at high risk of PE development, early in pregnancy, would help in clinical management of the pregnancy. Additionally, finding factors that differentiate between PE and non-PE pregnancies provides a window into molecular processes that may be dysregulated, which contributes to our understanding of the disease.

The search for PE biomarkers was first focused on angiogenesis-related factors, in line with the accepted pathophysiological paradigm of the disease[66,68].

Soluble fms-like tyrosine kinase 1 (sFLT) is perhaps the best known of these, as a truncated form of a VEGF receptor that segregates VEGFA in the circulation, therefore nullifying their proangiogenic effect. VEGF-A, placental growth factor (PlGF), and soluble endoglin (sENG), were similarly investigated. sENG, an endogenous inhibitor of TGF-β1, is similarly elevated in PE serum[69,78]. There is evidence that these markers are moderately efficient in predicting PE (early-onset better than late-onset, a proxy of severity), especially when combined with clinical characteristics and placental perfusion data[79,80].

Today, most research agrees that a panel of biomarkers will likely be more effective, since it could encompass the multifactorial nature of PE. This would not only increase the predictive capability of these biomarkers for maternal and fetal outcomes of the pregnancy, but also increase our understanding of the multiple pathways possibly dysregulated in PE.

1.3.4. Resolving PE heterogeneity

The notable heterogeneity in clinical presentation and placental pathology of PE has led our group and others to investigate the potential existence of PE subclasses, driven by different forms of placental disease[74,75]. Using an unsupervised clustering approach that integrates transcriptional and histopathological profiles of placentas from women across the clinical PE spectrum, we identified and characterized three distinct and clinically relevant disease subtypes. Cluster 1 was largely comprised of healthy placentas, with only 23% of cluster membership with a PE diagnosis. Their transcriptional and histological

profiles demonstrated no overt pathology, and clustered alongside gestational age-matched healthy controls, such that it is postulated that this PE subtype is primarily driven by maternal factors, with minimal placental dysfunction. This maternal PE subtype accounted for 18% of all preeclamptics in this cohort. Cluster 2 was heavily dominated by preeclamptic samples (89%), and accounted for 63% of cohort preeclamptics. These samples demonstrated transcriptional profiles consistent with the current PE paradigm of placental hypoxia as the underlying disease pathophysiology (canonical PE), with upregulation of known PE biomarkers such as *FLT1* and *ENG*. Histologically, these placentas demonstrated lesions consistent with maternal vascular malperfusion, such as distal villous hypoplasia, placental infarctions, advanced villous maturity, and increased syncytial knots. The few healthy control samples that clustered alongside these patients also demonstrated transcriptional and histological evidence of placental malperfusion and hypoxia, despite the absence of clinical manifestation of disease in the mother. Membership in cluster 3 also predominantly included preeclamptic samples (73%), which represented 16% of all PE patients in our cohort. This immunological PE subtype demonstrated an intriguing transcriptional and histopathological profile, marked by an increase in immune and pro-inflammatory genes (i.e.TNFα and IFNγ), and placental lesions consistent with chronic inflammation and maternal-fetal interface disturbances, such as villitis of unknown etiology (VUE) or massive perivillous fibrin deposition (MPFD). Interestingly, the healthy control patients that clustered alongside these PE patients also demonstrated transcriptional and histological

findings consistent with heightened placental inflammation, despite the absence of PE maternal symptoms[74,75,81].

1.4. Fibrinogen-like protein 2 (FGL2)

1.4.1. Gene, transcripts, and protein

In 1995, Parr *et al.* sought to identify the protein conferring pro-coagulant properties to primary peritoneal macrophages in culture, after induction by mouse hepatitis virus strain 3 (MHV-3)[82]. Cloning, sequencing, and subsequent comparison to a cDNA library revealed this gene to be *Musfiblp* (originally called *pT49*), which had been previously cloned and described as a constitutively expressed, cytotoxic T-cell-specific gene[83]. The transcript name *Musfiblp* and the eventual name Fibrinogen-like protein 2 (FGL2) originate in its homology with the β and γ subunits of fibrinogen. The protein is sometimes called Fibroleukin[84]. The C terminal of the protein presents about 36% homology with the β and γ subunits, the same as the fibrinogen subunits have between each other, while much lower homology is observed at the N terminal[83]. The C terminal of the α, β, and γ chains of fibrinogen contain Fib-related domains (FREDs), and FGL2 contains a domain homologous to them[85]. Beyond coagulation, these domains are involved in leukocyte and endothelial cell adhesion and migration. Overall, the amino acid (aa) sequences of mouse and human FGL2 are 78% similar, with up to 90% identity within the FRED[84,85]. A signal peptide for transport of the protein across the cell membrane was initially identified for mouse *Fgl2*, and a cleavage site was predicted, but not confirmed[83]. The putative cleavage site is a different one in human *FGL2,* but the

protein was detected in both cell lysates and supernatants[85,86]. Importantly, as detection of the FGL2 protein can be dubious, this was confirmed by detecting a tag from the *FGL2*-tag fused cDNA used for overexpression, not solely using an anti-FGL2 antibody. Based on aa sequence analysis, human FGL2 was predicted to be a type II protein[84]. The identified sequence for both mouse and human *FGL2* contains several consensus sequences for N-linked glycosylation, another indicator that it is secreted, and glycosylation was later shown to be critical for its solubility[85,87,88]. The *FGL2* gene was mapped, in the mouse, to proximal regions of chromosome 5 and in the human, to the short arm of chromosome 7[87,89]. Native FGL2 presents as an oligomer; it is composed of four monomers joined together by disulfide bonds[86,87]. The FGL2 monomer has a molecular weight of about 65kDa, and the oligomer (tetramer), of 260kDa[87,88].

1.4.2. Prothrombinase activity of FGL2

As FGL2 was initially discovered as an MHV-3-induced prothrombinase, causing fibrin deposition within liver endothelium, it was heavily studied in other MHV-dependent diseases and MHV-susceptible tissues, in the mouse[89]. Within a few years, it was investigated as a potential player in pregnancy pathologies (spontaneous miscarriage and preeclampsia), as the focus of the field was the role clotting may play in these pathologies[90]. A high rate of spontaneous abortions was first correlated, in the mouse, with increased FGL2 expression in the trophoblast and certain decidual cell populations[91,92]. This was confirmed, at the time, in human tissue, when trophoblast was shown to be positive for FGL2 (1st and 3rd trimester

tissue), along with invaded trophoblast and decidual vessels of miscarriage tissue. This was also the first link made between fibrin deposition and FGL2 in preeclamptic placentas[90].

FGL2 provides a bypass of both the intrinsic and the extrinsic pathways of the traditional coagulation cascade. FGL2 can be used for prothrombin recognition in place of factor Xa, which is normally where the intrinsic and extrinsic pathways converge[93]. The prothrombinase activity of FGL2 was first localized within its gene sequence when an antibody to an early sequence of the gene abrogated its coagulation activity[94]. Its serine protease function was later localized to Ser89 in the mouse, and Ser 91 in the human[84,93]. Importantly, soluble (secreted) FGL2 does not exhibit prothrombinase activity, as this activity is exclusive to the membrane-bound form[87].

1.4.3. Function: immunosuppression

The initial discovery that FGL2 could be induced by MHV-3, an inflammatory coronavirus, led to the investigation that other inflammatory cytokines could also induce it. The induction of FGL2 expression by IFNγ was first observed in primary human PBMCs[86]. In the CBA X DBA/2 mouse model, prone to cytokine-dependent abortions, both TNFα and IFNγ, independently and in synergy, were shown to upregulate FGL2 in the trophoblast and some decidual cells[90,91]. In natural mouse pregnancy (no induction of miscarriage), correlative expression of TNFα and FGL2 was shown in the decidua and in the trophoblast[90]. Treatment with IL-12, which is

normally secreted by antigen-presenting cells (APCs), increased both TNFα and IFNγ, and FGL2 was proposed to cause the resulting inflammatory abortion[95].

After delineating what induces FGL2, its own potential immunoregulatory effects were studied. The effect of a lack of FGL2 was investigated using knockout mice (*Fgl2*$^{ko/ko}$) and FGL2 antibodies, and the effect of its presence or excess, with recombinant soluble FGL2 and overexpressing mice (*Fgl2*$^{ko/tg}$). *Fgl2*$^{ko/ko}$ mice tended to polarize their immune profile to a Th1, inflammatory profile: increased T cell proliferation, increased numbers of antibody-producing B cells, DCs, and Tregs, which were however dysfunctional. Bone marrow-derived DCs (BMDCs) in these mice had increased MHCII and CD80 expression[94,96]. Due to these effects, these mice developed autoimmune glomerulonephritis by one year of age[96]. Heterozygous matings (*Fgl2*$^{wt/ko}$ x *Fgl2*$^{wt/ko}$) led to a a 40% reduction in *Fgl2*$^{ko/ko}$ pups, due to hemorrhage at the feto-maternal interface, observed at e7.5[97]. Also in heterozygous matings, a subsequent paper from the same group reported neonatal deaths (also preferential to *Fgl2*$^{ko/ko}$ pups), in which mild cardiac dysfunction was observed, but no clear cause could be determined, despite expression in cardiomyocytes[98,99]. These findings were opposed by another group's *Fgl2* knockout mice, who were reportedly immunologically normal and had no subfertility[100].

Fgl2 overexpressing mice were generated many years later and have an interesting phenotype of their own. $CD4^+$ T cells had reduced proliferation in response to alloantigens or CD3/CD28 stimulation, BMDCs had reduced expansion and secreted more IL-10. Tregs numbers were increased, and they had enhanced immunosuppressive activity. This immune profile allows the mice to accept a heart

allograft without the need for further immunosuppression[101]. As both these mouse lines were used in our experiments, the details of how they were generated can be found in **Materials and Methods**.

1.4.4. Immunosuppressive effect of soluble FGL2

The specific immunosuppressive activities of the soluble form of FGL2 were investigated. First, it inhibits dendritic cell (DC) maturation by affecting NF-κB nuclear translocation, which can directly reduce T cell proliferation, and causes B cell apoptosis[94,102]. These effects are mediated by FGL2 binding to FcγRIIB (CD32B), a low-affinity inhibitory receptor expressed by most antigen presenting cells (APCs), including macrophages, DCs, and B cells, as well as some endothelial cells[103]. It was also shown to bind FcγRIIIA/B (CD16A/B), an activating receptor, although the effects of this binding have not been characterized[102]. Of note, when tested separately, the FGL2 monomer had enhanced cell type-specific immunosuppressive activity (inhibition of T cell proliferation), compared to the tetramer[88].

FGL2 has also been shown to play a role in polarization of the Th1/Th2 cytokine profile toward the secretion of Th2, anti-inflammatory cytokines, by direct binding to T lymphocytes. It induces the secretion of IL-4 and IL-10 and inhibits secretion of IL-2 and IFNy[94,96].

1.4.5. Aberrant FGL2 in disease pathophysiology

Aside from the involvement in reproductive pathologies noted in *Fgl2*$^{ko/ko}$ and *Fgl2*$^{ko/tg}$ mice, FGL2 came to be associated with several other conditions known to be immune-mediated and/or where fibrin deposition is a factor. MHV-3-induced viral hepatitis in mice was shown to occur through the procoagulant effect of FGL2[87,89]. In mice, development of collagen-induced arthritis, with fibrin deposition in joints was associated with an increase in FGL2 expression[104]. Injection of FGL2-recombinant adenovirus in rats, or recombinant FGL2, ameliorated heart allograft through Treg suppression of $CD4^+$ T cell proliferation[105,106]. A similar phenotype was observed in liver allografts in the rat, where high FGL2 polarized macrophages to an M2 phenotype and contributed to transplant tolerance[107]. In a xenograft mouse model of hepatocellular carcinoma, injection of tumour cells with low *Fgl2* resulted in decreased angiogenesis and slower tumour growth[108]. The same phenotype was observed in a xenograft mouse model of prostate cancer[109]. It has also been suggested to be involved in human parturition, as high FGL2 expression could increase thrombin in the myometrium, which acts on calcium physiology to promote myometrial smooth muscle contraction[92].

Overall, the aberrant expression of FGL2 has been linked to numerous pathological conditions. It is interesting to note that both a lack and an excess seem to be problematic, either *in vitro*, in animal models or in human disease. Neither absolutely essential to normal function nor the sole cause of a dysfunction, the concept of equilibrium seems to be central to the role of FGL2.

1.5. Rationale, Hypothesis and Aims

Previously, our lab identified FGL2 as a target of SNF2L, an imitation switch (ISWI) protein that contributes to nucleosome positioning as the catalytic subunit of a chromatin remodeling complex[110]. This relationship was explored in a mouse line with an inactivating mutation of the *Snf2L* exon that carries ATPase activity (*Snf2L* Ex6DEL). SNF2L expression being mostly restricted to reproductive tissues (male and female), reproductive capacity in this line was fully characterized, first identifying a decreased response to superovulation despite cumulative reproductive output over a set time period being comparable to *Snf2L* WT mice. Histological examination of the *Snf2L* Ex6DEL ovaries revealed lower counts of secondary follicles and more abnormal antral follicles (hemorrhagic follicles, trapped oocytes). When granulosa cells were collected following gonadotropin stimulation, an induction of *Fgl2* was noticed in *Snf2L* WT mice, specifically 8 hours after hCG injection. Interestingly, this induction was not present in *Snf2L* Ex6DEL mice, suggesting that SNF2L is required for FGL2 to exert its time-specific function, and that its lack, caused by SNF2L inactivation, may be responsible for the defective response to superovulation hormones[110].

This identification of FGL2 as a target of SNF2L in the ovary, coupled with previous literature showing a role for FGL2 in pregnancy, led us to hypothesize that ***aberrant FGL2 regulates the establishment of pregnancy and optimal fetal and placental outcomes, through its immune modulator and prothrombinase functions.***

We explored this hypothesis through three specific aims:

1. To evaluate the effect of aberrant *Fgl2* expression on the establishment and outcomes of mouse pregnancy;
2. To determine the role played by FGL2 in trophoblast function and response to inflammation;
3. To identify features associated with placental *FGL2* expression in an immune-mediated subtype of preeclampsia.

CHAPTER 2: MATERIALS & METHODS

2.1. Animal work

2.1.1. Mouse lines and colony maintenance

The *Fgl2*$^{ko/tg}$ mouse line, used to generate *Fgl2*$^{ko/ko}$ *and Fgl2*$^{ko/tg}$ mice used in our experiments, was gifted by Dr. Gary Levy (Toronto General Hospital, University Health Network, Toronto, ON). Briefly, *Fgl2*$^{ko/ko}$ mice were generated by inserting a *LacZ* and *PGK-Neo* cassette in a *BamH1* site substituted for the initiating codon of exon 1 of the *Fgl2* gene}. Therefore, in *Fgl2*$^{ko/ko}$ mice, β*-gal* expression is driven by the *Fgl2* promoter and can be visualized with Xgal staining[97]. *Fgl2*$^{ko/tg}$ mice were generated by first mutating S89, the known serine protease conferring prothrombinase activity, in an *Fgl2* cDNA cloned from C57BL/6 mouse heart RNA. This mutated *Fgl2* was cloned into the iZ/EG targeting vector, and embryonic stem cells clones were selected for single copy insertion. Cre-mediated excision results in ubiquitous expression of *Fgl2*^{S89A}*-EGFP*, driven by the cytomegalovirus early enhancer/chicken β actin (CAG) promoter. Mice were crossed to *Fgl2*$^{ko/ko}$ mice to eliminate endogenous *Fgl2* expression, and to Ella-cre mice for ubiquitous expression of Cre[101]. These mice are maintained as one line in our colony, using *Fgl2*$^{ko/ko}$ X *Fgl2*$^{ko/tg}$ mating pairs. Live pups from these pairs are determined as either *Fgl2*$^{ko/ko}$ or *Fgl2*$^{ko/tg}$ by verifying ubiquitous GFP positivity. To produce suitable control mice for our experiments, *Fgl2*$^{ko/ko}$ mice were backcrossed with C57BL/6 mice newly acquired from Jackson Laboratories to produce our *Fgl2* BL6/J WT line, called *Fgl2*$^{wt/wt}$ throughout this thesis. Genotyping primer sequences for all possible alleles of *Fgl2*, used to confirm mouse genotype in our experiments, can be found in **Table 1**).

All animal husbandry, experiments and euthanasia procedures were conducted according to guidelines and under ethics protocol approval at the Animal Care and Veterinary Service of the University of Ottawa.

2.1.2. Timed matings for pregnancy timepoints

Females to be mated were primed and their estrous cycle synchronized by adding male bedding to their cage. 48 hours later, females were moved to a male's cage at a 2:1 ratio. For all experiments involving timed matings, with or without superovulation, females were mated to a male of identical genotype (*Fgl2*$^{wt/wt}$, *Fgl2*$^{ko/ko}$, or *Fgl2*$^{ko/tg}$). All mice were kept on a 12-hour light/dark cycle. In experiments involving the natural estrous cycle, ovulation was assumed to occur at 12am. The day following mating was considered day 0.5 of pregnancy (e0.5), if a vaginal plug was observed, and females were returned to their home cage on that day, to ensure precise dating of the pregnancy.

2.1.3. Superovulation

Females received an intra-peritoneal (IP) injection of 5IU equine chorionic gonadotropin (eCG, Calbiochem) to stimulate follicle maturation. 42 to 48 hours later, they received an IP injection of 5IU human chorionic gonadotropin (hCG, Sigma), to induce ovulation. Ovulation was assumed to occur 12 hours after hCG injection. Females were then either mated, as described previously, or used for sample collection, as follows.

2.2 Reproductive tract dissection for collection of oocytes and embryos

2.2.1. Collection of oocytes (ovulation)

Collection of cumulus-oocyte complexes (COCs) was performed 2-6 hours after ovulation, either natural or induced. The reproductive tract was grossly dissected and under a dissection microscope, and the ovary was detached. The connective tissue supporting the structure of the oviduct was sheared to uncoil it and the mass of COCs was squeezed out of the fimbrial end using tweezers. The mass was transferred to a drop of hyaluronidase (Milipore Sigma) to disperse cumulus granulosa cells, and oocytes were counted. Three to five mice per genotype were used for natural cycling ovulation, and eight to twelve for superovulation. Each data point represents the sum of ovulated oocytes from both ovaries of the same animal.

2.2.2. Collection of two-cell embryos (fertilization)

Collection of two-cell embryos was performed 40-46 hours after hCG injection and mating. The ovary was removed, and the oviduct was uncoiled and flushed with 100-200μL PBS from the fimbrial end, using a blunted 30G needle. The number of morphologically normal two-cell embryos was determined, as well as the number of unfertilized oocytes (whole, fragmented or degenerated). The fraction of two-cell embryos over the total number of structures recovered was calculated. 3-6 pregnancies per genotype were counted, and each data point represents this fraction for an independent animal (sum of both oviducts).

2.2.3. Collection of pregnant uteri (implantation)

Collection of pregnant uteri was first done at e5.5. The whole uterus was dissected and stretched to make implantation sites easily discernable. 4-6 pregnancies per genotype were counted, and each data point represents the number of implantations (sum of both horns of uterus).

2.2.4. Collection of near-term pregnancies (outcomes)

Collection of near-term pregnancies was done at e18.5. The whole uterus was dissected out. Implantation sites were counted and dissected one at a time to separate fetus and placenta, which were weighed and stored appropriately for their downstream uses. 3-4 pregnancies per genotype were counted, and each data point represents the number of implantation sites (sum of both horns of uterus). In the case of fetal or placental weight, each data point represents the average measure for all fetuses or placentas of the same pregnancy.

2.3. Histology

2.3.1. Tissue collection and processing

Tissues were collected, trimmed of fat when appropriate and immediately placed in 10% buffered formalin (Fisher Scientific) for 24 hours. Tissues were then moved to 70% ethanol until embedding into paraffin blocks. For immunohistochemistry (IHC) and hematoxylin and eosin (H&E) staining, 5μm tissue sections were cut using a microtome. In the case of IHC, positively charged glass slides were used (Fisher Scientific).

2.3.2. X-gal staining

Following dissection of tissues of interest, they were fixed in a solution of 1% formaldehyde and 0.5% glutaraldehyde in PBS, for 30 minutes. Tissues were washed 3 times in detergent buffer (5 mM potassium ferricyanide, 5 mM potassium ferrocyanide, 2 mM MgCl2, 0.01% sodium deoxycholate, 0.02% NP-40 in PBS), and subsequently incubated in the staining solution (1 mg/mL X-gal in detergent buffer), overnight. Tissues were washed 3 times in PBS to remove background stain and photographed using a dissection microscope.

2.3.3. Immunohistochemistry

5μm tissue sections were deparaffinized and rehydrated in successive xylenes and ethanol gradient baths. They were submitted to heat-mediated antigen unmasking in a citrate-based solution (Vector Laboratories) in a pressure cooker. After cooling, endogenous peroxidase activity was blocked by applying a solution of 3% hydrogen peroxide (H_2O_2) to tissues for 10 minutes. A serum-free protein blocking reagent (Agilent Dako) was applied to the slides for 30 minutes, followed by overnight incubation at 4°C with the primary antibody, appropriately diluted in Antibody Diluent (Agilent Dako). All antibodies and their specific working concentrations can be found in **Table 2**. Slides were washed with PBS and then incubated at room temperature for 30 minutes with a horseradish peroxidase-labeled secondary antibody (Agilent Dako) and subsequently developed for 5 minutes, using diaminobenzidine (DAB) as a chromogen. Slides were counterstained with

hematoxylin, dehydrated in ethanol gradient baths and mounted using Permount (Fisher Scientific).

2.4. Histological analysis

Slides were scanned using the ScanScope CS2 (Aperio) or the AxioScan (Zeiss). Snapshots presented here were taken using either FIJI 3 (ImageJ version 2.0.0-rc-69/1.52p), ImageScope (Aperio) or Zen v3.1 (Zeiss). For quantification of pixel positivity on DAB-stained images, we used the Pixel Positivity v9.1 algorithm on the ImageScope software, which automatically detects and counts weakly/strongly positive and negative pixels. Otherwise, manual counting was achieved using the cell counter functions on either ImageScope or FIJI 3, as described below for specific experiments.

2.4.1. Abnormal/total follicles

In 2 sections from the same ovary, at least 200µm apart, we first counted all visible follicles, at all stages of development. We then counted, within these, those with abnormal features: degenerated oocyte, trapped oocyte, hemorrhagic follicle, etc. One ovary from 4 animals per genotype was counted, and each animal is represented as a data point.

2.4.2. CD206-positive cells in CL

In 1 ovary section (roughly midway through the embedded tissue) per animal, all CD206-positive cells were counted. These were localized to the ovarian stroma, the

theca cell layer, or the CL. The total area occupied by ovarian tissue was measured in mm^2, using ImageScope, and the CD206-positive cell count was divided by this area to obtain macrophage density. One ovary from 3 independent animals per genotype was quantified, and each animal is represented as a data point.

2.4.3. Vascular density in the CL (CD31 positivity)

In 1 ovary section (roughly midway through the embedded tissue) per animal, all CLs were identified, and in each CL, the largest possible rectangular field of view (FOV) was drawn. The pixel positivity algorithm on ImageScope determined the fraction of DAB-positive pixels (CD31 positive) over the total pixels of the FOV. Vasculature density was determined in this manner for all CLs present (4-10 CLs per ovary) and averaged for each animal. One ovary from 3 independent animals per genotype were counted, and each animal is represented as a data point.

2.4.4. Placental stereology

Mouse placentas (e18.5) were collected and processed for histology work as described above. As little trimming as possible was done, to preserve the decidua basalis, which can easily be removed by mistake. Before embedding, the placentas were sliced vertically, at the site of umbilical cord insertion, to ensure that sectioning would produce midline sections for analysis. Midline sections (thickness of 5μm) were obtained, stained with hematoxylin and eosin (H&E) and scanned for image analysis. For each placenta, the total volume was estimated, to use as a reference space value for compartment and subcompartment measurements. This was

calculated using the measured placental weight and a known value for estimation of tissue density, 1.05g/cm^3 (Jackson 1987). For determining the volume of the labyrinth and the junctional zone (main compartments), the point counting system was used. In a field of view (FOV) comprising the whole section, a grid was overlayed on the image, using FIJI, aiming for a total of ~200 points covering the tissue. Points falling in either compartment were manually counted, and the result was expressed as a ratio to total point count. The ratio of the total volume occupied by each compartment was converted to absolute compartment volume using the total placental volume, previously calculated. Sub-compartment (spongiotrophoblast and glycogen cells) volumes were determined in the same manner. Three different placentas from the same pregnancy were quantified, and three to four pregnancies per genotype were used for comparisons. This protocol was based on “Best Practices for Quantifying the Microscopic Structure of Mouse Placenta: The Stereological Approach”[111].

2.5. Molecular and *in vitro* work

2.5.1. Live cell imaging proliferation assay

An equal number of cells was plated in 12 wells of a 96-well plate, per cell line. Well confluence was monitored every 2 hours, starting 6 hours after plating and ending 72 hours after, using the Incucyte Live-Cell Imaging System and software (Essen Instruments). At each timepoint, cell confluence was measured from an image of each well and averaged across 8-12 wells per sample (N=3).

2.5.2. Live cell imaging migration assay

An equal number of cells, optimized to form a confluent monolayer, was plated in 12 wells of a 96-well plate, for each sample. A scratch wound was made using the Wound Maker (Essen Instruments), and cell confluence within the wound was monitored every 2 hours, until wound closure, using the Incucyte Live-Cell Imaging System and software (Essen Instruments). At each timepoint, cell confluence was measured from an image of each well and averaged across 8-12 wells per sample (N=3).

2.5.3. Transwell invasion assay

Matrigel-coated Boyden chamber inserts with 8 μm pores (Corning) were rehydrated and placed in wells containing RPMI with 10% FBS. An equal number of serum-starved (24 hours) HTR-8/SVneo cells was resuspended in RPMI with 0% FBS and pipetted into the upper chambers of 3 inserts per cell line. After 24 hours, the Matrigel layer and any cells remaining in the upper chamber were scrubbed off the membrane, which was then stained with crystal violet and left to dry. The membranes were excised from the inserts and mounted on microscope slides, and the invaded cells on the lower chamber side of the membrane, which took up the stain, were counted. All cells were counted using FIJI cell counter function, and numbers for each cell line were averaged across three technical replicates (N=3).

2.5.4. Forskolin and cytokine treatments

For forskolin (FSK) and cytokine (TNFα, IFNγ) treatments, all plates containing samples to be compared were plated at the same time, using the same number of cells (HTR-8/SVneo or BeWo). 72-hour treatments were initiated 24 hours after plating, and 24-hour treatments were initiated 72 hours after plating, so as to collect all plates at the same time and ensure consistency in cell confluence and culture period. Human TNFα (Thermo Fisher Scientific) was prepared at 0.5ng/mL and 10ng/mL and human IFNγ (Peprotech) was prepared at 5ng/mL and 50ng/mL. Forskolin (Millipore Sigma) was used at 100μM.

2.5.5. Human *FGL2* overexpression (h*FGL2*)

A human *FGL2* cDNA was purchased (Integrated DNA Technologies) and cloned into the pWPI vector (Addgene plasmid #12254), using the In-Fusion PCR Cloning system (Clontech) and isolated using GenElute Maxiprep Kit (Sigma-Aldrich). Pure plasmid DNA from pWPI and pWPI-hFGL2 preps was obtained using GeneJET plasmid DNA purification kit (Thermo Fisher). Both plasmids were packaged into a lentivirus, by transfecting HEK293 cells with purified DNA and packaging components. Lentiviruses were collected 48 hours after transfection and filtered at 45μm. The HTR-8/SVneo and BeWo cell lines were infected with both viruses (polybrene) and the successfully infected cells were isolated using fluorescence-activated cell sorting (FACS) for GFP expression.

2.5.6. Quantitative RT-PCR (qPCR)

All primer pairs were designed with the NCBI primer design tool to produce a single amplicon 75-200bp in length and spanning an exon-exon junction, whenever possible. Potential primer pairs were analyzed using OligoAnalyzer (Integrated DNA Technologies) and pairs were chosen for a minimal likelihood of hairpin, homodimer and heterodimer formation, and for similar melting temperatures. Primers were then tested in qPCR on a pooled cDNA sample. The melt curve was analyzed, and the product was run on an agarose gel to ensure presence of a single amplicon. This amplicon was serially diluted and used in a standard curve, which was then used to calculate the amplification efficiency using the formula: $E = -1+10^{(-1/slope)}$. Only primers with satisfactory efficiency of 95-105% were used in this work. Primer sequences can be found in **Table 1**.

To conduct qPCR, RNA was first extracted from cell lysates using the RNAspin kit (GE Healthcare Life Sciences) or the RNeasy Mini Kit (Qiagen) and cDNA was synthesized using iScript (Bio-Rad) reagents and protocols. cDNA was mixed at assay-specific concentrations (200-1000ng per well) with ddH_2, the primer mix and SsoFast EvaGreen enzyme mix (Bio-Rad). The ABI 7500 FAST (Applied Biosystems) and its software were used to run qPCR. The relative expression presented in plots throughout this thesis represents $2^{(-\Delta\Delta CT)}$, where the geometric mean of the cycle threshold (CT) of endogenous control genes was subtracted from the CT of the target gene to obtain ΔCT. This number was normalized to either an external positive control or the control condition of specific experiments, to obtain

ΔΔCT. Technical replicates are always 3 wells per sample, biological replicate number is indicated in individual figure captions.

2.5.7. Western blot

Protein extraction from cell lysates was done using Mammalian Protein Extraction Reagent (M-PER, Thermo Fisher Scientific). β-mercaptoethanol and sodium dodecyl sulfate (SDS) loading buffer were added to the lysate and heated, and samples were run on NuPAGE 4-12% Bis-Tris gradient gels (Life Technologies). Protein was transferred to a polyvinylidene difluoride (PVDF) membrane in Tris-glycine buffer with 20% methanol and blocked with 5% skim milk in Tris-buffered saline with Tween 20 (TBST). The membrane was incubated in primary antibody as described in **Table 2** and in a 1/10000 dilution of an appropriate secondary antibody. The membrane was developed using Clarity Western ECL Substrate (Bio-Rad) and imaged using the ChemiDoc system (Bio-Rad).

2.5.8. Enzyme-Linked Immunosorbent Assay (ELISA)

Culture medium was collected from cells (HTR-8/SVneo or BeWo; parental or *Fgl2*-overexpressing) that had been plated 48 hours prior to collection. Two independent wells per sample were collected. The cells in the wells were counted at the time of collection, to express results of the assay as FGL2 concentration per 100 000 cells. The reagents and the protocol used were those provided with the LEGEND MAX Human FGL2 ELISA (BioLegend). The plate was read at both 450nm and 570nm, and the 570nm reading was subtracted from the 450nm reading. The

FGL2 concentration in each well was calculated using the standard curve run in the same assay.

Table 1. List of primers

Gene	Species	Application	Sequence (5'-3')
ALPP	Human	qPCR	F – CTCAGACGTTCCATACCCCC R – GAGGGACCTTTGGCTCTCG
CGB3	Human	qPCR	F – CACCCCAGCATCCTATCACC R – ATCTCCATCCTTGGTGCGTC
ERVW-1	Human	qPCR	F – ATAACCCATACCTCAAACCTCACC R – GGCACTAAGAATGAGAGGAAGCA
Fgl2	Mouse	Genotyping (amplicon in $Fgl2^{wt/wt}$ and $Fgl2^{ko/ko}$)	F – TTGATAACACCAGTTGGTTCT R – TGCTGTTTCTGTGATCAGGGG
Fgl2	Mouse	Genotyping (amplicon only in $Fgl2^{ko/tg}$)	F – AACAGTTTGGATGGCAAGTGT R – TGCTGTTTCTGTGATCAGGGG
Fgl2	Mouse	Genotyping (amplicon only in $Fgl2^{wt/wt}$)	F – GGAAGCAGTGGACAGTCTGAA R – CTCCCTCGGGTTAATGTTTAT
FGL2	Human	qPCR	F – CAGGCAGAAACGGACTGTTG R – CCAGGCGACCATGAAGTACA
GCM1	Human	qPCR	F – GATGACAAGGAACCTGACCTAACC R – AAACAAGAGGCAAGGAGACCAC

Table 2. List of antibodies and conditions

Protein	Source	Type	Application	Specific conditions
CD31	Abcam (ab28364)	Rabbit polyclonal	IHC-P	1:100
CD206	Abcam (ab64693)	Rabbit polyclonal	IHC-P	1:500
FGL2	LSBio (LS-C293889)	Polyclonal rabbit anti-mouse	IHC-P (mouse tissue)	1:500-1:1000
FGL2	Abnova (H00010875-M01, clone 6D9)	Monoclonal mouse anti-human	IHC-P (human tissue)	1:1000
			WB (human cell lines)	1:500
αSMA	Abcam (ab5694)	Rabbit polyclonal	IHC	1:750

2.6. Computational analysis and statistics

2.6.1. Microarray dataset assembly, clustering and processing

Selection and processing of samples from the Research Centre for Women's and Infants' Health BioBank (Mount Sinai Hospital, Toronto, Canada), as well as procedures for microarray and unsupervised clustering analysis of a combined dataset were previously described. Clinical information from available samples was collected and analyzed[74,75,81].

The initial transcriptional clustering of samples, as previously described, resulted in 5 clusters. The lack of clear phenotype (via gene expression, histological and clinical profiling), coupled to the presence of genomic copy number gains for specific chromosomes (via array-based comparative genomic hybridization analysis), indicate that the formation of cluster 5 was likely driven by site-specific sampling artifacts related to confined placental chromosomal mosaicism, rather than distinct preeclampsia pathophysiology[75]. Our group has previously published a small highly discriminatory panel of genes that can be used to assign patient samples into the unique transcriptional clusters using standard qPCR methods. When these original cluster 5 patients' samples (N=15) were re-screened using this discriminatory gene panel, they were re-assigned into clusters 1-3. Following cluster reassignment, placental histopathology was assessed and in support of this reassignment exercise, histopathology findings of each patient were concordant to those of their reassigned cluster. For the present study, after cluster 5 sample reassignment, the dataset was filtered for samples belonging to transcriptional clusters 1, 2 and 3. All analyses were accomplished using RStudio, version 1.1.453

(R version 3.5.0). Network analysis was accomplished using R package *WGCNA*[112]. All gene ontology analyses were performed using R package *g:Profiler*[113].

2.6.2. Gene module detection, enrichment and visualization

Network analysis based on weighted gene correlations in our dataset was accomplished using R package WGCNA. Gene expression data derived from the microarray and clinical information about samples was loaded. For network construction and module detection, a threshold of 5 was used, the dendogram cut height was set to 0.25 and the minimal module size was set to 30 genes. Module enrichment was examined in our 6 diagnostic groups, which are based on cluster membership and diagnosis given to each sample: cluster 1 & healthy, cluster 1 & PE, cluster 2 & healthy, cluster 2 & PE, cluster 3 & healthy, cluster 3 & PE. An average gene expression z-score was calculated for all genes belonging to a given module. Scores of all samples in a diagnostic group were averaged, and the resulting module enrichment was represented as a heatmap. For network structure visualization of relevant modules (yellow and purple), weighted gene correlation values calculated previously using WGCNA were converted to an *igraph* network using the *WGCNA2igraph* function from the *limmaDE2* package (https://github.com/jtlovell/limmaDE2/). Values were filtered for genes belonging to modules of interest, and network plots were created using R package *igraph.* Hub genes (genes with degree > 30) and genes of interest were colour-coded and labelled.

2.6.3. GO terms enrichment

R package *g:Profiler* was used for all gene ontology analyses. To determine GO terms associated with specific gene modules, a vector containing all genes belonging to a module (non-ranked) was set as query. Hierarchical filtering strength was set to “none”, and we used an fdr-corrected maximal p-value of 0.05 to exclude non-significant terms. For both gene modules analyzed, the top 15 terms are presented. To determine GO terms associated with upregulated genes in MVM lesions, we first compiled a list of genes that were common among genes upregulated in placentas affected by each lesion. A vector containing this ranked gene list was used as query. Hierarchical filtering strength was set to “moderate” to reduce redundancy of terms presented, and we used an fdr-corrected maximal p-value of 0.05 to exclude non-significant terms. The same parameters were applied when determining GO terms associated with upregulated genes in single inflammatory lesions, but a ranked list of upregulated genes was directly used as query instead of pooling commonly upregulated genes.

2.6.4. Statistical analysis

R (version 3.6.2) and RStudio (version 1.2.5019), and occasionally, GraphPad Prism (version 9.0.0) were used to perform statistical analyses. The Shapiro test was used to verify normality of the data, and the F-test was used to measure variance, and together with the data type, were used to justify the use of a parametric vs. a nonparametric test. Specific tests are noted in figure captions. In general, to test the difference of means between two groups, Student’s t test was

used for normally distributed data (parametric), and Welch's t test (nonparametric) was used for non-normal data. To test the difference of means between three groups or more, analysis of variance (ANOVA) was used for normal data (parametric) and Kruskal-Wallis rank-sum test was used for non-normal data (nonparametric).

In analyses where factors external to those being tested were suspected to have an effect on the main outcome, regression analysis was used (clinical data, fertility study). This allowed us to account for this effect when describing the statistical significance of the conclusion, if necessary. In all cases, regression models were built using the linear model (lm) function of base R language, using only the main dependent and independent variables at first, and progressively testing the addition of other variables, independently and in interaction with each other. The "best" model was chosen to optimize the normal distribution of residuals and secondarily, a high R^2 value. In those cases, our results report what variables were included in the model, interactions between them (if applicable), and the calculated p value associated with them. Statistical significance was conferred when $p<0.05$.

CHAPTER 3 (RESULTS): ESSENTIAL EQUILIBRIUM OF *FGL2* EXPRESSION FOR SUCCESSFUL PREGNANCY ESTABLISHMENT AND OPTIMAL OUTCOMES

3.1. Validation of mouse models

We acquired two mouse models to conduct our studies, *Fgl2*$^{ko/ko}$ (knockout) and *Fgl2*$^{ko/tg}$ (overexpressing), described in *Materials and Methods*[97,101]. Several FGL2 detection antibodies exist, and most are predicted to react with both the mouse and human form of the protein, while some claim to be specific but, in preliminary experiments, were shown not to be. We therefore aimed, first, to confirm complete knockout in *Fgl2*$^{ko/ko}$ animals, using a method that is not antibody dependent. To generate this model, *LacZ* was inserted within the first exon of *Fgl2*, driven by the *Fgl2* promoter, which should result in β-galactosidase expression in cells that are normally positive for FGL2. We stained dissected reproductive tracts from *Fgl2*$^{wt/wt}$ and *Fgl2*$^{ko/ko}$ mice with X-gal and observed strong staining in the *Fgl2*$^{wt/wt}$ oviduct and uterine lumen, as well as scattered on the visible surface of the ovary (**Figure 1A**). In contrast, only weak background staining is evident in all *Fgl2*$^{ko/ko}$ tissues, confirming successful knockout. *Fgl2*$^{ko/tg}$ mice are genotyped easily, as they ubiquitously express the FGL2-GFP fusion protein. We observed a strong GFP signal in *Fgl2*$^{ko/tg}$ reproductive tracts, but none in *Fgl2*$^{wt/wt}$ (**Figure 1B**). We further validated these models by testing *Fgl2*$^{wt/wt}$, *Fgl2*$^{ko/ko}$ and *Fgl2*$^{ko/tg}$ tissues by immunohistochemistry and confirmed reliable detection of FGL2 for our studies by determining that protein expression matched the tissue genotype (**Figure 1C**).

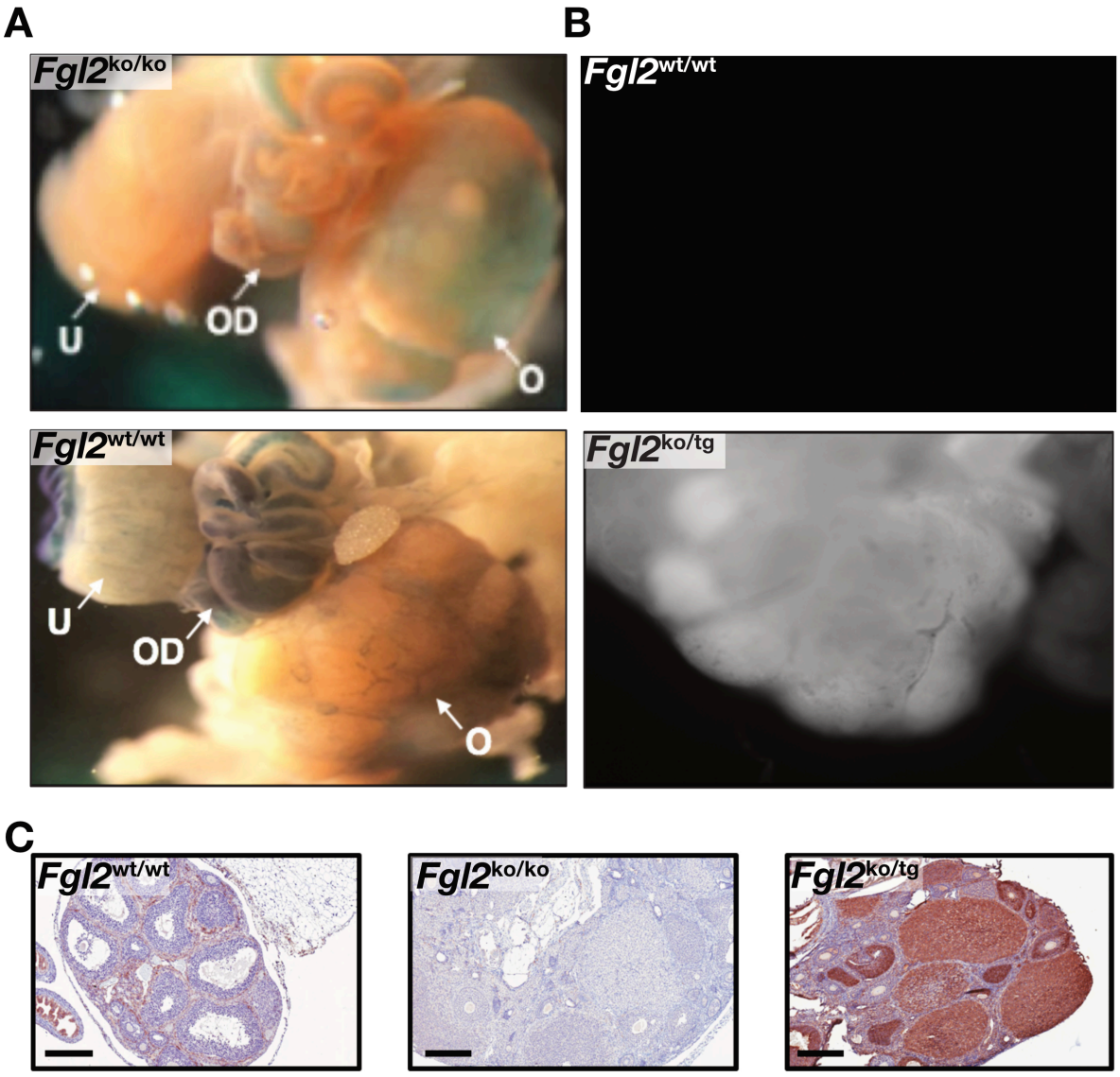

Figure 1: Validation of *Fgl2* knockout (*Fgl2*$^{ko/ko}$) and overexpression (*Fgl2*$^{ko/tg}$) mouse models. A) X-gal staining of whole reproductive tract fresh tissues. B-galactosidase is absent from *Fgl2*$^{ko/ko}$ tissues but expressed in *Fgl2*$^{wt/wt}$ tissues. **B)** GFP is absent from *Fgl2*$^{wt/wt}$ but present in *Fgl2*$^{ko/tg}$ tissues (U, uterus; O, ovary; OD, oviduct). **C)** Immunohistochemistry of ovary section from randomly cycling *Fgl2*$^{wt/wt}$, *Fgl2*$^{ko/ko}$, and *Fgl2*$^{ko/tg}$ animals (rabbit anti-mouse FGL2, LSBio). Positive staining is concordant with *Fgl2* genotype. Scale bars = 200μm.

3.2. Aberrant FGL2 expression causes subfertility in mouse colony

In order to investigate the effect of FGL2 on fertility in mice, we retrospectively examined several parameters of breeding success, using accumulated data from our mouse colony management database. Between *Fgl2*$^{wt/wt}$, *Fgl2*$^{ko/ko}$ and *Fgl2*$^{ko/tg}$ breeding pairs (as indicated in **Figure 2A**), we first compared the number of pups produced over a set period of time, by calculating the number produced, on average, over 90 days, taking into account all pups produced by that pair until the mating was disbanded. In the same way, we compared the number of litters produced over a set time period, and the number of pups per litter. We used linear regression modeling to identify independent variables that influence the measurements of breeding success (dependent variables), hypothesizing that genotype would be the significant factor in any variation observed in dependent variables. We first noticed that compared to *Fgl2*$^{wt/wt}$ pairs, *Fgl2*$^{ko/ko}$ and *Fgl2*$^{ko/tg}$ pairs produce fewer pups over a set period of time, with *Fgl2*$^{ko/ko}$ having a larger decrease than *Fgl2*$^{ko/tg}$ (**Figure 2A**). Our optimal linear regression model ($p = 6.79e\text{-}6$, $R^2 = 0.98$) included a significant interaction between the *Fgl2*$^{ko/ko}$ genotype and the number of pups per litter ($p = 0.0476$), and a near-significant one between the *Fgl2*$^{ko/tg}$ (female) genotype and the number of pups per litter ($p = 0.0666$). The effect of each genotype, by itself (without interaction with another variable), did not reach significance ($p = 0.3408$, *Fgl2*$^{ko/ko}$; $p=0.9159$, *Fgl2*$^{ko/tg}$ male; $p=0.0584$, *Fgl2*$^{ko/tg}$ female). Independently, the number of litters over 90 days and the number of pups per litters had a significant effect on the total number of pups over 90 days ($p = 2.0e\text{-}16$ and $p = 1.39e\text{-}11$, respectively). Therefore, we next looked at the variation between genotypes of the number of

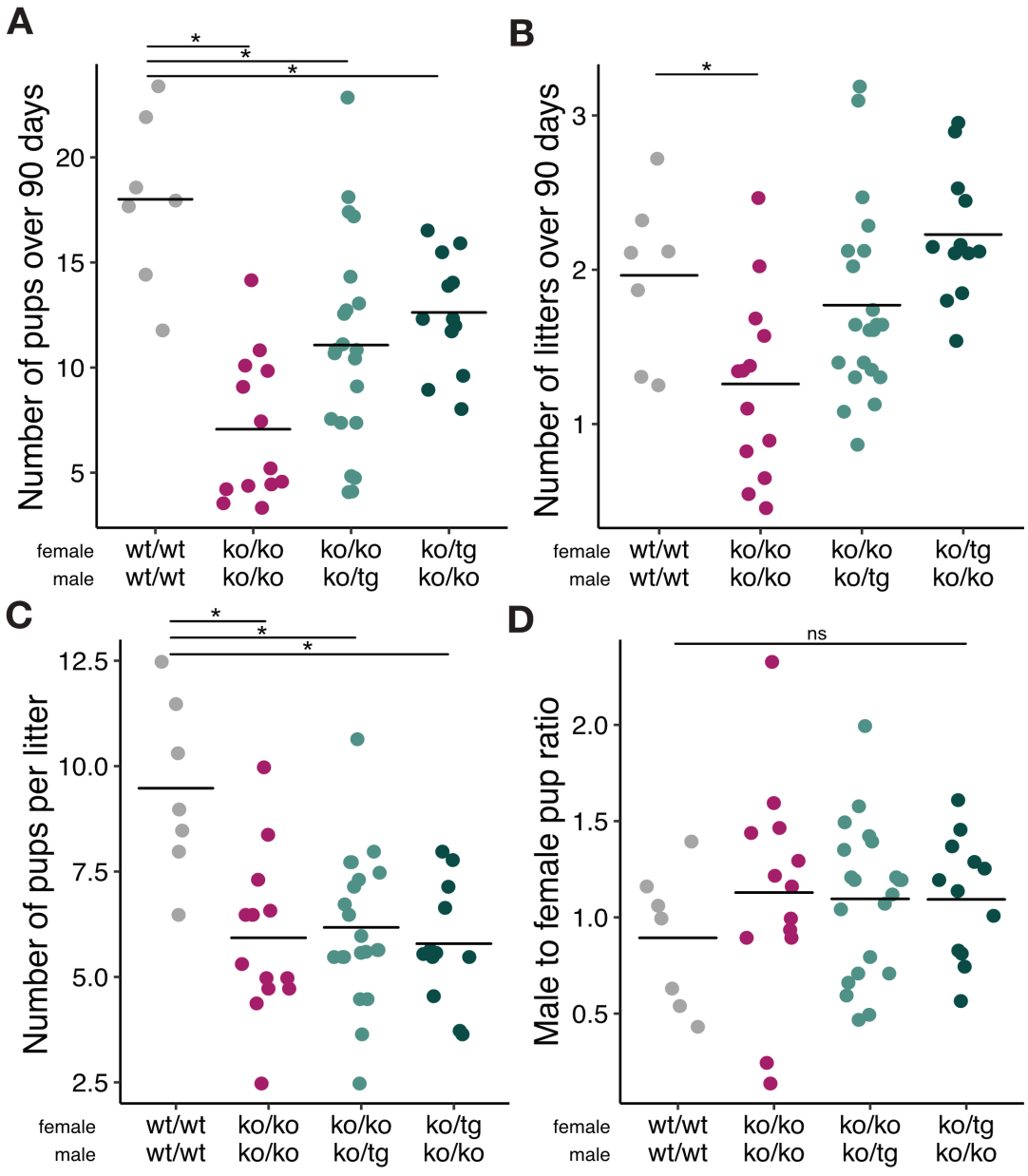

Figure 2: *Fgl2* knockout and overexpression cause subfertility in a retrospective assessment in mouse colony mating pairs. A) Fewer total pups produced from *Fgl2*$^{ko/ko}$ pairs. Best fitting linear regression model (p=6.79e-6, R^2=0.98) includes interaction between number of pups per litter and genotype (p=0.0476, *Fgl2*$^{ko/ko}$; p=0.8697, *Fgl2*$^{ko/tg\ male}$; p=0.0666, *Fgl2*$^{ko/tg\ female}$) and independent effect of the number of litters over 90 days (p=2.0e-16) and number of pups per litter (p=1.39e11). Effects of all other variables or interactions are not significant. **B)** Fewer total litters produced from *Fgl2*$^{ko/ko}$ pairs (p=0.01) but not from *Fgl2*$^{ko/tg\ male}$(p=0.434) or *Fgl2*$^{ko/tg\ female}$(p=0.426). **C)** Fewer pups per litter in *Fgl2*$^{ko/ko}$ (p=8.91e-5), *Fgl2*$^{ko/tg\ male}$ (p=8.92e-5) and *Fgl2*$^{ko/tg\ female}$ (p=6.32e-5) pairs. **D)** Pup sex ratio is similar in all genotypes (p=0.56). Kruskal-Wallis rank sum test with Dunn's test for multiple comparisons.

litters over 90 days, where a significant reduction was only seen in *Fgl2*$^{ko/ko}$ pairs (p = 0.01, *Fgl2*$^{wt/wt}$-*Fgl2*$^{ko/ko}$; p = 0.434, *Fgl2*$^{wt/wt}$-*Fgl2*$^{ko/tg}$ male; p = 0.426, *Fgl2*$^{wt/wt}$-*Fgl2*$^{ko/tg}$ female) (**Figure 2B**). When comparing the number of pups per litter, we observed significant reductions in all groups, compared to *Fgl2*$^{wt/wt}$ (p = 8.91e-5, *Fgl2*$^{wt/wt}$-*Fgl2*$^{ko/ko}$; p = 8.92e-5, *Fgl2*$^{wt/wt}$-*Fgl2*$^{ko/tg}$ male; p = 6.32e-5, *Fgl2*$^{wt/wt}$- *Fgl2*$^{ko/tg}$ female) (**Figure 2C**). As fewer pups per litter suggest embryo loss, we investigated a potential bias in the sex of live pups. The ratio of male to female pups born to breeding pairs of all genotypes was unchanged (p = 0.56) (**Figure 2D**).

Taken together, these data reveal that *Fgl2*$^{ko/ko}$ pairs produce fewer pups over a set period of time than *Fgl2*$^{wt/wt}$ pairs, as a result of fewer, smaller litters. *Fgl2*$^{ko/tg}$ pairs, when either the male or the female is *Fgl2*$^{ko/tg}$, have smaller litters but at higher frequencies than *Fgl2*$^{ko/ko}$, leading to a reduced number of pups over a set time period, but not as severe as in *Fgl2*$^{ko/ko}$ pairs.

3.3. Expression dynamics and functionality of FGL2 in ovarian morphology and function

Previously, our lab identified FGL2 as a target of SNF2L, in the ovarian function of *Snf2L* Ex6DEL (knockout) mice (**see Introduction**). Taken together, the ovarian phenotype observed in *Snf2L* Ex6DEL mice, the evidence for SNF2L regulation of *Fgl2* levels at a functionally important stage, and the subfertility of *Fgl2* ko mice led us to consider whether a lack of *Fgl2*, on its own, could lead to morphological and/or functional defects in the ovary.

3.3.1. Cell-type specific ovarian FGL2 expression varies temporally through the estrous cycle

As cell type specificity and variation in expression intensity through the estrous cycle provide hints towards functional role, we first aimed to resolve the dynamics of FGL2 expression around ovulation. We collected tissues from WT mice at strategic timepoints after exogenous gonadotropin stimulation, to pinpoint possible peaks in intensity or changes in localization of FGL2 expression. Twenty-four hours after PMSG injection, a timepoint analogous to the pre-estrous phase of the natural cycle, baseline expression of FGL2 was first observed in ovarian stroma, and in the theca cell layer that surrounds growing follicles. No difference in intensity was noted between follicles at different stages of maturation (**Figure 3**). We noted perinuclear cellular localization in all positive cells, consistent with knowledge from the literature that FGL2 can be either embedded in the plasma membrane or secreted, but through an unknown mechanism.

FGL2 protein expression is increased by hCG, with expression intensity peaking 8 hours after injection, remaining high through ovulation (12 hours post hCG) and gradually decreasing back to pre-hCG levels around 24 hours post hCG (**Figure 3**). As theca cells chiefly contribute to steroid hormone synthesis through crosstalk with granulosa cells, this suggests FGL2 to

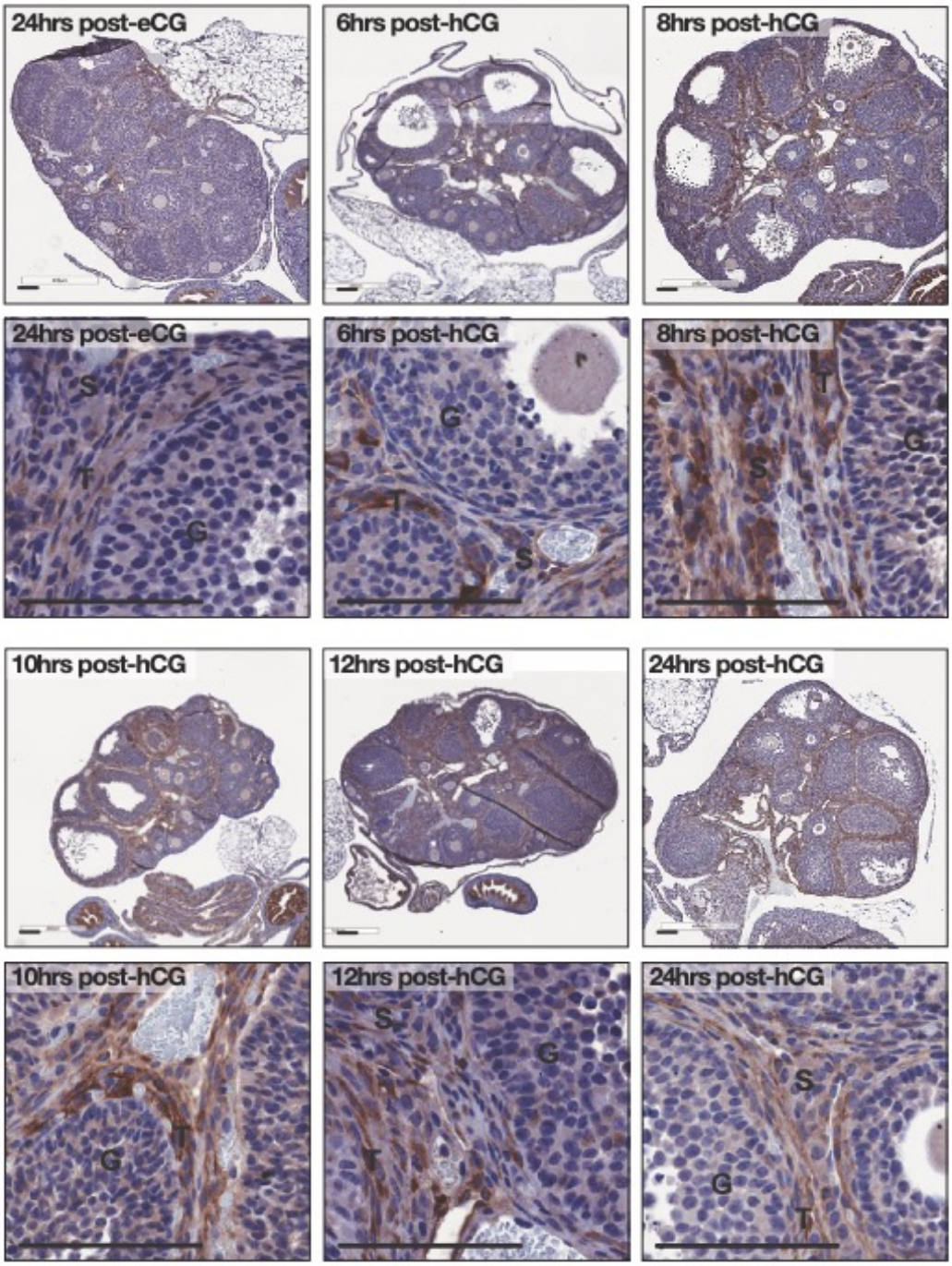

Figure 3: Ovarian cell type specificity of FGL2 expression and temporal dynamics through induced ovulation. Immunohistochemistry staining of ovaries from gonadotropin-stimulated animals at various timepoints after hCG injection (rabbit anti-mouse FGL2, LSBio). Ovarian FGL2 expression is restricted to theca cells and stroma, and peaks in intensity 8hrs after hCG injection. Representative images of tissues from 3 animals/timepoint. T, theca; S, stroma; G, granulosa. Scale bars = 100μm.

be involved in the preovulatory stage of follicle maturation. While granulosa cells and oocytes of developing follicles are devoid of FGL2 expression, a subset of cumulus granulosa cells acquires expression after hCG injection, first noticed at 6 hours post hCG (**Figure 4**). This persisted through ovulation, where some positive granulosa cells were observed at the ovulatory wound site, and beyond, as ovulated oocytes surrounded by FGL2-positive cumulus granulosa cells (COCs) were observed in the ampulla of the oviduct (**Figure 4**). Overall, this dynamic pattern of expression suggests FGL2 to be involved in late-stage follicle maturation or ovulation – either as a regulator of the necessary signals or responding to the precisely-timed molecular cues that govern the process.

3.3.2. Aberrant FGL2 expression does not alter ovarian morphology or ovulation efficiency

We next aimed to determine if the functionality of ovaries was affected in our *Fgl2*$^{ko/ko}$ and *Fgl2*$^{ko/tg}$ mouse lines, and if this potential defect could account for their reduced fertility. Considering the decrease in secondary follicle counts and the numerous abnormal follicles observed in *Snf2L* Ex6DEL mice, we first investigated potential morphological differences between the ovaries of *Fgl2*$^{wt/wt}$, *Fgl2*$^{ko/ko}$, and *Fgl2*$^{ko/tg}$ mice. As FGL2 is expressed in theca cells and peaks shortly before ovulation, we hypothesized that its lack or excess could be directly responsible for a deficient progression to the late antral/preovulatory stage of follicle development, as

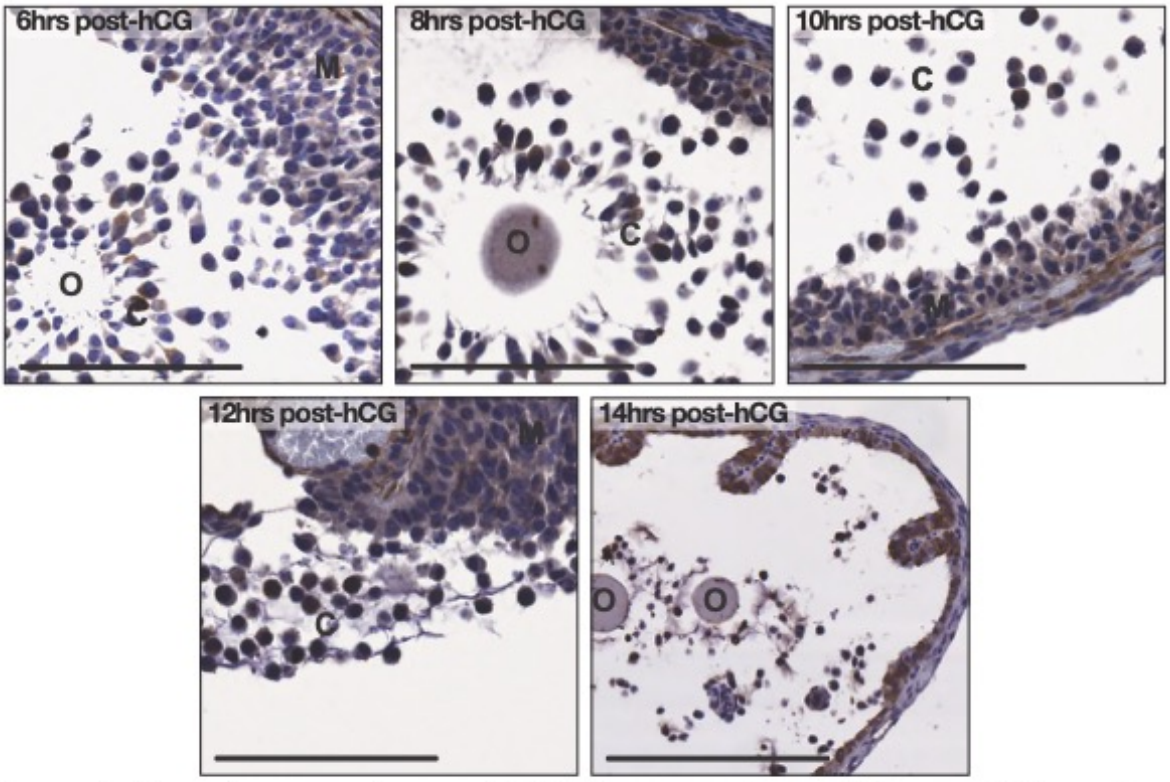

Figure 4: Cumulus granulosa cell FGL2 expression and temporal dynamics through induced ovulation. Immunohistochemistry staining of antral follicles and cumulus-oocyte complexes (COCs) from gonadotropin-stimulated animals at various timepoints after hCG injection (rabbit anti-mouse FGL2, LSBio). FGL2 expression is acquired by cumulus granulosa cells 6hrs after hCG injection and persists in ovulated COCs. Representative images of tissues from 3 animals/ timepoint. O, oocyte; C, cumulus granulosa cells; M, mural granulosa cells. Scale bars = 100μm.

in *Snf2L* Ex6DEL mice. We counted and calculated the ratio of abnormal to total follicles in H&E-stained ovary sections. We found comparable ratios in all 3 genotypes ($p = 0.3024$) (**Figure 5A-B**).

We next examined the effect of that genotype on the capacity of these mice to ovulate, as morphologically normal follicles could be dysfunctional. We first asked whether *Fgl2*$^{ko/ko}$ mice produce fewer oocytes per ovulation, as fewer pups are produced from each litter. We collected COCs from the ampulla region of the oviduct, using naturally cycling, non-induced mice, and found similar numbers in all 3 female genotypes (~9 COCs, *Fgl2*$^{wt/wt}$; ~10 COCs, *Fgl2*$^{ko/ko}$; ~8 COCs, *Fgl2*$^{ko/tg}$) (**Figure 6A-C**). Interestingly, in *Fgl2*$^{ko/ko}$ mice, this number is, on average, higher than the number of live pups per litter (~10 COCs, ~6 pups), while *Fgl2*$^{wt/wt}$ mice have an ovulation number that roughly corresponds to the number of live pups in each litter (~9 COCs, ~9 pups) (**Figures 2 and 6**). This suggests the possibility of embryo loss in the pre- or post-implantation period, rather than a lack of oocytes to be fertilized, as a cause of the smaller litters. In *Snf2L* Ex6DEL mice, where the lack of *Snf2L* activity leads to the loss of *Fgl2* induction in granulosa cells, an ovulation defect was only evident upon stimulation with exogenous gonadotropins. We therefore examined the possibility that similarly, *Fgl2*$^{ko/ko}$ mice would show a decreased yield when superovulated. We collected and counted COCs from gonadotropin-induced mice, and found similar number in all three genotypes, suggesting that FGL2 lack or excess does not affect response to superovulation (~22 COCs, *Fgl2*$^{wt/wt}$; ~20 COCs, *Fgl2*$^{ko/ko}$; ~23 COCs, *Fgl2*$^{ko/tg}$) (**Figure 6A-D**). We conclude that neither follicle maturation

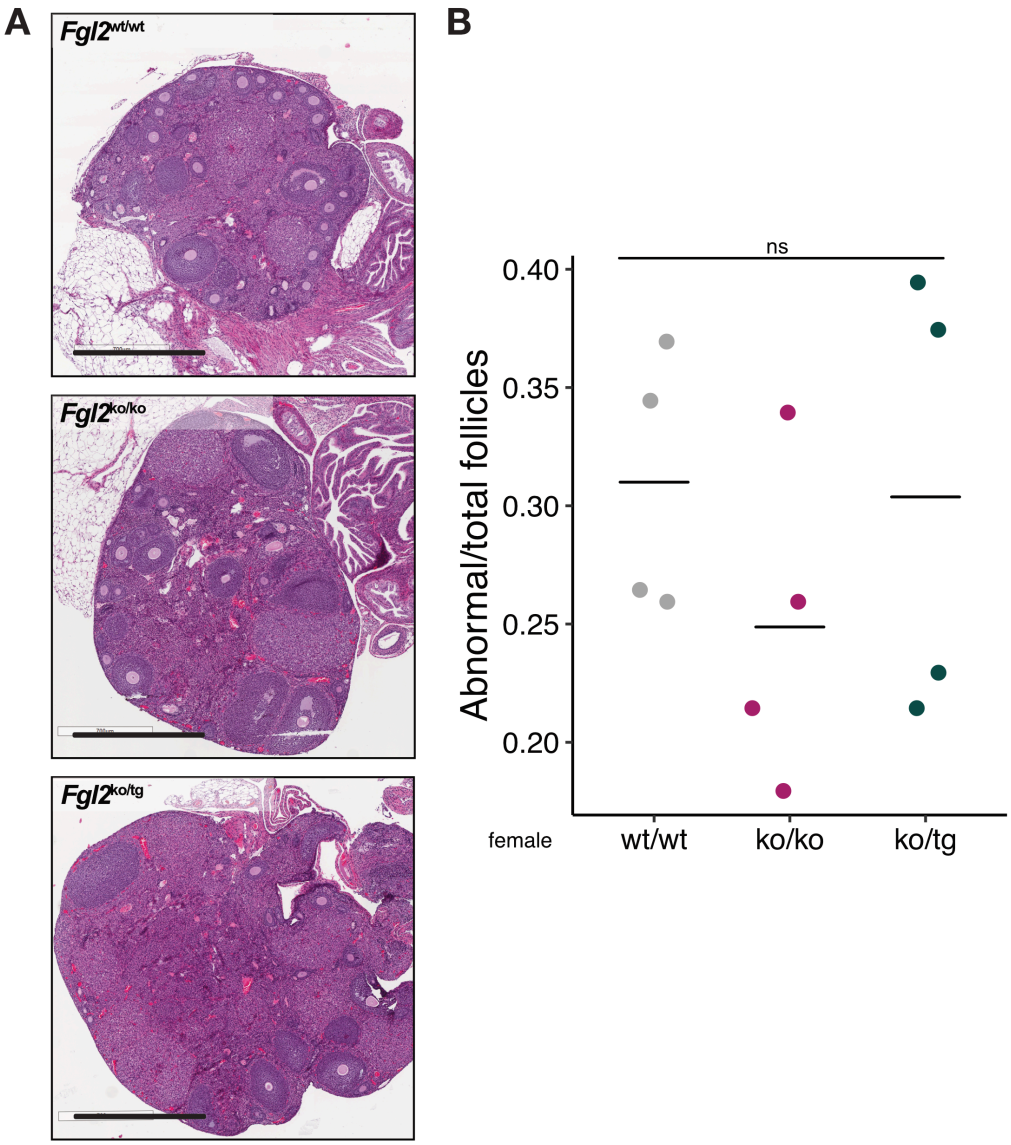

Figure 5: Effect of aberrant *Fgl2* expression on ovarian morphology and follicle health. A) Hematoxylin and eosin (H&E) staining of ovaries from *Fgl2*$^{wt/wt}$, *Fgl2*$^{ko/ko}$, and *Fgl2*$^{ko/tg}$ mice. Aberrant *Fgl2* does not cause obvious morphological defects. Representative images of tissues from 4 animals/genotype, 2 sections/ ovary, at least 200µm apart. Scale bars = 1mm. **B)** Abnormal to total follicle count in ovaries of *Fgl2*$^{wt/wt}$, *Fgl2*$^{ko/ko}$, and *Fgl2*$^{ko/tg}$ mice are similar but highly variable (p=0.3024, Kruskal-Wallis rank sum test). Each data point represents the average ratio found in 2 sections from the ovary of the same animal.

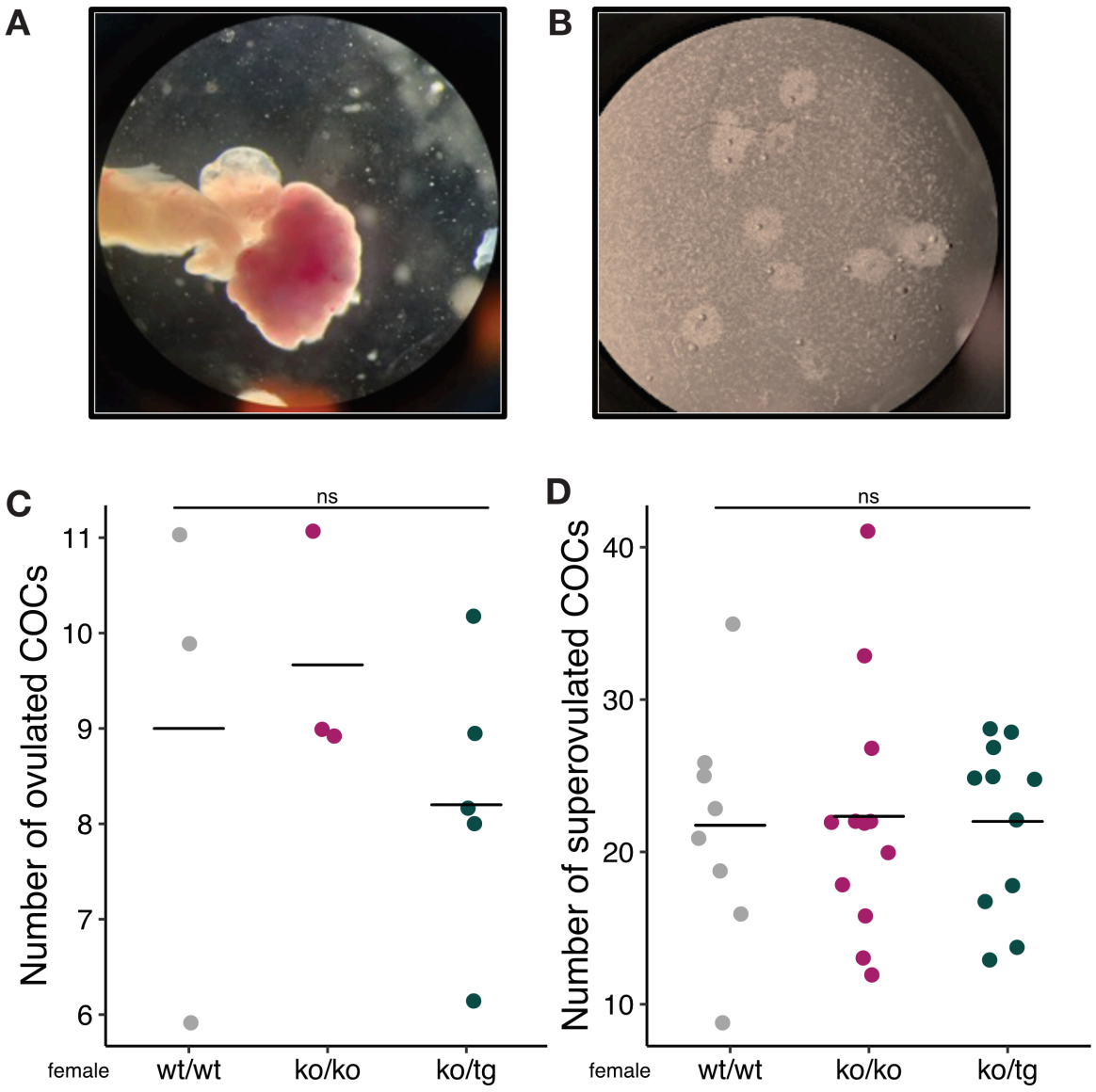

Figure 6: Aberrant *Fgl2* expression does not affect ovulation efficiency in mice. A) Representative image of the ampulla at the time of COC collection. **B)** Representative image of the dissociation of oocytes and their cumulus granulosa cells by hyaluronidase. **C)** *Fgl2*$^{wt/wt}$, *Fgl2*$^{ko/ko}$, and *Fgl2*$^{ko/tg}$ females produce equivalent number of COCs when naturally cycling (p=0.4152, Kruskal-Wallis rank sum test), and **D)** when induced with exogenous gonadotropins (p=0.8948, Kruskal-Wallis rank sum test).

or ovulation is impaired by a lack or excess of FGL2, and therefore do not explain the subfertility of our mouse lines.

3.4 FGL2 as a regulator of luteal angiogenesis

The predominant localization of FGL2 expression in theca cells, the previously reported loss of e7.5 *Fgl2*$^{ko/ko}$ embryos from *Fgl2*$^{wt/ko}$ X *Fgl2*$^{wt/ko}$ mating pairs (see **1.4.3.**), and the known M2-polarizing effect of FGL2 on macrophages combine to suggest a role for FGL2 in luteal angiogenesis. Therefore, we tested the specific hypothesis that aberrant FGL2 expression in the ovary creates imbalanced macrophage populations, dysregulating angiogenesis regulation signals in the developing CL.

3.4.1. Dynamics of FGL2 and CD206 expression in luteinizing follicles

We first verified the localization of macrophages within the ovary, using CD206 immunoreactivity – a commonly used marker of M2 polarization[114,115]. We examined its dynamics around induced ovulation, and how it relates to FGL2 expression intensity and localization. Until ovulation, 12 hours after hCG injection in mice, CD206-positive cells are absent from maturing follicles, and are exclusively found within the theca cell layer – where FGL2 is highly expressed at that stage (**Figure 7A**). After ovulation, M2 macrophages can still be found within the thickening theca cell layer, but they are also seen at the luteinizing front, at the periphery of the luteinizing follicle, making their way inwards. Twenty-four hours after hCG, they can be found within the

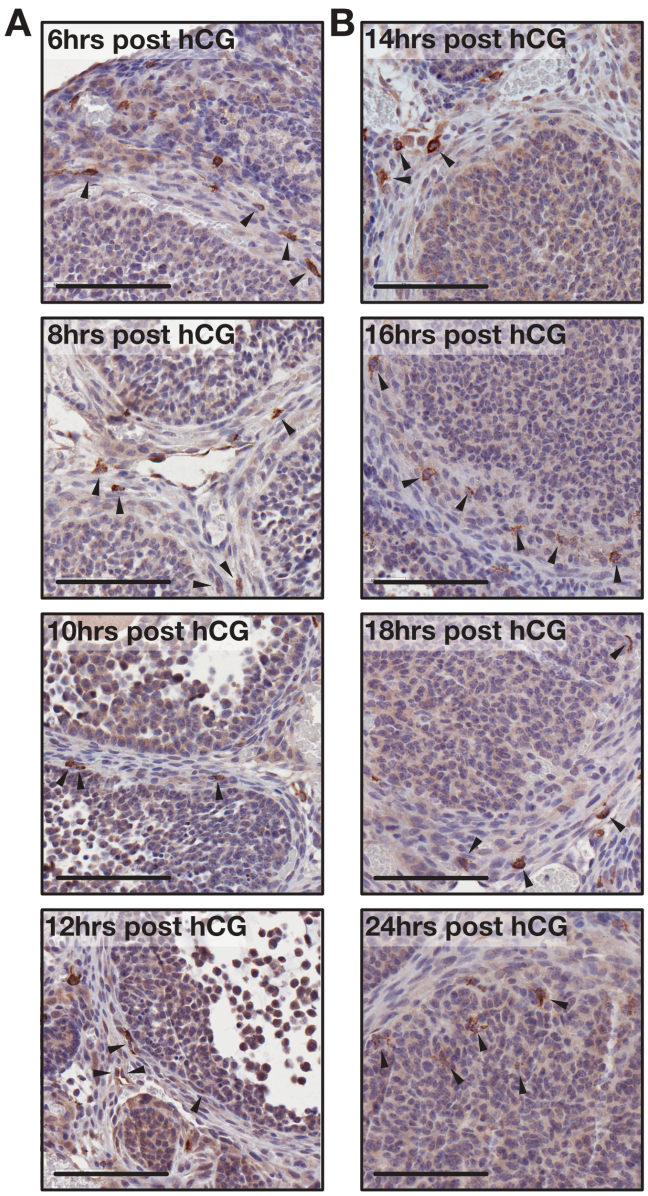

Figure 7: Dynamics of M2 macrophage localization through follicle maturation and corpus luteum formation (superovulation). A) Immunohistochemistry staining for CD206, a marker or M2 polarization in macrophages. Prior to ovulation, M2 macrophages are found within the theca cell layer of maturing follicles, which expresses FGL2. **B)** Following ovulation, as luteinization progresses, M2 macrophages are found more and more towards the center of the developing CL. Scale bars = 100μm, arrowheads indicate individual macrophages.

developing CL (**Figure 7B**). In contrast, FGL2 expression remains restricted to theca cells, even after ovulation when its intensity decreases. Proximal expression of FGL2 and CD206, within the theca layer at the onset of luteinization, suggests possible regulation of macrophages by FGL2, by contributing to either their initial recruitment or polarization.

To examine this hypothesis more closely, the abundance of M2-polarized macrophages was determined in our three FGL2 mice lines – comparing CD206 expression in *Fgl2*$^{wt/wt}$, *Fgl2*$^{ko/ko}$ and *Fgl2*$^{ko/tg}$ ovaries. We observed an average of 34 and 21 CD206-positive cells per mm^2, respectively, in *Fgl2*$^{wt/wt}$ and *Fgl2*$^{ko/ko}$ ovaries, and a marked increase in *Fgl2*$^{ko/tg}$ ovaries, at 199 positive cells/mm^2 (p=0.2280, *Fgl2*$^{wt/wt}$-*Fgl2*$^{ko/ko}$; p=0.0758, *Fgl2*$^{wt/wt}$-*Fgl2*$^{ko/tg}$; p=0.0256, *Fgl2*$^{ko/ko}$ -*Fgl2*$^{ko/tg}$) (**Figure 8A-B**). CD206-positive cells were found mainly through theca cell layers of developing follicles and the ovarian stroma, with few populating the CL at this mature stage. It is still uncertain whether FGL2 is essential to recruitment or M2 polarization, as our quantification showed an apparent decrease in numbers that was not statistically significant, in *Fgl2*$^{ko/ko}$ ovaries. The marked increase in M2 macrophages observed in *Fgl2*$^{ko/tg}$ ovaries however suggests that if not absolutely required, FGL2 certainly enhances the process.

3.4.2. *Fgl2* overexpression promotes luteal angiogenesis

As M2 macrophages secrete angiogenic factors, which guide vessel branching from the theca cell layer towards the center of the luteinizing follicle, we first characterized the timeline of vasculature formation in the CL. The

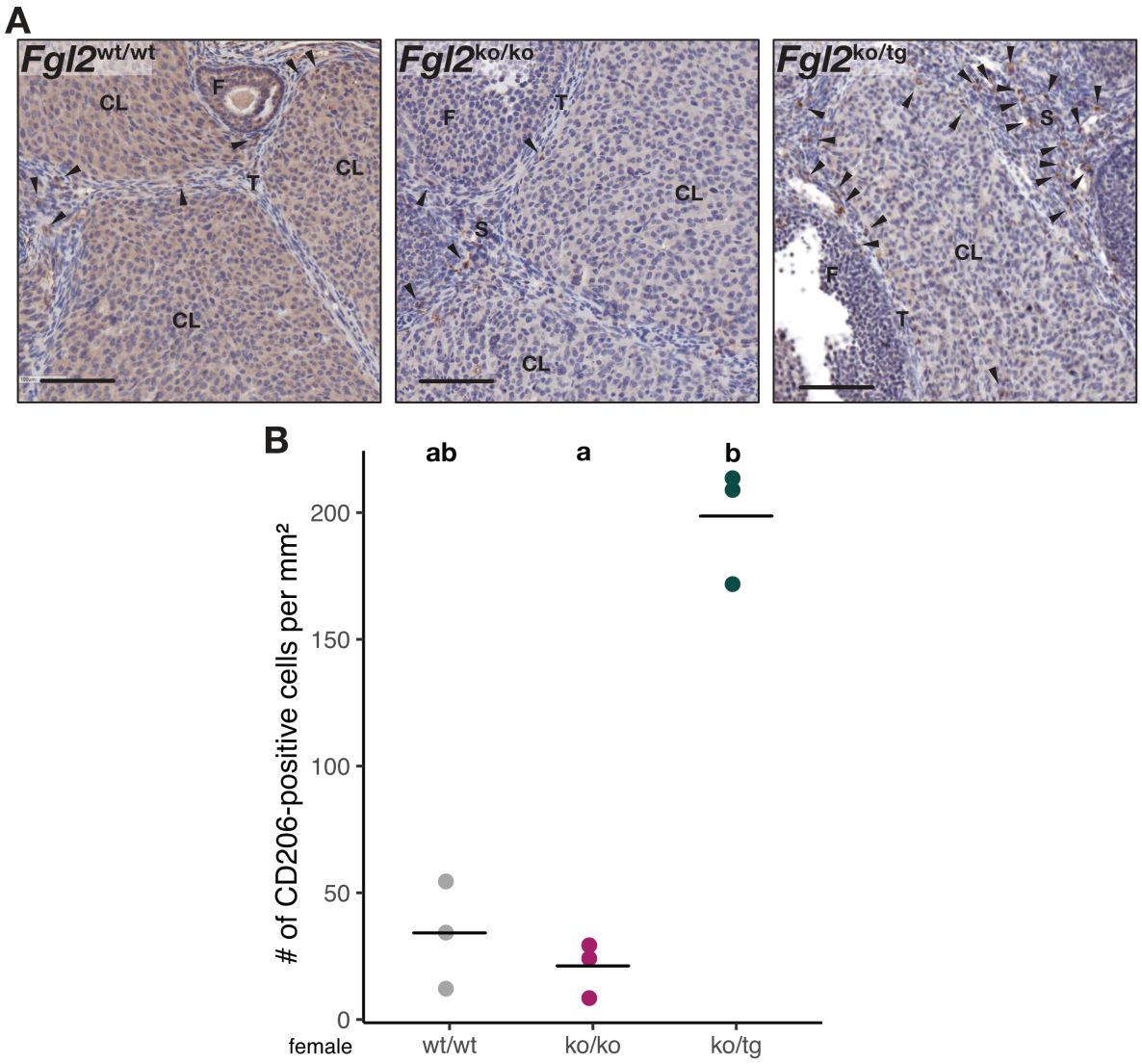

Figure 8: *Fgl2* overexpression leads to an increase in CD206-positive macrophage density in the ovary. A) Immunohistochemistry staining of CD206 in ovaries from gonadotropin-stimulated animals at 48 hours after hCG injection. Representative pictures of tissues from 3 animals/genotype. Arrowheads point to positive cells. CL = corpus luteum, T = theca cell layer, F = developing follicle, S = stroma. Scale bars = 100µm. **B)** CD206-positive cell density is higher in *Fgl2*$^{ko/tg}$ ovaries. Data points are individual animals, each represents total positive cell count/ovarian tissue area on the slide. Different letters indicate statistical difference between groups, Kruskal-Wallis rank sum test with Dunn's test for multiple comparisons (p=0.2280, *Fgl2*$^{wt/wt}$-*Fgl2*$^{ko/ko}$; p=0.0758, *Fgl2*$^{wt/wt}$-*Fgl2*$^{ko/tg}$; p=0.0256, *Fgl2*$^{ko/ko}$-*Fgl2*$^{ko/tg}$).

presence of pericytes normally precedes the appearance of functional vessels, and we therefore assessed the localization of α-SMA, a marker of pericytes, and of CD31, which marks endothelial cells, through the luteinizing process. At the time of ovulation, 12 hours after hCG injection, vasculature is restricted to the thickened theca cell layer, but progressively branches towards the center of the follicle - pericytes slightly ahead of endothelial cells. By 24 hours after hCG, α-SMA expression is uniform throughout the follicle, while CD31 expression has almost reached the center (**Figure 9**). This timeline is concordant with the theory that a CL would be fully vascularized and functional, able to fulfil its endocrine role, by e2.5, if fertilization occurs.

Lastly, we sought to determine the effect of M2 macrophage density, affected by aberrant *Fgl2*, on this vascularization process. Forty-eight hours after hCG injection, we observed a marked increase in CD31 positivity (density) in CLs from $Fgl2^{ko/tg}$ mice, where M2 macrophages were found to be more numerous (p = 0.3274, $Fgl2^{wt/wt}$-$Fgl2^{ko/ko}$; p = 0.0380, $Fgl2^{wt/wt}$-$Fgl2^{ko/tg}$; p = 0.0550, $Fgl2^{ko/ko}$-$Fgl2^{ko/tg}$) (**Figure 10A-B**). Interestingly, the opposite phenotype was not present in $Fgl2^{ko/ko}$ ovaries, which have a vasculature density comparable to that of $Fgl2^{wt/wt}$ ovaries.

3.5. Expression dynamics and functionality of FGL2 in oviductal function

The absence of an ovulatory defect to explain the subfertility of *Fgl2* ko mice led us to investigate tissues and mechanisms further down the female reproductive tract. The oviduct isn't a simple transit site but can host important

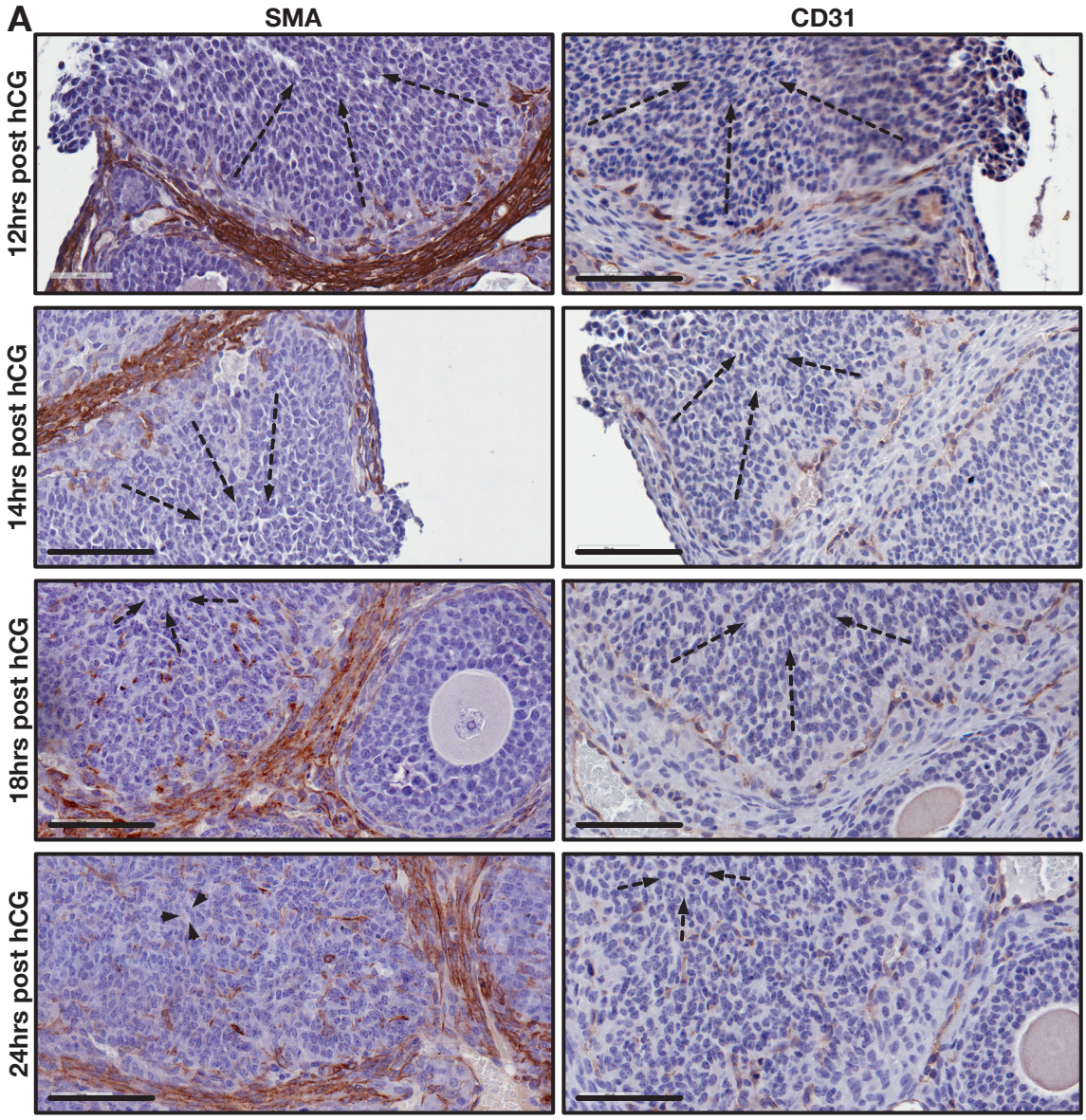

Figure 9: Dynamics of angiogenesis in the developing CL. A) Immunohistochemistry staining for SMA, a marker of pericytes, and CD31, a marker of endothelial cells, through CL development. Following ovulation, vasculature branches from existing vessels in the theca cell layer, towards the center of the follicle. Arrows indicate the direction and approximate progression of angiogenesis. SMA expression precedes CD31 expression. Scale bars = 100μm.

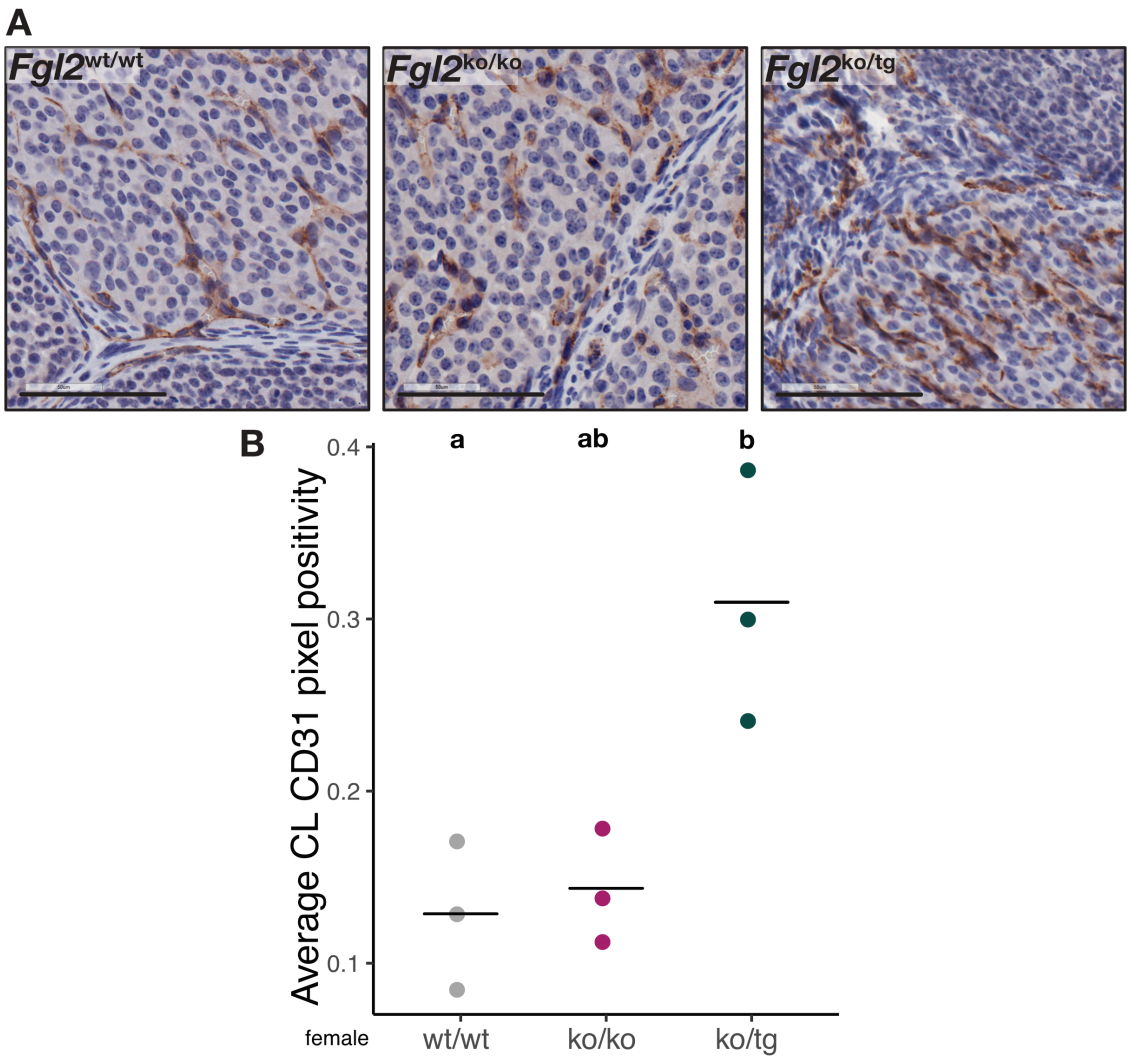

Figure 10: Aberrant *Fgl2* expression affects corpus luteum vasculature density. A) Immunohistochemistry staining of CD31 in ovaries from gonadotropin-stimulated animals 48 hours after hCG injection. Representative images of tissues from 3 animals/genotype. Scale bars = 100µm. **B)** CD31 positivity is higher in $Fgl2^{ko/tg}$ ovaries. Data points are individual animals, each represents the average CD31 positivity for 4-10 distinct CLs from the same tissue section (DAB positive pixels/total pixels of field of view, for each CL). Different letters indicate statistical difference between groups, Kruskal-Wallis rank sum test with Dunn's test for multiple comparisons (p=0.3274, $Fgl2^{wt/wt}$-$Fgl2^{ko/ko}$; p=0.0380, $Fgl2^{wt/wt}$-$Fgl2^{ko/tg}$; p=0.0550, $Fgl2^{ko/ko}$-$Fgl2^{ko/tg}$).

immunoregulatory steps of the mating process. Several factors affect the composition and immune profile of oviductal fluid, and FGL2 presents as a possible regulator of this immunosuppressive environment.

3.5.1 FGL2 oviductal expression fluctuates temporally through estrous cycle

We first examined localization of FGL2 expression, by immunohistochemistry, in tissues collected at several timepoints after ovulation induction. In the fimbria, where ciliated cells represent a high proportion of the epithelial layer, FGL2 was exclusively expressed in secretory cells. This restricted expression was maintained through the ampulla, where cell type proportion approximates 50%, and the isthmus, where secretory cells are in majority (**Figure 11**). All secretory cells demonstrated FGL2 immunopositivity, resulting in more abundant FGL2 staining from the fimbrial to the isthmal end of the oviduct, a gradient driven by cell type abundance. Cellular localization was, again, perinuclear/cytoplasmic. Although the secretion mechanism is unknown, and we could not confirm whether FGL2 is found in the oviductal fluid, its likely presence could contribute to the environment in which important processes, such as fertilization, take place.

3.5.2. *Fgl2* knockout reduces fertilization efficiency in mice

To test the hypothesis that aberrant FGL2 could alter the oviductal environment in a functionally meaningful way, we compared fertilization efficiency in our 3 mouse lines. The contents of oviduct flushes, at the stage where 2-cell

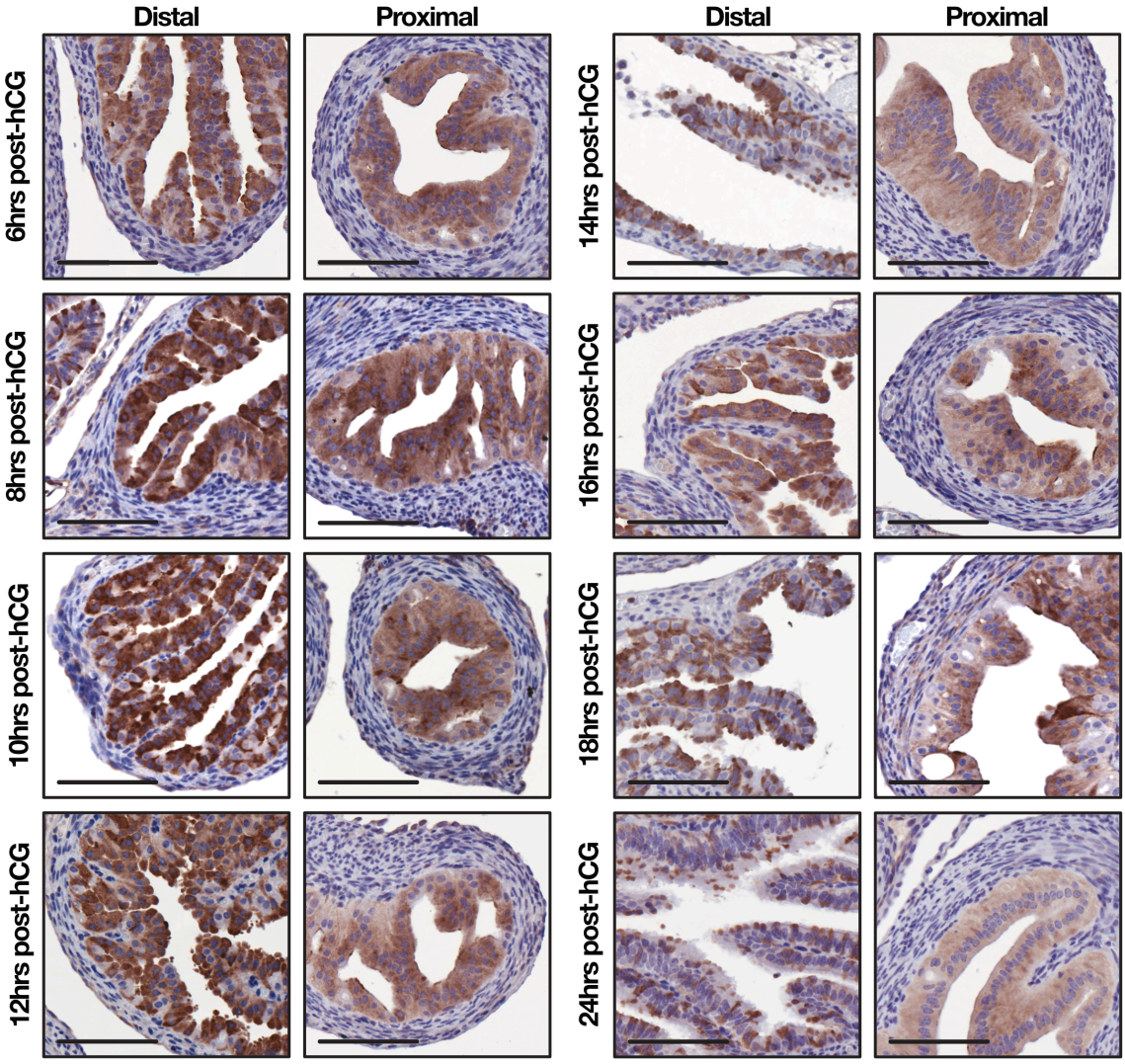

Figure 11: Oviductal cell type specificity of FGL2 expression and temporal dynamics through induced ovulation. Immunohistochemistry staining of distal (ampulla region) and proximal (isthmus region) oviduct from gonadotropin-stimulated animals at various timepoints after hCG injection (rabbit anti-mouse FGL2, LSBio). FGL2 expression is prominent in secretory cells of the oviductal epithelium. Expression peaks in intensity 8-12hrs after hCG injection. Representative pictures of tissues from 3 animals/timepoint. Scale bars = 100μm.

embryos should be found in the reproductive tract of mated females, were collected. We counted the number of morphologically normal 2-cell embryos, as well as unfertilized oocytes (whole or fragmented), and calculated the fraction of structures that were embryos. This fraction was lower in *Fgl2*$^{ko/ko}$ females (0.62), than in *Fgl2*$^{wt/wt}$ (0.75) and *Fgl2*$^{ko/tg}$ (0.73) females, a difference that was statistically significant (p = 0.0303, *Fgl2*$^{wt/wt}$-*Fgl2*$^{ko/ko}$; p = 0.3569 *Fgl2*$^{wt/wt}$-*Fgl2*$^{ko/tg}$; p = 0.0437, *Fgl2*$^{ko/ko}$-*Fgl2*$^{ko/tg}$) (**Figure 12A-B**). This suggests that in *Fgl2*$^{ko/ko}$ mice, fewer embryos make it to the implantation stage.

3.6. Aberrant FGL2 increases suboptimal fetal pregnancy outcomes

3.6.1. Aberrant FGL2 may reduce the number of implantations and term fetuses

To identify other steps of the reproductive process possibly defective in *Fgl2*$^{ko/ko}$ and *Fgl2*$^{ko/tg}$ mice, we next considered the impact of FGL2 expression on post-implantation reproductive parameters. At e5.5, a timepoint of mouse pregnancy where implantation is complete and macroscopically visible in the dissected uterus, we observed a trend of fewer implantations sites in *Fgl2*$^{ko/ko}$ (~7) and *Fgl2*$^{ko/tg}$ (~6) than in *Fgl2*$^{wt/wt}$ (~10) mice, although pairwise comparisons between genotypes did not reach statistical significance (p = 0.0875, *Fgl2*$^{wt/wt}$-*Fgl2*$^{ko/ko}$; p = 0.0587, *Fgl2*$^{wt/wt}$-*Fgl2*$^{ko/tg}$; p = 0.2450, *Fgl2*$^{ko/ko}$-*Fgl2*$^{ko/tg}$) (**Figure 13A**). We then compared near-term pregnancy outcomes, by taking samples at e18.5. We observed fewer fetuses in *Fgl2*$^{ko/ko}$ (~5) and *Fgl2*$^{ko/tg}$ (~6) than in *Fgl2*$^{wt/wt}$ (~9) mice (p = 0.0146, *Fgl2*$^{wt/wt}$-*Fgl2*$^{ko/ko}$; p = 0.0606, *Fgl2*$^{wt/wt}$ - *Fgl2*$^{ko/tg}$; p

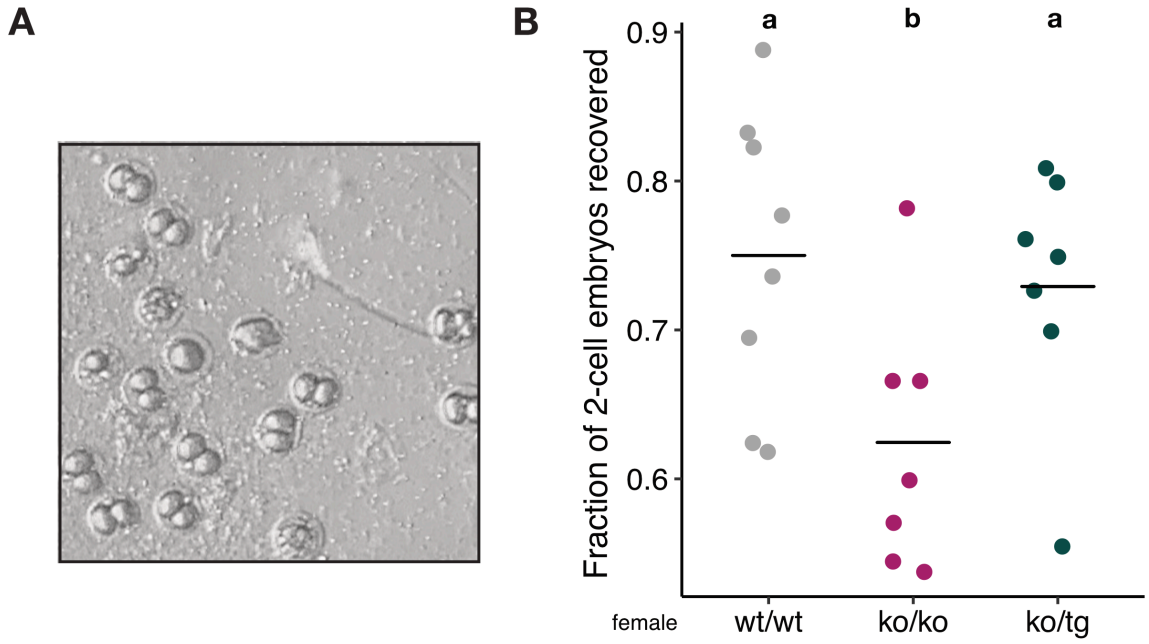

Figure 12: *Fgl2* knockout reduces fertilization efficiency in mice. A) Representative image of the contents of an oviduct flush. **B)** Comparison of the fraction of 2-cell embryos recovered in the oviducts of $Fgl2^{wt/wt}$, $Fgl2^{ko/ko}$, and $Fgl2^{ko/tg}$ mice. Different letters indicate statistical difference between groups, Kruskal-Wallis rank sum test with Dunn's test for multiple comparisons (p=0.0303, $Fgl2^{wt/wt}$-$Fgl2^{ko/ko}$; p=0.3569, $Fgl2^{wt/wt}$-$Fgl2^{ko/tg}$; p=0.0437, $Fgl2^{ko/ko}$-$Fgl2^{ko/tg}$).

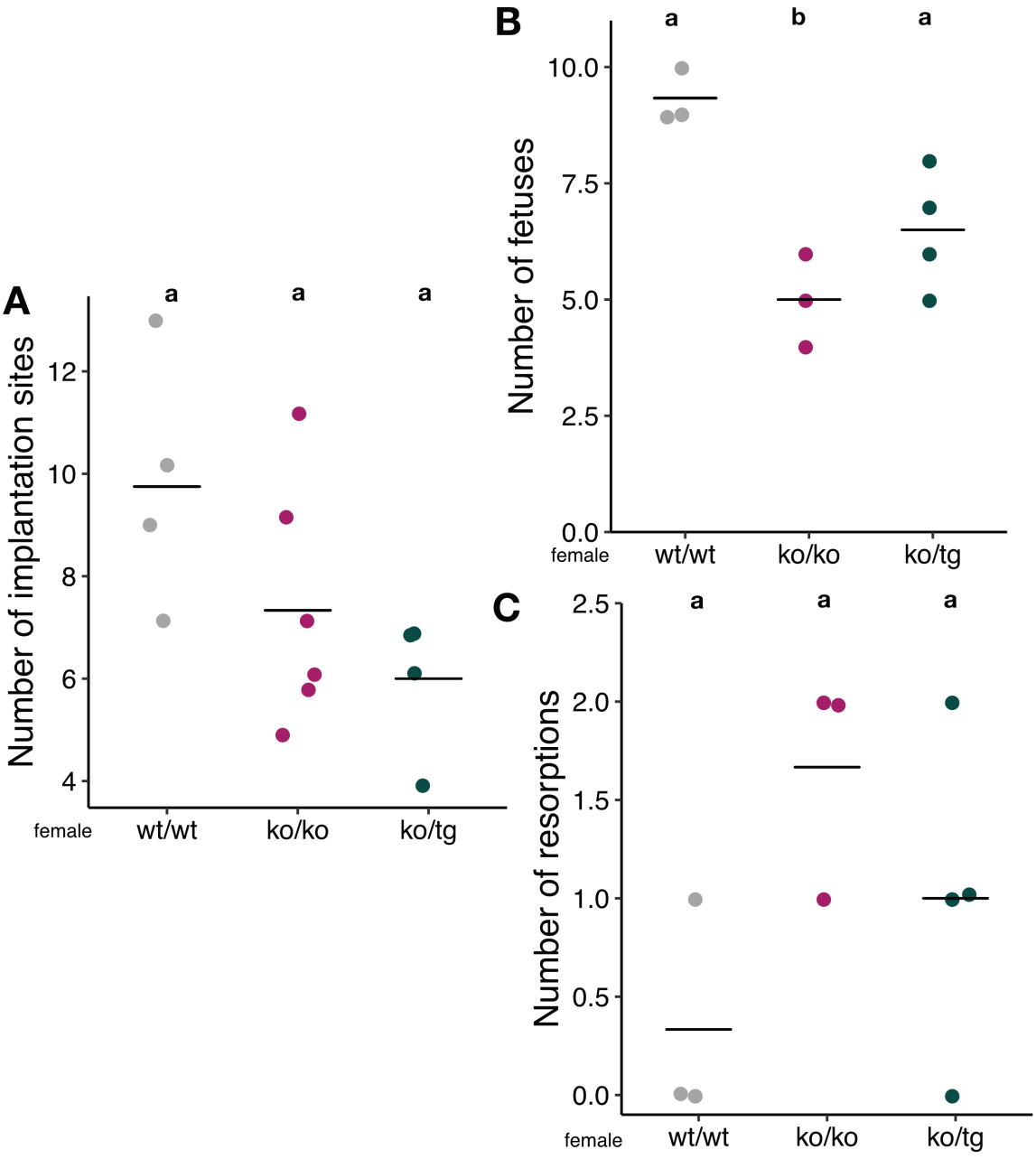

Figure 13: Aberrant FGL2 expression may lead to fewer implantations (e5.5) and term fetuses (e18.5). A) Comparison of the number of implantations (e5.5) in *Fgl2*$^{wt/wt}$, *Fgl2*$^{ko/ko}$ and *Fgl2*$^{ko/tg}$ mice (p = 0.0875, *Fgl2*$^{wt/wt}$ - *Fgl2*$^{ko/ko}$, p = 0.0587, *Fgl2*$^{wt/wt}$ - *Fgl2*$^{ko/tg}$; p = 0.2450, *Fgl2*$^{ko/ko}$ - *Fgl2*$^{ko/tg}$). **B)** Comparison of the number of fetuses in the uterus (e18.5) in *Fgl2*$^{wt/wt}$, *Fgl2*$^{ko/ko}$ and *Fgl2*$^{ko/tg}$ mice (p = 0.0146, *Fgl2*$^{wt/wt}$ - *Fgl2*$^{ko/ko}$, p = 0.0606, *Fgl2*$^{wt/wt}$ - *Fgl2*$^{ko/tg}$; p = 0.1543, *Fgl2*$^{ko/ko}$ - *Fgl2*$^{ko/tg}$). **C)** Comparison of the number of resorptions in the uterus (e18.5) in *Fgl2*$^{wt/wt}$, *Fgl2*$^{ko/ko}$ and *Fgl2*$^{ko/tg}$ mice (p = 0.0683, *Fgl2*$^{wt/wt}$ - *Fgl2*$^{ko/ko}$; p = 0.2138, *Fgl2*$^{wt/wt}$ - *Fgl2*$^{ko/tg}$; p = 0.1425, *Fgl2*$^{ko/ko}$ - *Fgl2*$^{ko/tg}$). For all plots, different letters indicate statistical difference between groups, Kruskal-Wallis rank sum test with Dunn's test for multiple comparisons.

= 0.1543, *Fgl2*$^{ko/ko}$ - *Fgl2*$^{ko/tg}$) (**Figure 13B**). Finally, we observed that the number of resorptions visible in the uterus at e18.5 was slightly, albeit not significantly, increased in *Fgl2*$^{ko/ko}$ (~2) only, compared to *Fgl2*$^{wt/wt}$ (~0) and *Fgl2*$^{ko/tg}$ (~1) mice (p = 0.0683, *Fgl2*$^{wt/wt}$-*Fgl2*$^{ko/ko}$; p = 0.2138, *Fgl2*$^{wt/wt}$-*Fgl2*$^{ko/tg}$; p = 0.1425, *Fgl2*$^{ko/ko}$ - *Fgl2*$^{ko/tg}$) (**Figure 13C**). While not all parameters showed a significant difference between genotypes, these trends combine to point to a hypothesis for the cause of the subfertility of *Fgl2*$^{ko/ko}$ mice. In these mice, the difference in the number of fetuses in the uterus at e5.5 (~7) and e18.5 (~5) can be accounted for by the number of resorptions observed (~2), as is the case for *Fgl2*$^{wt/wt}$ mice. Additionally, the decrease, in *Fgl2*$^{ko/ko}$, in e5.5 implantations and in live pups per litter is similar (~-3), which suggests that embryo loss occurs in the pre-implantation period. Our numbers suggest that the same hypothesis could apply to *Fgl2*$^{ko/tg}$ mice, which would similarly account for the reduction in live pups per litter.

3.6.2 Aberrant FGL2 causes suboptimal fetal parameters

As the subfertility of *Fgl2*$^{ko/ko}$ and *Fgl2*$^{ko/tg}$ leads them to have fewer pups overall, we next sought to evaluate if their term pups were phenotypically comparable to *Fgl2*$^{wt/wt}$ pups. At e18.5, we noticed that *Fgl2*$^{ko/tg}$ fetuses seemed abnormally small, leading us to record fetal and placental weight, as well as fetal length. Several factors (i.e., litter size) are known to affect fetal size in mice, independently of any gene of interest. As such, we used linear regression to statistically compare fetal length and weight in our three mouse lines. We first evaluated the impact of genotype on fetal crown-rump length, and our best

regression model (R^2 = 0.9842, overall p = 8.52E-3) included fetal weight as an independent term, and an interaction term between fetal length and the number of fetuses in the litter. Compared to *Fgl2*$^{wt/wt}$, *Fgl2*$^{ko/ko}$ fetuses tend to be longer when the length variable is considered independently (p = 0.0824), but that effect shrinks when the model corrects for litter size (p = 0.1196). *Fgl2*$^{ko/tg}$ fetuses, on the other hand, are significantly shorter even after correcting for litter size (p = 0.0380) (**Figure 14A**). Independently, litter size has a significant effect on fetal length (p = 0.0461), statistically confirming the common observation that larger litters produce smaller pups. Unsurprisingly, we observed a similar trend with fetal weight, with a similarly constructed regression model (R^2 = 0.8760, p = 0.0591). Fetal weight tends to be different between *Fgl2*$^{wt/wt}$ and *Fgl2*$^{ko/ko}$, when that variable is considered independently (p = 0.0831), but not when corrected for litter size (p = 0.1453). The lower weight of *Fgl2*$^{ko/tg}$ fetuses, compared to *Fgl2*$^{wt/wt}$, retains significance after correction (p = 0.0372) (**Figure 14B**). Litter size, as an independent variable, is close to significance (p = 0.0679). Measured placental weights were highly variable, and our best regression model (R^2 = 0.7225, p = 0.4477), included fetal weight (independently) and litter size (interacting with genotype). No other variable had a significant effect on placental weight, including *Fgl2*$^{ko/ko}$ (p = 0.2200) and *Fgl2*$^{ko/tg}$ (p = 0.2780) genotypes (**Figure 14C**). We then calculated fetal/placental weight ratios, as a crude measure of placental efficiency, for pregnancies of all three genotypes. While the ratios also present with appreciable variability, the average ratio for *Fgl2*$^{ko/tg}$ pregnancies (5.93) is lower, denoting a less efficient placenta, than

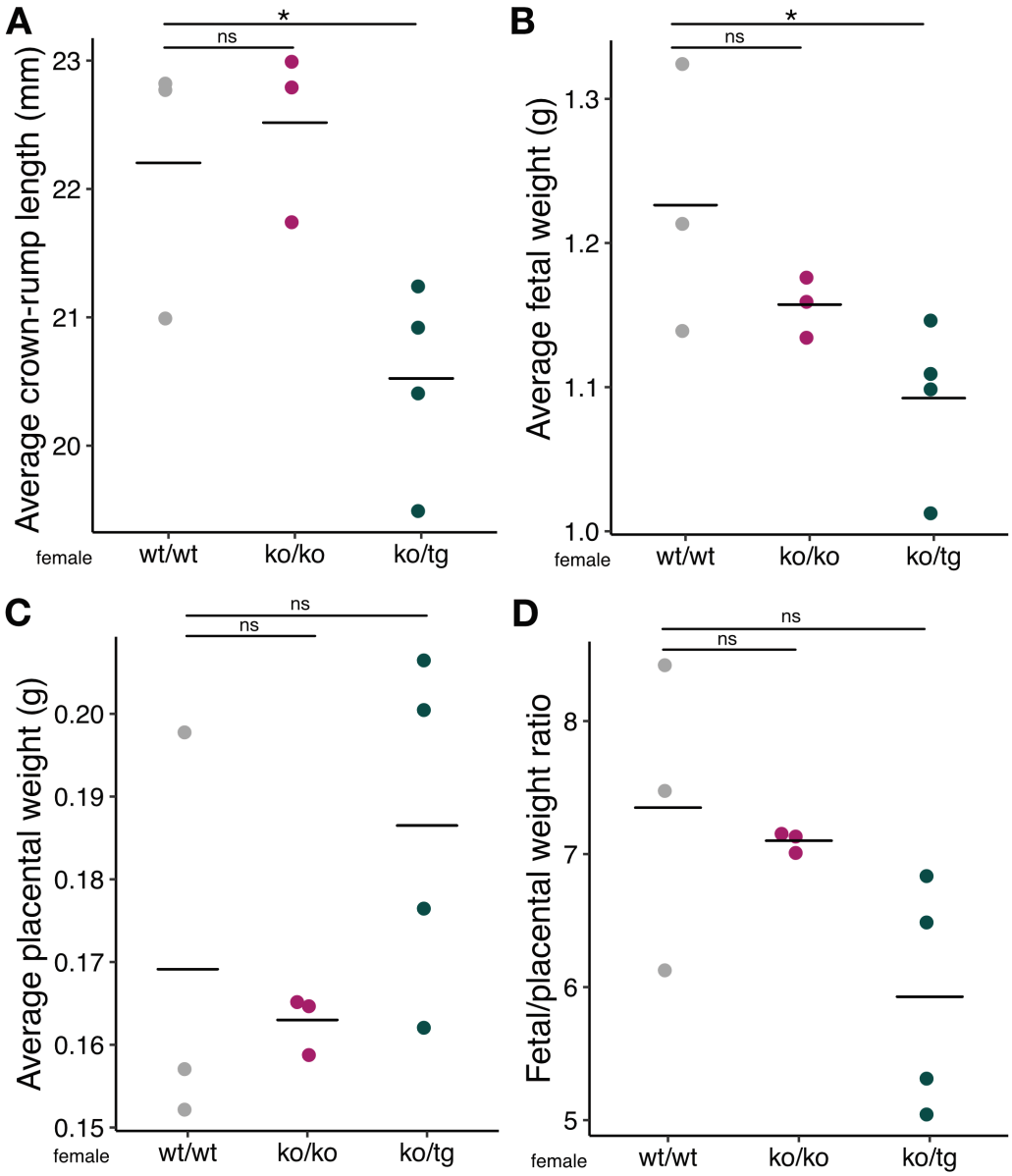

Figure 14: *Fgl2* overexpression may result in smaller pups and lower fetal to placental weight ratios in mice. A) Effect of *Fgl2* genotype on fetal crown-rump length. At e18.5, crown-rump length is reduced in $Fgl2^{ko/tg}$ mice (p=0.0380) but unchanged in $Fgl2^{ko/ko}$ mice (p=0.1196). Best regression model (R^2=0.9842, p=8.52E-3) corrects for litter size and fetal weight. **B)** Effect of *Fgl2* genotype on fetal weight. At e18.5, fetal weight is reduced in $Fgl2^{ko/tg}$ mice (p=0.0372) but unchanged in $Fgl2^{ko/ko}$ mice (p=0.1453). Best regression model (R^2=0.8760, p=0.0591) corrects for litter size. **C)** Effect of *Fgl2* genotype on placental weight. At e18.5, placental weight is unchanged in $Fgl2^{ko/ko}$ (p=0.2200) and $Fgl2^{ko/tg}$ mice (p=0.2780). Best regression model (R^2=0.7225, p=0.4477) corrects for litter size and fetal weight. **D)** Effect of *Fgl2* genotype on fetal/placental weight ratio. At e18.5, ratio tends to be reduced in $Fgl2^{ko/tg}$ (p=0.0628) but is unchanged in $Fgl2^{ko/ko}$ mice (p=0.7284). Best regression model (R^2=0.4542, p=0.1201). For all parameters, each data point is the average of all fetuses or placentas of one pregnancy (n=3-4 pregnancies per genotype). Horizontal bars represent group mean.

for *Fgl2*$^{wt/wt}$ (7.10) and *Fgl2*$^{ko/ko}$ (7.35) pregnancies, suggesting reduced efficiency of the placenta. The best fitting regression model (R^2 = 0.4542, p = 0.1201) includes only the genotype, an indication that some unmeasured factors affect these ratios. *Fgl2*$^{ko/ko}$ ratios were similar to *Fgl2*$^{wt/wt}$ (p = 0.7284), but *Fgl2*$^{ko/tg}$ ratios were lower than *Fgl2*$^{wt/wt}$, a difference that approached significance (p = 0.0628) (**Figure 14D**). While not a perfect indicator (see Discussion), the fetal to placental weight ratio is used for both murine and human pregnancies and has clinical relevance – providing a measurement of how efficient the placenta is at delivering required oxygen and nutrients to the developing fetus. The observation of reduced placental efficiency, therefore, may explain the smaller pup size in this mouse line.

3.7. Fgl2 overexpression reduces placental efficiency

3.7.1. Aberrant *Fgl2* expression does not affect placental compartment volume and volume ratio

Stereology is a standardized method for quantifying potential differences in mouse placental morphology, useful for identification of placental dysfunction[111,116]. With the goal of identifying placental features that could explain the lower fetal weight (and the trend towards lower fetal/placental weight ratios) seen in *Fgl2*$^{ko/tg}$ near-term pregnancies, we applied stereology to e18.5 placentas of all three genotypes. Using the point-counting method, we first determined the area ratio occupied by the labyrinth and the junctional zone, the two major fetal compartments of the mouse placenta (**Figure 15A-B**). Using the placental weights previously

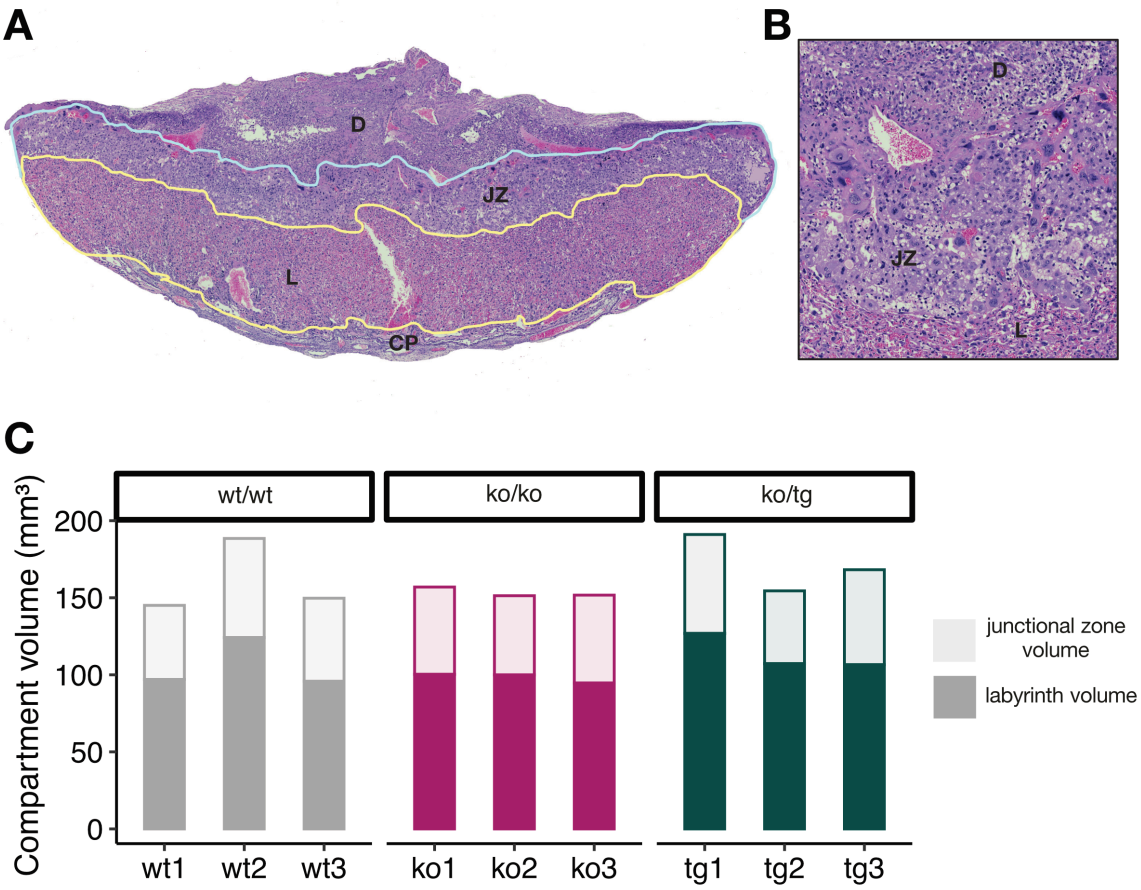

Figure 15: *Fgl2* knockout and overexpression do not alter major placental compartment volumes in mice. A) Representation (H&E stain) of major placental compartments within the mouse placenta. Labyrinth (L, yellow outline) and junctional zone (JZ, blue outline) volumes were measured. **B)** Representative image (H&E stain) of interface between labyrinth, junctional zone and decidua basalis. **C)** Absolute volume (mm^3) occupied by each compartment, in $Fgl2^{wt/wt}$, $Fgl2^{ko/ko}$ and $Fgl2^{ko/tg}$ mice. Each bar represents a different pregnancy and is the average compartment volume of 3 separate placentas from that pregnancy. For each placenta, area ratios were obtained by point counting using a grid overlaying a stained midline placenta section, and absolute values were calculated by multiplying the ratio by the total placental volume.

measured, and a standard value for mouse placental tissue density (1.05g/cm^3), we calculated the absolute volume of each compartment, for each placenta (**Figure 15C**)[111]. Each layer (compartment) is composed of specific trophoblast populations, and over- or under-representation of either would point to lineage-specific trophoblast differentiation defects. Therefore, we calculated and compared between genotypes the ratio of total placental volume occupied by each layer. We found no difference in this ratio in either *Fgl2*$^{ko/ko}$ or *Fgl2*$^{ko/tg}$ mice, compared to *Fgl2*$^{wt/wt}$ (p = 0.4144, *Fgl2*$^{wt/wt}$-*Fgl2*$^{ko/ko}$; p = 0.4415, *Fgl2*$^{wt/wt}$- *Fgl2*$^{ko/tg}$; p = 0.6735, *Fgl2*$^{ko/ko}$-*Fgl2*$^{ko/tg}$) (**Figure 16A**).

3.7.2. Fgl2 overexpression causes a reduction in glycogen cell volume ratio

The subcompartments of the junctional zone, glycogen (trophoblast) cells and the spongiotrophoblast, can be distinguished using simple H&E staining, and were therefore measured using the point counting method (**Figure 17A**). Subcompartment absolute volume was calculated using total junctional zone volume and results of point counting (**Figure 17B**). These subcompartments represent terminally differentiated trophoblast populations, and alteration of their volume ratio could point to the signaling mechanisms affected by the lack or excess of FGL2. Independent quantification of placentas from the same pregnancy yielded similar subcompartment volume ratios, conferring validity to our method. Interestingly, in *Fgl2*$^{ko/tg}$ placentas, the total volume proportion

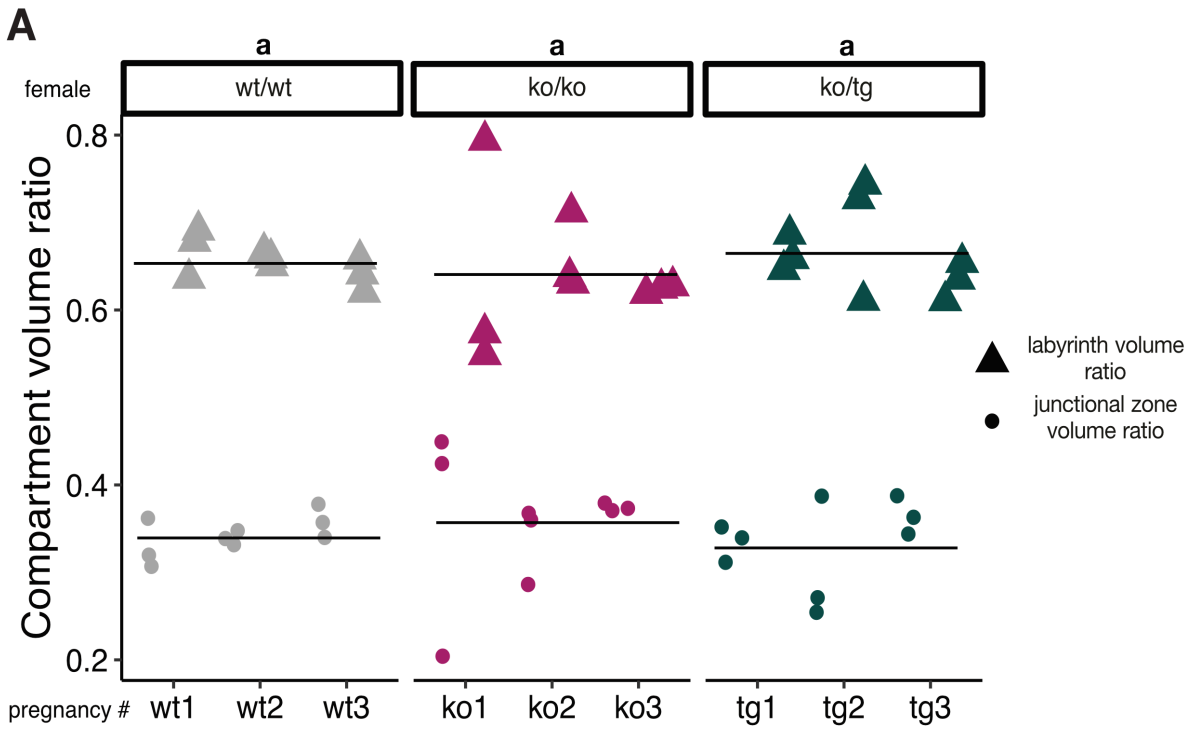

Figure 16: *Fgl2* knockout and overexpression do not alter the volume ratios of major placental compartments in mice. A) Volume ratios of compartments. Junctional zone (and labyrinth) volume ratio is equal in *Fgl2*$^{wt/wt}$, *Fgl2*$^{ko/ko}$, and *Fgl2*$^{ko/tg}$ placentas. Each data point is a separate placenta, and columns (tick marks) group placentas from the same pregnancy, horizontal bars represent average value for a genotype. For each placenta, area ratios were obtained by point counting using a grid overlaying a stained midline placenta section, and absolute values were calculated by multiplying the ratio by the total placental volume. Different letters indicate statistical difference between groups, Kruskal-Wallis rank sum test with Dunn's test for multiple comparisons (p=0.4144, *Fgl2*$^{wt/wt}$-*Fgl2*$^{ko/ko}$; p=0.4415, *Fgl2*$^{wt/wt}$-*Fgl2*$^{ko/tg}$; p=0.6735, *Fgl2*$^{ko/ko}$-*Fgl2*$^{ko/tg}$).

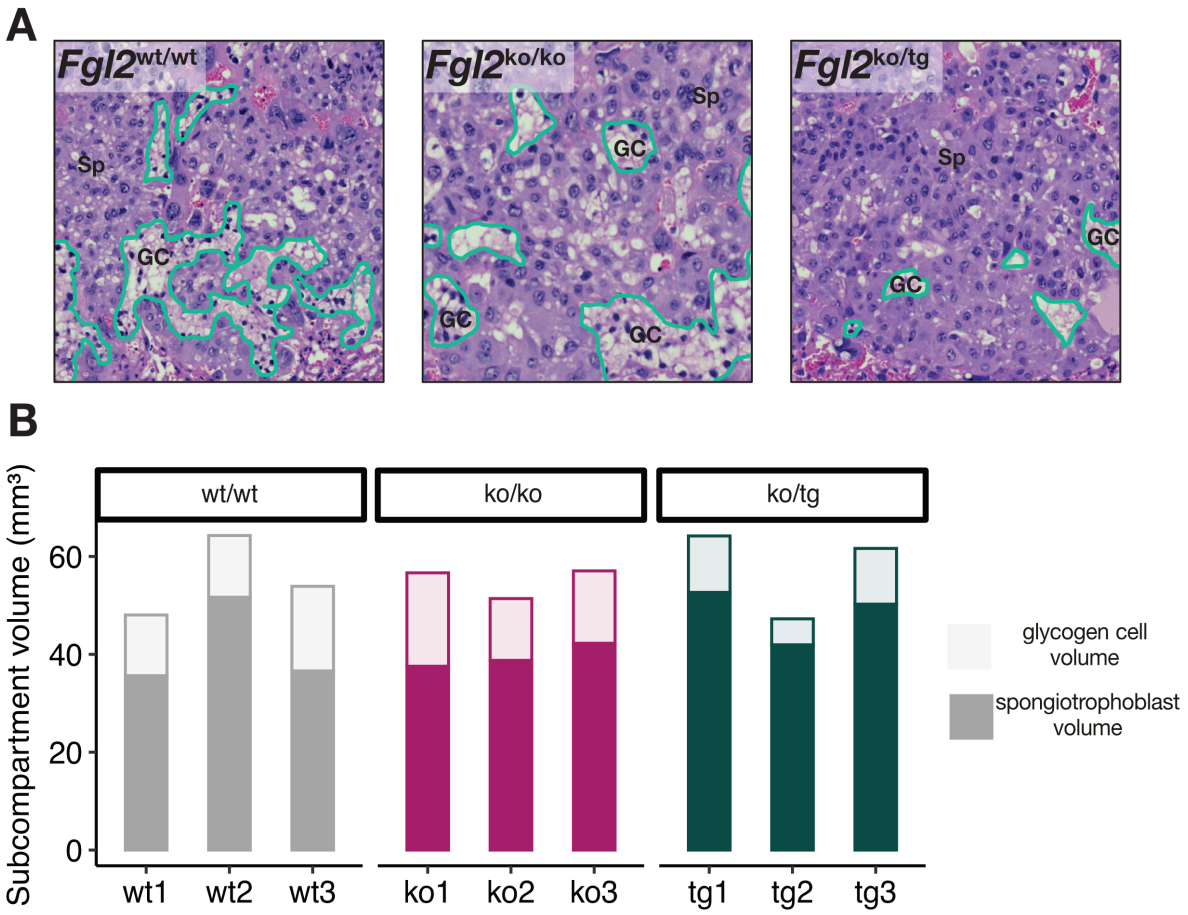

Figure 17: *Fgl2* overexpression causes a reduction of junctional zone glycogen cell abundance in mice. A) Representative pictures (H&E stain) of relative volumes occupied by glycogen cell (GC, outlined in turquoise) and spongiotrophoblast (Sp) within the junctional zone of placentas from each genotype. **B)** Absolute volume (mm^3) occupied by each subcompartment within the junctional zone. Each bar represents a different pregnancy and is the average subcompartment volume of 3 separate placentas from that pregnancy. For each placenta, area ratios were obtained by point counting using a grid overlaying a stained midline placenta section, and absolute values were calculated by multiplying the ratio by the total junctional zone volume.

occupied by glycogen cells is lower than in *Fgl2*$^{wt/wt}$ and *Fgl2*$^{ko/ko}$mice (p = 0.4407, *Fgl2*$^{wt/wt}$*Fgl2*$^{ko/ko}$; p = 0.0553, *Fgl2*$^{wt/wt}$ - *Fgl2*$^{ko/tg}$; p = 0.0385 *Fgl2*$^{ko/ko}$*Fgl2*$^{ko/tg}$) (**Figure 18A**). While syncytiotrophoblast layers of the mouse placenta are more commonly associated with a placental insufficiency phenotype, glycogen cells also play a role as conceptus energy stores, and low counts are often associated with reduced fetal weight[116,117]. As such, this lower proportion of glycogen cells in *Fgl2*$^{ko/tg}$ placentas may explain, in part, the reduced fetal weights and fetal to placental weight ratios that we observe in this mouse line.

3.8. Summary

Fgl2 knockout in mice causes subfertility (small, infrequent litters), while *Fgl2* overexpression causes slight subfertility (small litters) and small pups. To determine the cause of these phenotypes, we mapped FGL2 protein expression in female reproductive tissues, and assessed various parameters of reproductive function in knockout and overexpressing animals. FGL2 is expressed in the ovarian stroma and theca cells throughout the estrous cycle, peaking shortly before ovulation. Ovarian morphology and ovulation output are unaffected by both knockout and overexpression. Luteal angiogenesis, likely through M2 macrophages, is not decreased in the absence of *Fgl2*, but is significantly enhanced when *Fgl2* is in excess. FGL2 is strongly expressed by secretory cells of the oviductal epithelium. Fertilization efficiency is slightly reduced, although not significantly, in *Fgl2*$^{ko/ko}$ mice, which could explain their subfertility. The number of

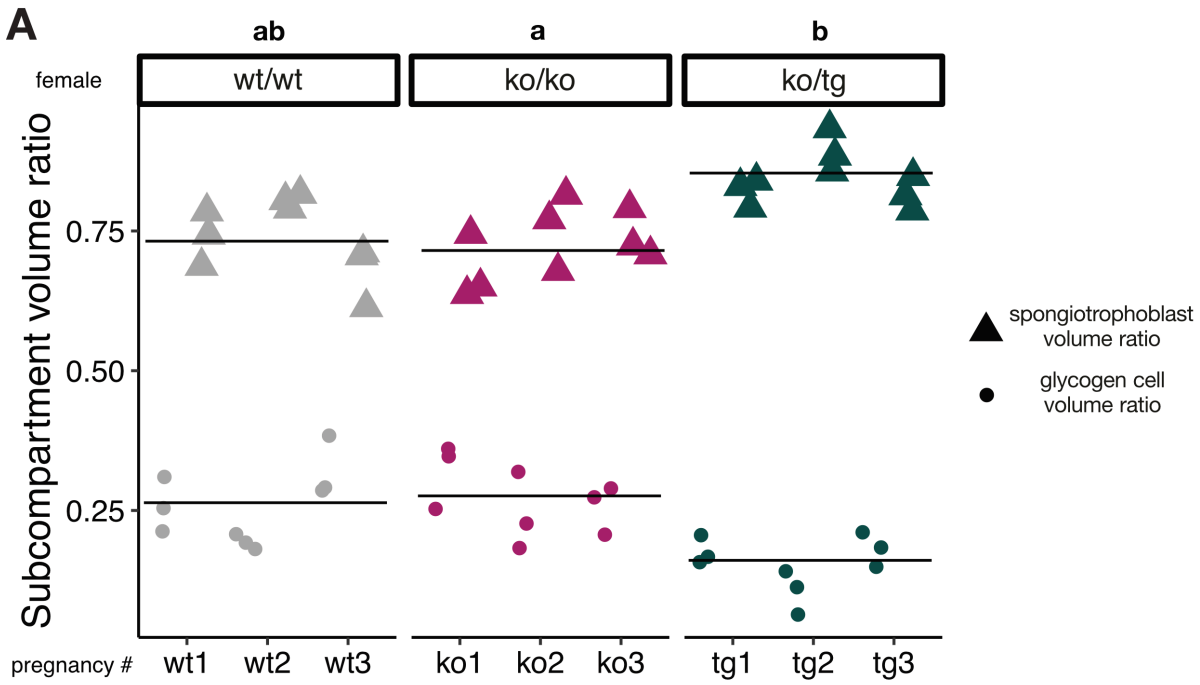

Figure 18: *Fgl2* overexpression causes a reduction of junctional zone glycogen cell abundance in mice. A) Volume ratios of junctional zone subcompartments. Glycogen cell volume ratio is decreased (and spongiotrophoblast volume ratio increased) in $Fgl2^{ko/tg}$ placentas. For each placenta, area ratios were obtained by point counting using a grid overlaying a stained midline placenta section, and absolute values were calculated by multiplying the ratio by the total junctional zone volume. Different letters indicate statistical difference between groups, Kruskal-Wallis rank sum test with Dunn's test for multiple comparisons (p=0.4407, $Fgl2^{wt/wt}$-$Fgl2^{ko/ko}$; p=0.0553, $Fgl2^{wt/wt}$-$Fgl2^{ko/tg}$; p=0.0385 $Fgl2^{ko/ko}$-$Fgl2^{ko/tg}$).

implantations and of term fetuses, in these mice, is lower than the number of oocytes naturally ovulated, and this reduction cannot be attributed to visible resorptions. Overall, this supports the hypothesis of a defect in the pre-implantation period, although this is a preliminary conclusion. *Fgl2*$^{ko/tg}$ fetuses are smaller, near term, than *Fgl2*$^{wt/wt}$ and *Fgl2*$^{ko/ko}$ fetuses. Their placentas do not show an alteration of compartment volume or volume ratio, but the junctional zones present a lower volume ratio of glycogen cells, potentially decreasing placental efficiency and slowing fetal growth.

CHAPTER 4 (RESULTS): MECHANISMS OF FGL2-MEDIATED TROPHOBLAST FUNCTION AND RESPONSE TO INFLAMMATION

4.1. Initial characterization of HTR-8/SVneo and BeWo *Fgl2* expression and secretion

Considering the placental abnormalities caused by *Fgl2* overexpression in the mouse, as well as the expression of FGL2, at various levels, by select trophoblast populations within the mouse placenta, we next sought to translate our findings to the human placenta. We aimed to delineate a biological role for FGL2 in human trophoblast function in the villous and extravillous compartments, under basal conditions and when its levels are modulated by other factors. Two commonly used human trophoblast cell lines were utilized to accomplish this: the HTR-8/SVneo – an SV40-transformed invasive trophoblast line representative of the extravillous cytotrophoblast lineage, and the BeWo cell line, generated from a choriocarcinoma and representative of the syncytiotrophoblast, when induced to fuse under certain conditions[118,119]. We first characterized, at the RNA and at the protein levels, basal levels of FGL2 in these cell lines. Curiously, we note an important discrepancy. By qPCR, BeWo express 6-fold more *FGL2* than HTR-8 (Student's t test, $p = 0.0281$) (**Figure 19A**). By western blot, however expression is much higher in HTR-8 than in BeWo (**Figure 19B**). As FGL2 is known to be secreted, albeit by an unknown mechanism, we quantified by ELISA the concentration of FGL2 in the cell culture media of both cell lines. In our hands, secreted FGL2 levels concur with our qPCR results, in that BeWo expresses higher levels than HTR-8 (Student's t test, $p = 0.0262$) (**Figure 19C**). Taken together, these results

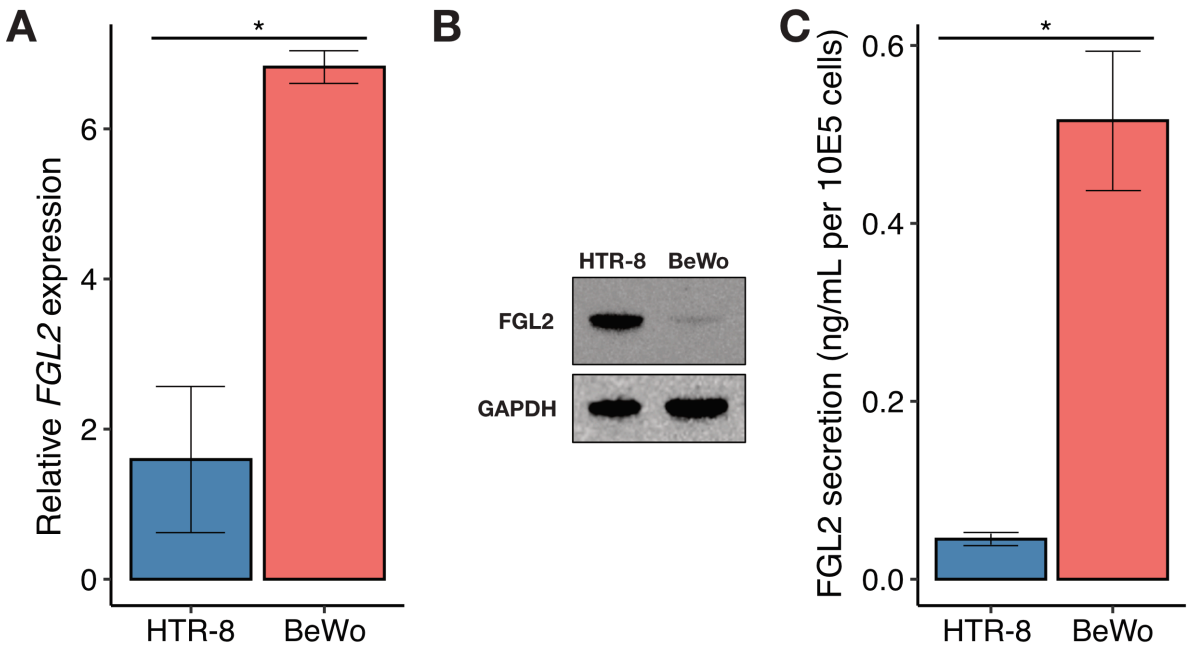

Figure 19: FGL2 is more highly expressed and secreted in BeWo than in HTR-8/SVneo. A) Relative *FGL2* expression after 72hrs culture (N=3). Expression is higher in BeWo than in HTR-8/Svneo (Student's t test, p=0.0281). **B)** FGL2 protein expression assessed by western blot, expression appears higher in HTR-8/Svneo than in BeWo. **C)** Absolute levels of secreted FGL2, assessed by ELISA (72hrs culture, N=3), per 10E5 cells (Student's t test, p=0.0262). Error bars represent SEM.

suggest that in BeWo, the abundant *FGL2* mRNA is translated and efficiently secreted, leading to low protein levels in cell lysates. In HTR-8, while a lower level of *FGL2* mRNA is generated, low levels of secretion lead to intracellular accumulation of the FGL2 protein.

4.2. Generation of Fgl2-overexpressing HTR-8/SVneo and BeWo cell lines

As a tool to decipher the effect of *FGL2* overexpression on trophoblast function, we overexpressed it using the pWPI vector and a human *FGL2* clone, packaging the resulting plasmid into a lentivirus. Puromycin selection and GFP expression confirmed success of the cell infection, and we validated overexpression using both western blot and ELISA. By western blot, the increase in FGL2 protein levels is evident much higher levels of FGL2 are detected in the hFGL2 (overexpressing) cell lines than in the pWPI (vector control) and the parental lines, for both HTR-8/SVneo and BeWo (**Figure 20A**). A striking increase in the amount of secreted FGL2 is also detected in these lines, by ELISA (**Figure 20B**).

4.2.1. *FGL2* overexpression decreases migration in HTR-8/SVneo, but does not affect proliferation or invasion

We evaluated the effect of *FGL2* overexpression in HTR-8-SVneo on three parameters of trophoblast function: proliferation, migration and invasion. Live

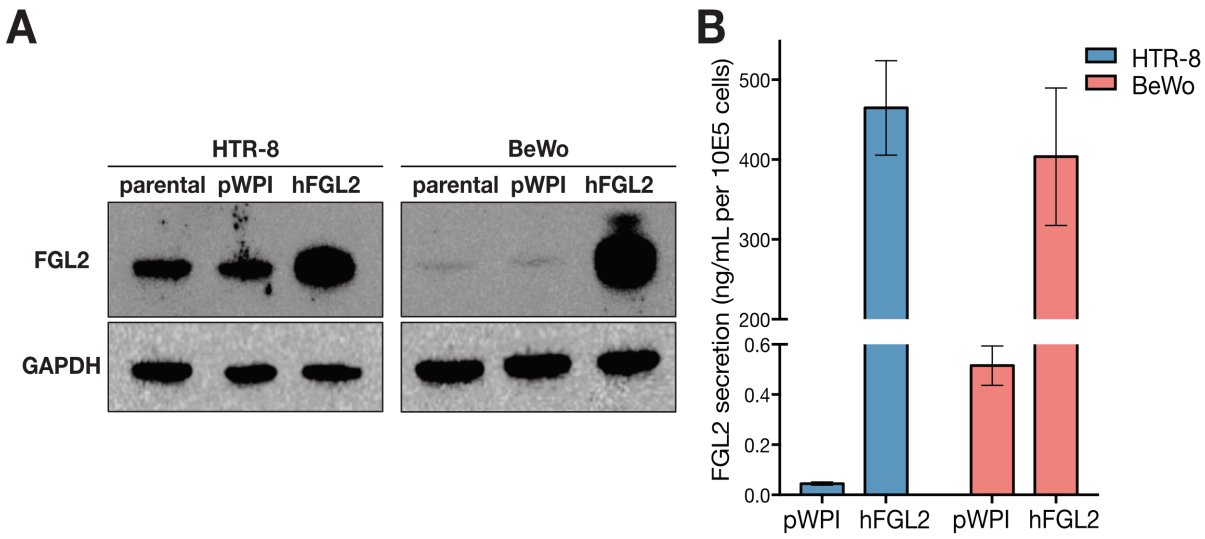

Figure 20: Successful FGL2 overexpression in BeWo and HTR-8/SVneo. A) FGL2 protein expression assessed by western blot after 72hrs in culture. Higher expression is evident in hFGL2 (overexpressing) than in pWPI (vector control) and in parental lines, for both HTR-8 and BeWo. **B)** Absolute levels of secreted FGL2, assessed by ELISA, per 10E5 cells after 72hrs in culture. Higher levels of secreted FGL2 are detected in hFGL2 than in pWPI lines, for both HTR-8 and BeWo.

cell imaging of well confluence over time revealed equal proliferation rates in HTR-8-parental, HTR-8-pWPI and HTR-8-hFGL2 (ANOVA comparing linear part of curves, p = 0.3679) (**Figure 21A**). Migration ability was evaluated using live cell imaging of cell confluence over time, following scratch wounding of a confluent monolayer. A slower rate of migration was observed of HTR-8-hFGL2, compared to both HTR-8 parental and HTR-8-pWPI (ANOVA comparing linear part of curves, p = 0.0378) (**Figure 21B**). It is however clear that this difference is not due to slower proliferation, as shown in Figure 21A. Interestingly, these inhibitory effects of excess FGL2 expression on migration were not seen on the invasive capacity of this cell line. Using a Matrigel-coated Boyden chamber serum gradient-mediated invasion assay, a similar number of HTR-8-hFGL2 cells were found to have invaded across the chamber membrane when compared to HTR-8 parental and HTR-8-pWPI cell lines (ANOVA comparing mean of groups, p=0.2198) (**Figure 21C**).

Overall, these results show that *FGL2* overexpression affects HTR-8/SVneo migration, but not proliferation or invasion. *In vivo*, the invasive ability of EVTs involves the degradation of the decidual extracellular matrix (ECM). An *in vitro* assay mimicking this process should therefore be more relevant. However, invasive and migratory capacity are often correlated, which raises the possibility that our assay didn't capture their full function under the current parameters.

Considering this decrease in migration in *FGL2* overexpressing cells, and as both IFNγ and TNFα were previously reported to directly upregulate FGL2 in other systems (see **1.4.3.**), we assessed their effect in HTR-8/SVneo. Following a 24-hour

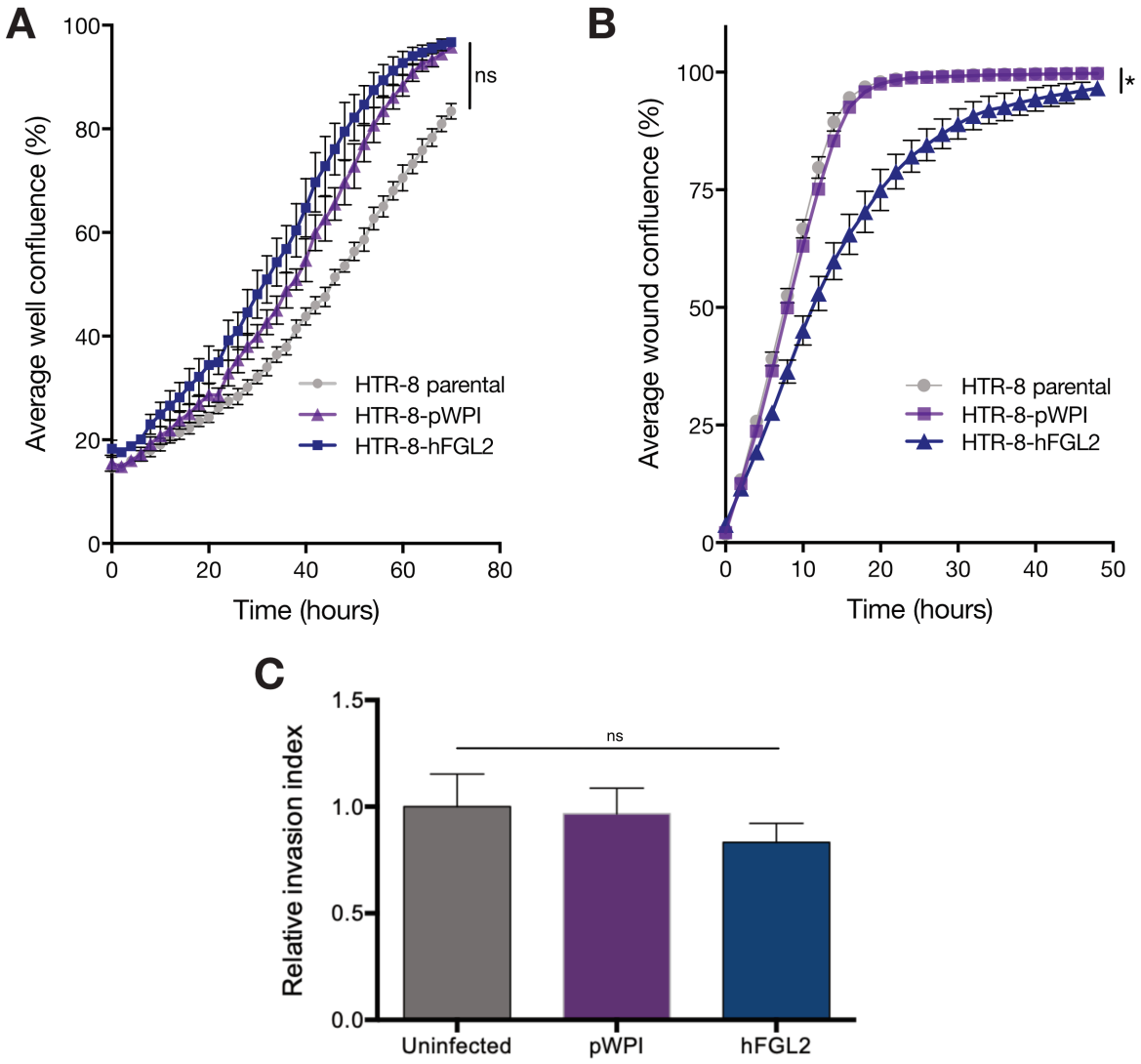

Figure 21: *FGL2* overexpression affects HTR-8/SVneo migration, but not proliferation or invasion. A) Well confluence over time. Proliferation rate is unaffected by *FGL2* overexpression (ANOVA comparing slopes of linear part of curves, p=0.3679). Data points represent average well confluence of 8-12 wells (N=3). **B)** Wound confluence over time after a scratch wound of a confluent monolayer. Migration rate is decreased by *FGL2* overexpression (ANOVA comparing slopes of linear part of curves, p=0.0378). Data points represent average well confluence of 8-12 wells (N=3). **C)** Invasion index relative to HTR-8 parental line. Invasion index is unaffected by *FGL2* overexpression (ANOVA comparing mean of groups, p=0.2198). Invaded cells were counted from entire membranes of three Boyden chamber inserts in each replicate (N=3).

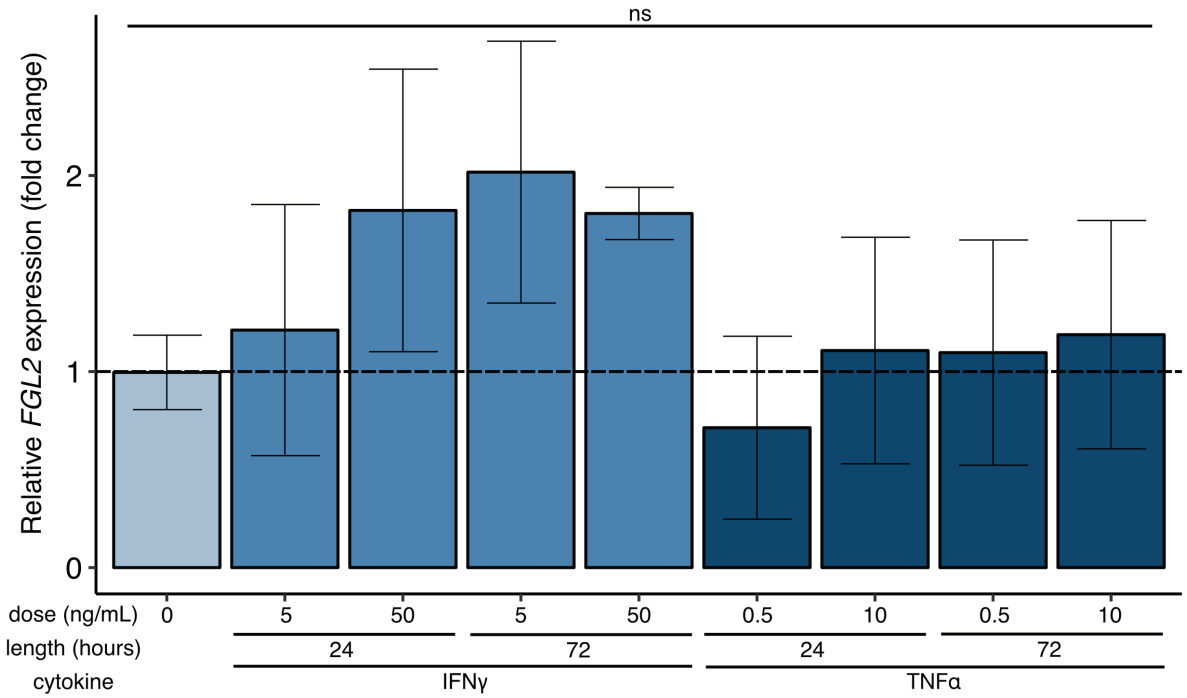

Figure 22: *FGL2* expression is unchanged by inflammatory cytokines in HTR-8/Svneo. Relative *FGL2* expression in HTR-8/SVneo cells in response to IFNγ and TNFα treatments (5 or 50ng/ml IFNγ, 0.5 or 10ng/ml TNFα for 24 or 72hrs, N=3). Expression is not significantly altered by either cytokine (one-way ANOVA, p = 0.7130). Error bars represent SEM.

and a 72-hour treatment with either cytokine, no significant change in *FGL2* expression was observed (one-way ANOVA, p = 0.713) (**Figure 22**).

4.2.2. Inflammatory cytokines may inhibit syncytialization and promote *FGL2* expression in BeWo

We next aimed to evaluate the role of FGL2 in the syncytiotrophoblast layer of chorionic villi, using the BeWo line, in its nascent cytotrophoblast state, or induced to syncytialize by forskolin (FSK) treatment. Both IFNγ and TNFα, two cytokines that are abundant in placental inflammation, were previously shown to inhibit villous cytotrophoblast fusion[120,121]. We verified this in our system, examining expression of *GCM1*, an upstream regulator essential to the syncytialization process, and of *CGB3*, which codes for a subunit of hCG and is only expressed once fusion has occurred[122]. FSK induced a 75-fold increase in *CGB3* expression compared to DMSO treatment (one-way ANOVA with Tukey's post hoc test, p = 0.0038), as expected, and this was non-significantly reduced by the addition of IFNγ (p = 0.0632), and unchanged by the addition of TNFα (p = 0.5461) (**Figure 23A**). The same trend was visible for *GCM1* expression, but no difference between groups reached statistical significance (one-way ANOVA, p = 0.3) (**Figure 23A**). As both IFNγ and TNFα were shown in other systems to upregulate *FGL2* expression, we tested this in BeWo. The addition of TNFα caused a 2-fold, significant increase in *FGL2* expression (one-way ANOVA with Dunnett's post hoc test, p = 0.0342), while the increase caused by IFNγ was not significant (p = 0.0985) (**Figure 23B**).

These data partly support the literature that inflammatory cytokines inhibit syncytialization. That they affect *CGB3* expression more than transcription factor *GCM1*expression, possibly indicates an effect on the pathway downstream of *GCM1*. These same cytokines had a modest effect on *FGL2* expression in both our cell lines. Considering this increase and its known immune regulating function, we chose to investigate the effect of an excess of FGL2 in the syncytiotrophoblast layer of the chorionic villi.

4.2.3. *FGL2* overexpression promotes FSK-mediated syncytialization in BeWo

To achieve this, we examined possible phenotypes in our *FGL2*-overexpressing BeWo line, in its cytotrophoblast state, or induced to syncytialize by FSK treatment. We first examined the effect of *FGL2* overexpression on BeWo proliferation. No effect was noted, as proliferation rates were equal between groups (one-way ANOVA, p=0.8772) (**Figure 24A**).

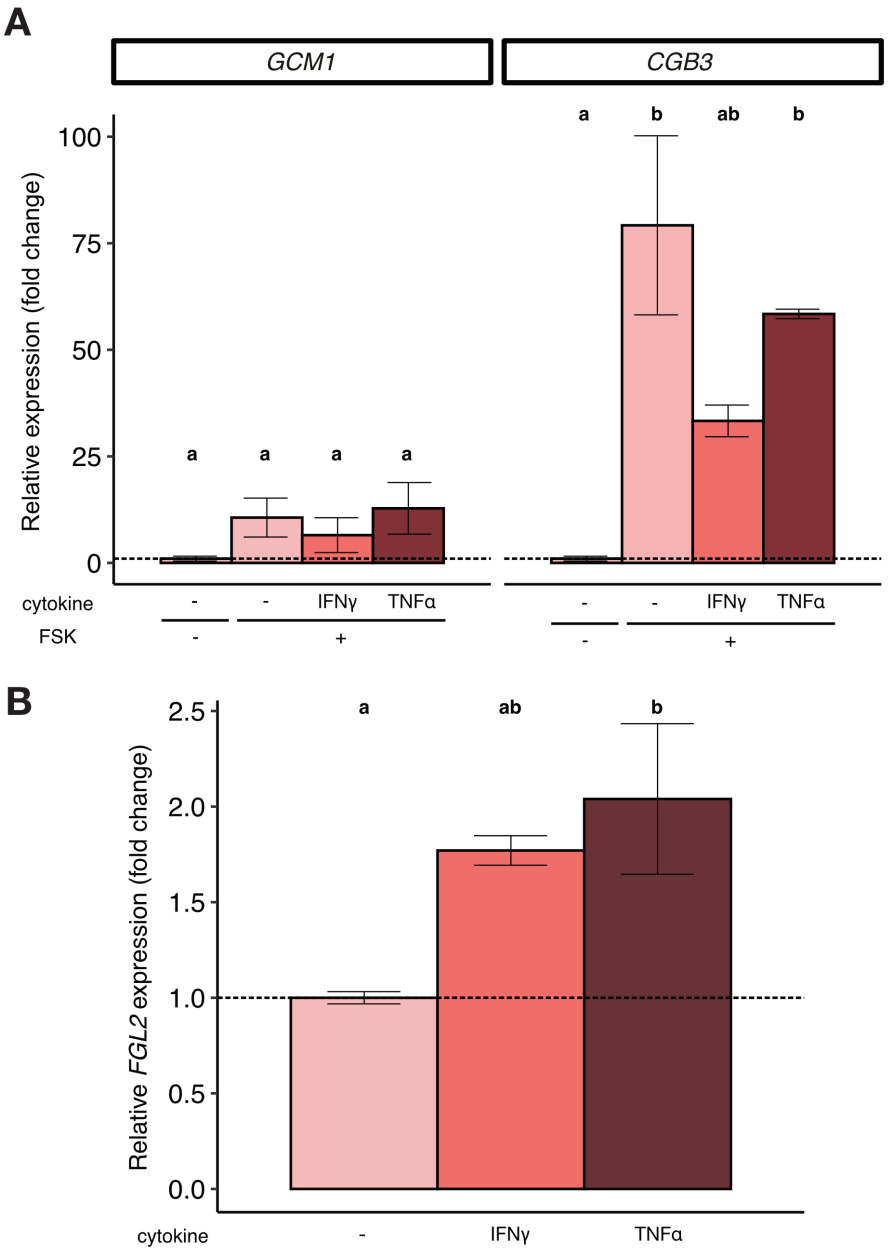

Figure 23: Inflammatory cytokines do not significantly alter syncytialization, but upregulate *FGL2* in BeWo. A) Relative expression of *GCM1* and *CGB3*, in response to IFNγ (50ng/ml) or TNFα (10ng/ml), in FSK-treated BeWo (100μM FSK for 72hrs, N=3). No changes are observed in *GCM1* (one-way ANOVA, p=0.3), and *CGB3* is induced by FSK (one-way ANOVA with Tukey's post hoc test, p=0.0038), and modestly reduced by IFNγ (p=0.0632) but not by TNFα (p=0.5461). **B)** Relative expression of *FGL2* in response to inflammatory cytokines (50ng/ml IFNγ or 10ng/ml TNFα for 72hrs, N=3). TNFα upregulates *FGL2* (one-way ANOVA with Dunnett's post hoc test, p=0.0342) but IFNγ does not (p=0.0985). Different letters indicate statistical difference between groups, error bars represent SEM.

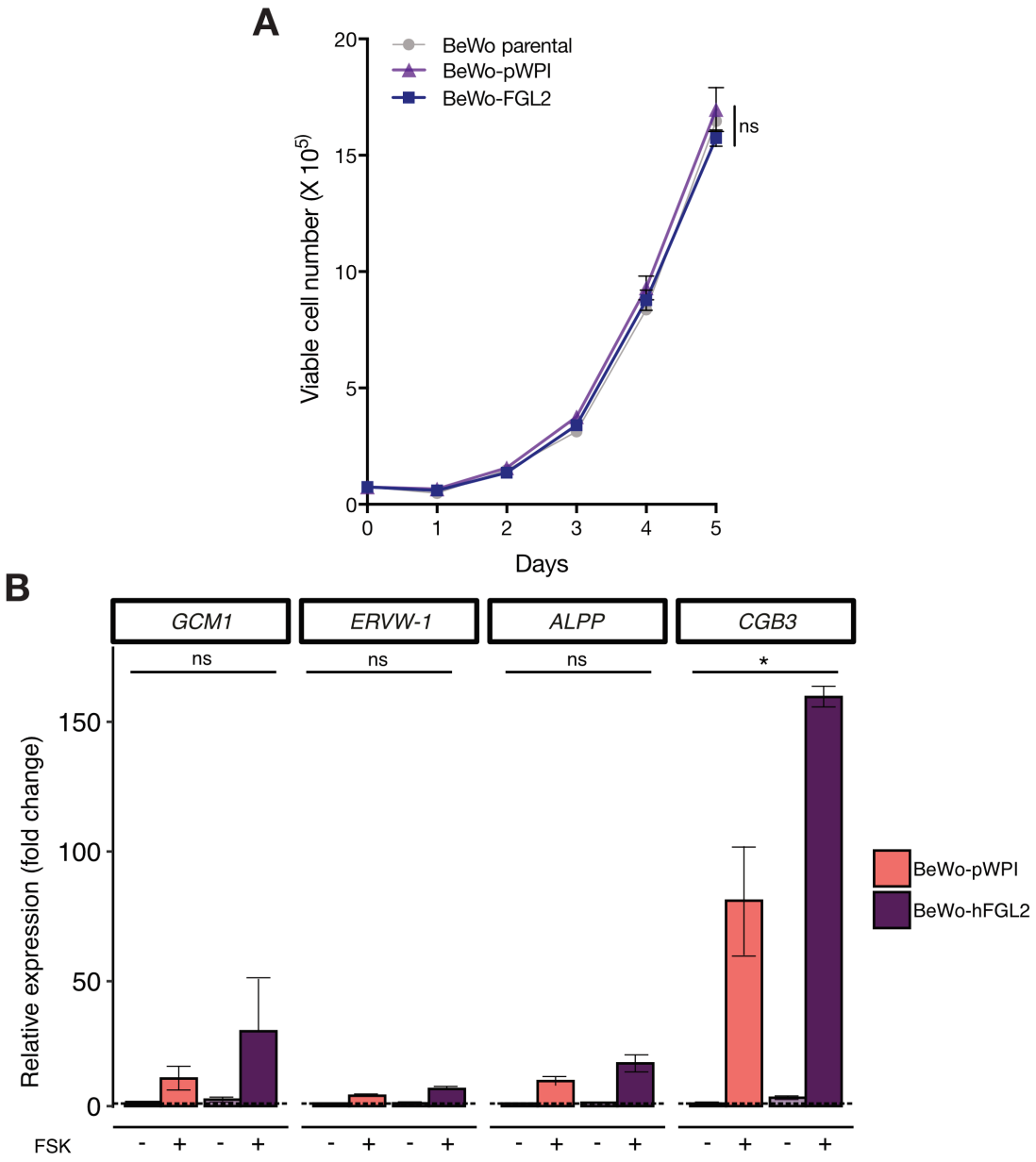

Figure 24: *FGL2* overexpression promotes FSK-mediated syncytialization in BeWo. A) 5-day growth curve in BeWo. Proliferation rate is unaffected by *FGL2* overexpression (one-way ANOVA with Dunnett's post hoc test, p=0.8772). Data points represent average cell number in 3 wells per line, per timepoint (N=3). **B)** Relative expression of *GCM1, ERVW-1, ALPP* and *CGB3* in DMSO and FSK-treated cells (100μM FSK for 72hrs, N=3). FSK upregulates all four genes (two-way ANOVA, p=0.003). The relative increase in *CGB3* is larger in BeWo-hFGL2 than in BeWo-pWPI (two-way ANOVA with Tukey's post-hoc test, p=0.0346), but this is not significant for *GCM1* (p=0.1051), *ERVW-1* (p=0.1051) and *ALPP* (p=0.1186). Error bars represent SEM.

We then treated BeWo-pWPI and BeWo-hFGL2 with FSK and compared their response by measuring *GCM1, ERVW-1* (syncytin-1, a mediator of syncytialization downstream of *GCM1*)*, ALPP* (placental alkaline phosphatase, an enzyme expressed only in fused cells)*,* and *CGB3*. FSK induced an increase in all four genes (two-way ANOVA, p=0.003), which was of larger magnitude in BeWo-hFGL2 than in BeWo-pWPI (**Figure 24B**). Of note, basal levels (in control, DMSO-treated cells) of all four genes were slightly higher in BeWo-hFGL2 than in BeWo-pWPI cells. We therefore compared the FSK-mediated increase between the two lines, each relative to its own DMSO-treated sample. *FGL2* overexpression caused a larger increase in *CGB3* (two-way ANOVA, p = 0.0346), while the difference between lines was not significant for *GCM1* (p = 0.1051)*, ERVW-1* (p = 0.1051) or *ALPP* (p = 0.1186). These data suggest that *FGL2* overexpression could increase the natural fusion rate of BeWo, and facilitates the cellular response to FSK, to more efficiently form a syncytium. However, it is also possible that the promotion of FSK response by excess FGL2 represents inappropriately fast syncytiotrophoblast turnover. Advanced villous maturation, which is reflective of placental dysfunction and can be observed in the histopathological profile of the term human placenta, could result from this accelerated syncytiotrophoblast turnover.

4.2.3. *FGL2* overexpression rescues the inhibitory effect of inflammatory cytokines on syncytialization

The syncytiotrophoblast is the cellular barrier of the maternal-fetal interface and has a large role to play in dictating the placental response to inflammatory insult. FGL2 was seen, in other systems, to mediate the response to inflammation – being induced by inflammatory cytokines and exerting an immunosuppressive effect (see **Introduction**). We therefore aimed to delineate the direct effect of an excess of *FGL2* overexpression on syncytiotrophoblast response to inflammatory insult.

We combined cytokine treatment with FSK induction and determined resulting expression of *GCM1* and *CGB3,* in BeWo-pWPI and BeWo-hFGL2. As presented in **Figure 23**, the addition of IFNγ to FSK reduced *CGB3* expression, in BeWo-pWPI. A strong increase in *CGB3* expression was observed in BeWo-hFGL2 ($p = 1.7E-5$), instead of the small decrease observed in BeWo-pWPI, suggesting that *FGL2* overexpression may reverse the inhibitory effect of IFNγ (**Figure 25**). While the inhibitory effect of TNFα on *CGB3* expression, and the effect of both cytokines on *GCM1* expression were not statistically significant, we also observe a rescue effect of *FGL2* overexpression in these cases. This was confirmed by an overall significant interaction of the effect of *FGL2* overexpression and the effect of treatment (two-way ANOVA, $p = 3.99E-6$) (**Figure 25A**).

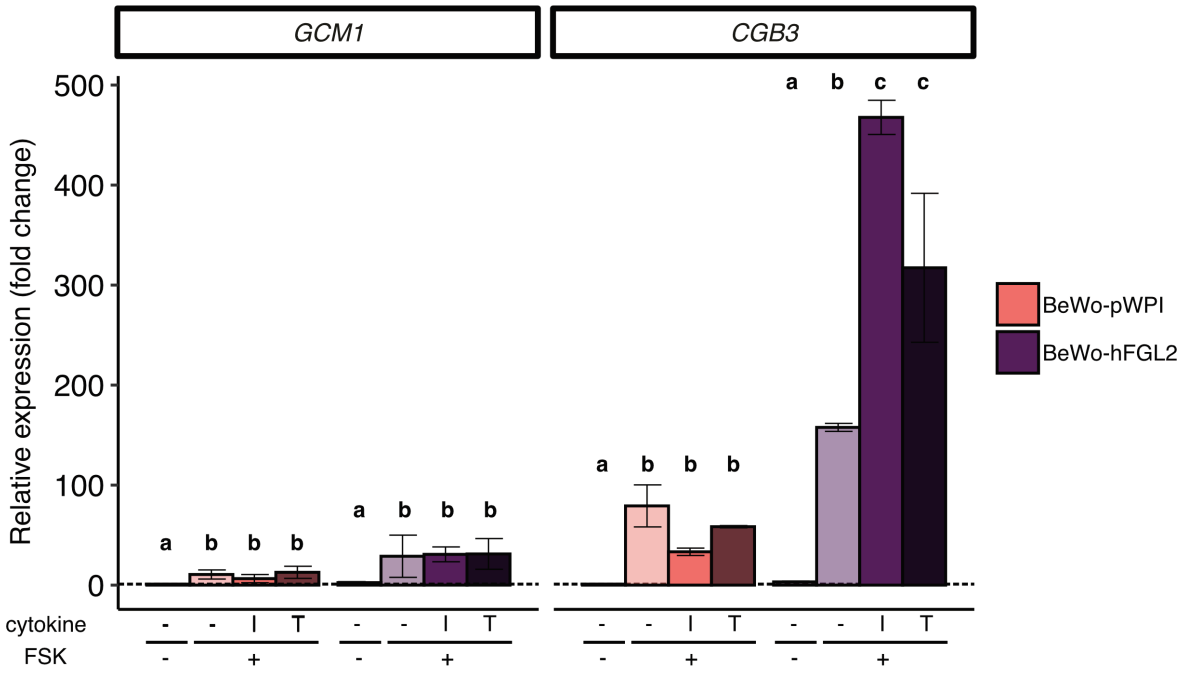

Figure 25: *FGL2* overexpression rescues inflammatory cytokine inhibition of syncytialization in BeWo. Relative expression of *GCM1* and *CGB3*, in response to IFNγ (I, 50ng/ml) or TNFα (T, 10ng/ml), in FSK-treated BeWo (100μM FSK for 72hrs, N=3). FSK upregulates *GCM1* and *CGB3* in both BeWo-pWPI and BeWo-hFGL2 (two-way ANOVA with Tukey's post hoc test, p=1.13E-10; significant interaction effect with cell line genotype, p=3.99E-6). *CGB3* is upregulated in BeWo-hFGL2 in response to IFNγ (p=1.7E-5), but not in BeWo-pWPI. Different letters indicate statistical difference between groups, error bars represent SEM.

4.3. Summary

Overall, these data suggest that *FGL2* overexpression may rescue the effect of IFNγ and TNFα to protect the process of syncytialization in a pro-inflammatory environment. As we also observed an increase in BeWo *FGL2* expression in response to IFNγ and to a lesser extent, TNFα, we propose that *in vivo*, FGL2 may be upregulated in the syncytiotrophoblast layer in response to inflammation, as a protective mechanism against the pro-inflammatory environment.

Previous studies by our lab have established that signaling pathways downstream of IFNγ and TNFα are central to the pathology of a clinically relevant subclass of preeclamptic placentas (see **1.3.4.**). Pregnancies affected by this immune-mediated PE subclass exhibit distinct maternal and fetal clinical profiles, and their placentas show evidence of chronic inflammatory histopathological lesions. The results of our *in vitro* investigation of the role of FGL2 in mediating the response to inflammation in the chorionic villous space warrant an examination of the patterns of expression of *FGL2* in this PE subtype.

CHAPTER 5 (RESULTS): FGL2-ASSOCIATED TRANSCRIPTIONAL AND HISTOPATHOLOGICAL FEATURES OF IMMUNOLOGICAL PREECLAMPSIA

5.1. Patterns of placental *FGL2* expression in a cohort of preeclamptic and non-preeclamptic pregnancies

Our phenotyping of the mouse placenta lacking or with excess of *Fgl2,* as well as our *in vitro* investigation of its role in trophoblast function in the villous space, suggest that aberrant placental *FGL2* is a factor in placental dysfunction. Previous literature on FGL2 has also suggested that its aberrant expression could be a cause in spontaneous miscarriage or preeclampsia but has not identified a mechanism (see **1.4.2.**). Its identified role of cleaving prothrombin suggests that an excess could promote fibrin deposition in the villous space, which can culminate in massive perivillous fibrin deposition (MPFD). Its known immunomodulating function, while still undefined in the context of the placenta, could play a part in maintaining the particular immunological balance demanded by pregnancy. These factors, combined, led us to examine its patterns of expression and associated features, in a cohort of preeclamptic and non-preeclamptic placentas which we previously characterized extensively.

Our understanding of the physiological mechanisms at the root of preeclampsia, which underlie placental dysfunction, is limited by the high degree of heterogeneity in clinical presentation and placental pathology findings. This heterogenous presentation, along with a lack of progress in the identification of accurate predictive biomarkers or effective therapeutics to prevent or treat preeclampsia has led to the hypothesis that the clinical diagnosis of preeclampsia may encompass a number of disease subclasses likely driven by distinct forms of

placental disease. Our group has played an important role in the identification of three distinct subclasses of preeclampsia through detailed placental profiling. In this chapter, we set out to investigate how placental *FGL2* expression may differ across these three preeclampsia subtypes and begin to determine if aberrant FGL2 expression may be associated with the distinct forms of placental dysfunction observed.

5.1.1. *FGL2* is unchanged by timing of preeclampsia disease onset

Our original patient cohort included both healthy controls and preeclamptic patients that spanned the clinical spectrum of the disease. We first investigated if placental *FGL2* mRNA expression could discriminate between clinically distinct groups of patients: first between preeclamptic and non-preeclamptic samples, and secondly, considering the time of delivery (term vs preterm) as an indicator of PE disease severity. Abundance of *FGL2* transcripts was unchanged in patient samples with a diagnosis of preeclampsia compared to non-preeclamptic controls ($p = 0.0951$), but a wide spread of FGL2 expression was noted across the cases, indicating a high degree of heterogeneity in these samples (**Figure 26A**). Existing studies commonly distinguish between early and late onset PE using a cutoff of 34 weeks of gestation, with considerable evidence to suggest different pathophysiology in early vs. late preeclampsia[41,123]. While this classification of cases does not perfectly align with ours, it shares some similarities in that placentas from preeclamptic pregnancies delivered early

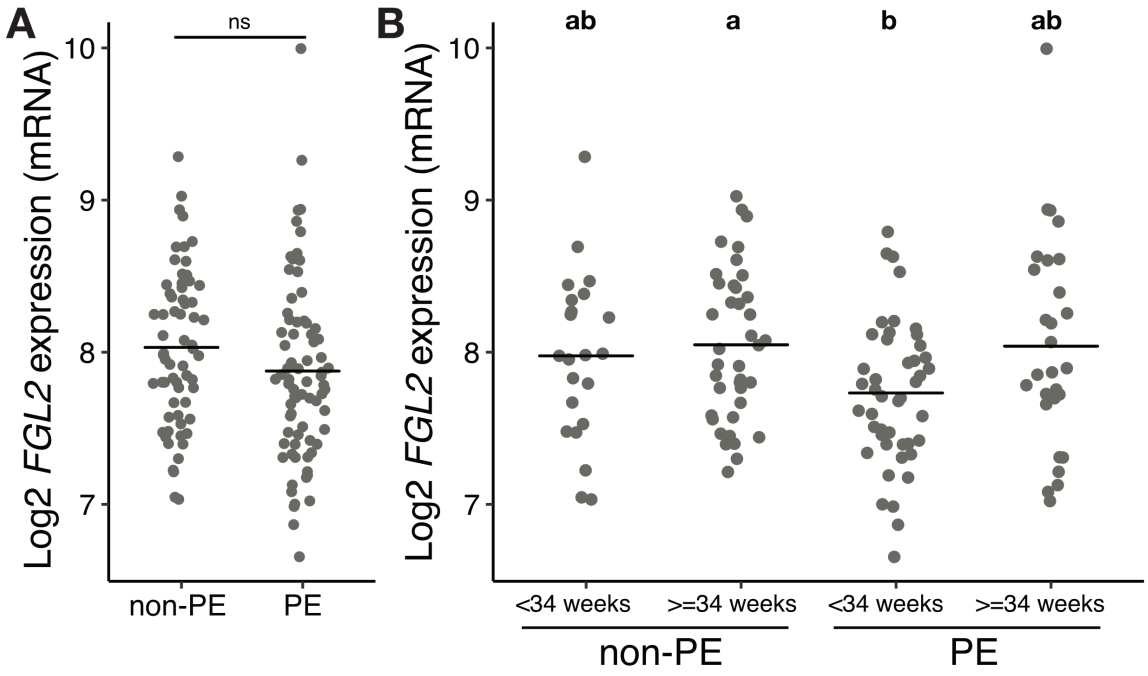

Figure 26: Placental *FGL2* expression is lower in early-onset PE, but does not discriminate between diagnoses. A) *FGL2* expression is unchanged between preeclamptic and non-preeclamptic samples (p=0.0951, Welch's t-test). **B)** *FGL2* expression is lower in preeclamptic samples with a gestational age below 34 weeks (p=0.0435; Kruskal-Wallis, Dunn's post-hoc test). Different letters indicate statistical differences between groups: p=0.4237 (non-PE<34wks/ non-PE>=34wks), p=0.0720 non-PE<34wks/PE<34wks), p=0.4980 (non-PE<34wks/PE>=34wks), p=0.0276 (non-PE>=34wks/PE<34wks), p=0.5082 (non-PE>=34wks/PE>=34wks), p=0.0749 (PE<34wks/PE >=34wks).

are transcriptionally and histopathologically different from those delivered closer to term. When using 34 weeks of gestation as a cutoff, we first observed that *FGL2* expression does not distinguish between term and preterm in non-PE pregnancies (p = 0.4980). However, *FGL2* expression is decreased in samples with early-onset PE compared to non-PE samples >= 34 weeks (p = 0.0276). In PE pregnancies, *FGL2* appears lower in early-onset than late-onset, but this decrease does not reach statistical significance (p = 0.0749) (**Figure 26B**). These data suggest that when using the catch-all clinical definition of PE (presence of de novo hypertension and proteinuria), or when defining PE according to time of disease onset, FGL2 expression does not appear to be meaningfully altered. These patterns show the potential of *FGL2* to distinguish between clinically relevant categories, but imperfectly. Moreover, considerable variation in FGL2 expression was noted across the cases, indicative of continued heterogeneity in our cases, even when split into dichotomous groups according to disease onset.

5.1.2. FGL2 is differentially expressed between transcriptional clusters

We have previously described and characterized clinically relevant transcriptional clusters of placental disease in a case-control series which included > 70 preeclampsia samples that spanned the clinical spectrum of disease[74,75,81]. We used these same characterized samples in the current analysis of FGL2 expression and were therefore able to assess placental FGL2 expression according to placental disease transcriptional cluster. A unique pattern of cluster-specific *FGL2* expression emerged (p = 6.794E-08; **Figure 27A**). Placentas from cluster 2, comprised

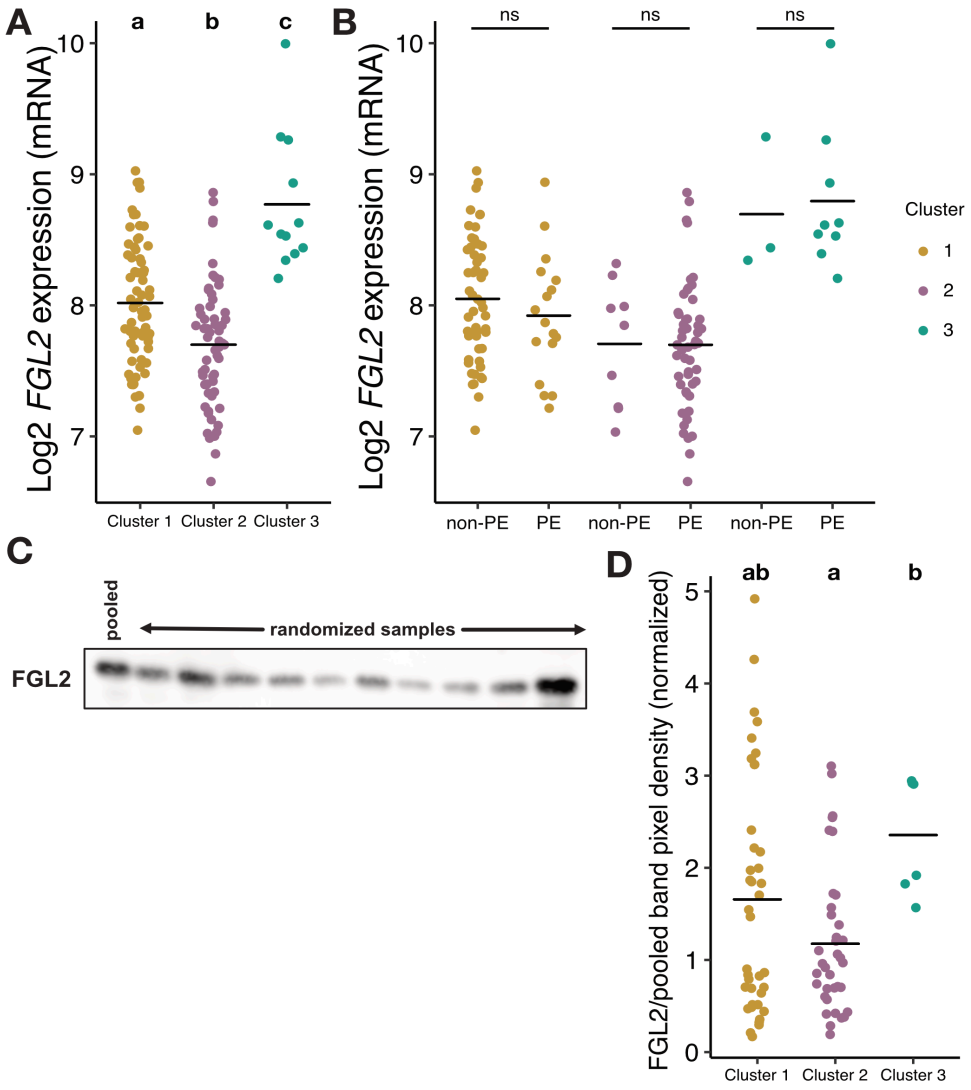

Figure 27: *Fgl2* is differentially expressed among gene expression clusters
A) *FGL2* expression is different among clusters (p=6.794E-8; Kruskal-Wallis, Dunn's post-hoc test). Different letters indicate statistical differences between groups: p=1.1246E-04 (clusters 1/2), p=8.9817E-04 (clusters 1/3), p=2.3702E-07 (clusters 2/3). **B)** *FGL2* expression is equal between healthy and preeclamptic samples from a same cluster (ns, non-significant, p=0.3425, cluster 1; p=0.9677, cluster 2; p=0.7907, cluster 3; multiple Welch's t-tests). **C)** Sample western blot for FGL2. Pooled sample was run on all blots to eliminate batch effect. Quantification was done by calculating the ratio of FGL2 band to pooled sample band pixel density, each normalized to whole lane protein. **D)** FGL2 protein expression is different among clusters (p=0.0362; Kruskal-Wallis, Dunn's post-hoc test). Different letters indicate statistical differences between groups: p=0.0972 (clusters 1/2), p=0.0514 (clusters 1/3), p=0.0191 (clusters 2/3). Horizontal bars represent group means.

primarily of canonical PE patients, showed significantly lower *FGL2* expression (p = 1.1246E-4) than placentas from cluster 1, used as the reference group as it included mostly non-preeclamptic term control patients[75]. Placentas from cluster 3 had higher *FGL2* expression relative to the same reference group (p = 8.8917E-04). While clusters 2 and 3 are heavily weighted with PE patient samples, some healthy controls clustered alongside and demonstrated similar placenta histopathology findings, despite no symptomatic evidence of maternal disease. Interestingly, we found that the pattern of cluster specific *FGL2* expression is unchanged by clinical diagnosis, as *FGL2* expression was similar between healthy and preeclamptic samples within each transcriptional cluster (p = 0.3425, cluster 1; p = 0.9677, cluster 2; p = 0.7907, cluster 3; **Figure 27B**). This finding highlights an important conclusion of our study of this cohort: that non-preeclamptic placentas are not necessarily "normal", as they share transcriptional and histopathological features with preeclamptic ones within their cluster. This concept and its possible causes are discussed below (see **Discussion**).

As clinical diagnosis often depends on protein detection, we confirmed cluster specific FGL2 expression by western blot, and quantified this by densitometry (**Figure 27C**). FGL2 protein was differentially expressed between clusters (p = 0.0362), with a modest decrease in FGL2 protein expression in cluster 2 (p = 0.0972) and increase in cluster 3 (p=0.0514), although not quite reaching statistical significance, relative to our cluster 1 reference group (**Figure 27D**). It is notable that sample number in each cluster is lower in our protein quantification than in our

analysis of the microarray data, as protein lysates were not available for all initial samples. This lowers the power of statistical analysis.

5.2. Placental FGL2 is expressed by cytotrophoblast, syncytiotrophoblast, and intravillous/intervillous histiocytes

As a first step towards understanding its action in the villous space, with potential consequences when it's lacking or in excess, we investigated FGL2 localization within the placenta by immunohistochemistry. We found FGL2 expression in the cytotrophoblast and syncytiotrophoblast layers of the chorionic villous structures (**Figure 28A**). Furthermore, strong expression was noted in some leukocytes present in fetal vessels within villi, and in leukocytes or lymphocytes in the intervillous space (**Figure 28B-D**). CD68 staining confirmed at least a subset of these FGL2-positive cells to be monocytes/histiocytes (**Figure 28B-D**). Syncytiotrophoblast positive staining is prominent in our tissue sections, but it is likely that FGL2 from both syncytiotrophoblast and monocyte/macrophages source contributes, perhaps differently. Whole tissue lysates were used to prepare the samples used for this study, and we therefore cannot determine the relative contribution of each of these cell types to our FGL2 profiling data.

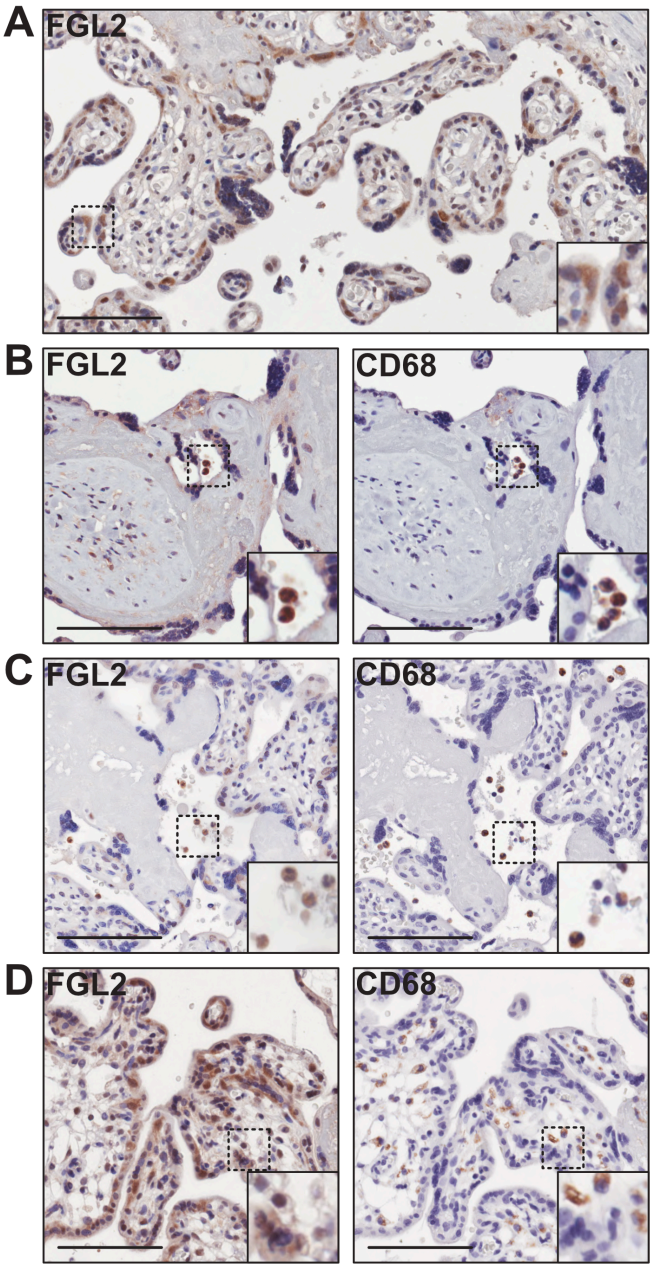

Figure 28: Localization of FGL2 expression within the villous space. Immunohistochemistry staining of villous tissue for FGL2 and CD68 in serial sections (images are representative of samples from all clusters). **A)** FGL2 is expressed by the cytotrophoblast and syncytiotrophoblast layers of the term villi. FGL2 and CD68 are co-expressed by subsets of **B)** leukocytes within fetal vessels **C)** intervillous leukocytes/lymphocytes and **D)** infiltrated leukocytes/ lymphocytes, identifying them as monocytes/macrophages. Scale bars = 100μm.

5.3. FGL2 is part of a gene module differentially enriched between PE disease subtypes

Given that the PE subtypes were derived from transcriptional profiles, the clinical phenotypes likely arise from expression of different functional gene sets. Any single gene of interest that contributes to cluster-specific features, either clinical or histopathological, does so as part of a broader inter-connected gene set. With the aim of identifying, without bias, gene sets to which *FGL2* belongs, and how those gene sets have functional relevance to our patient clusters, we applied network analysis to the gene expression dataset of our cohort[112]. This analysis identified 29 modules (gene sets) of co-expressed and correlated genes, which are often indicative of common function. We calculated and compared the enrichment of each module among diagnostic groups: preeclamptic and non-preeclamptic samples within each previously identified gene expression cluster. Broadly, three groups of modules with similar enrichment patterns could be observed (**Figure 29A**). While each module contains genes sets that potentially contribute to cluster-specific phenotypes, we chose to focus our analysis on genes well known for their potential as preeclampsia markers, and on *FGL2*. Of interest was a large module (yellow) that contained a panel of several such genes, that are known PE markers, or have been investigated as such, including: *FLT1, ENG, INHA/INHBA, FSTL3, PVRL4, NDRG1, SERPINA3, LEP, TREM1*[124-130]*.* Gene ontology analysis revealed that yellow module genes are primarily involved in regulating metabolic changes, cell

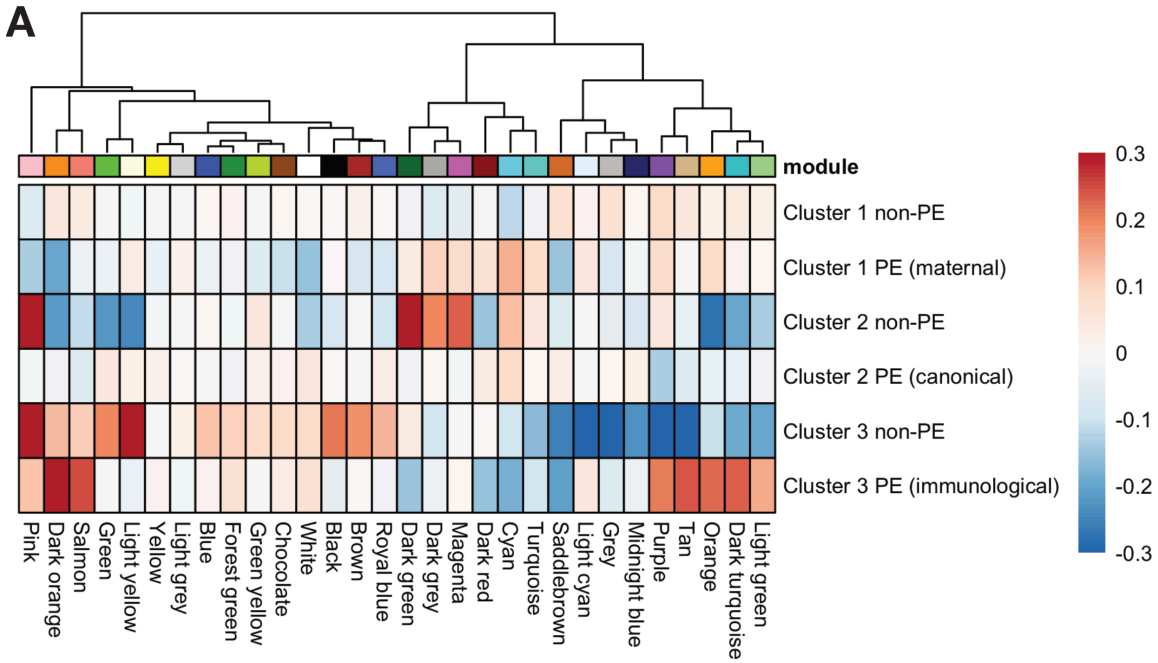

Figure 29: Weighted Gene Correlation Network Analysis (WGCNA) reveals discriminating gene modules. A) Gene module enrichment in cohort diagnostic groups (gene expression clusters divided into PE and non-PE). Modules were obtained with R package WGCNA with threshold of 5 used for network construction and module detection, dendogram cut height set to 0.25, minimal module size set to 30 genes. Grid square shade represents enrichment (average z-score of module genes for all samples in a diagnostic group).

death, and response to hypoxia (**Figure 30A**). Hub genes, in this network analysis, are defined as genes (vertices) that have the largest number of direct connections (degree over 30). High degree genes are usually central to their network, meaning their expression is correlated with a large number of others, and therefore tend to be the more important, biologically[112,131]. Hub genes of the yellow module included genes of this well-established gene panel and several others (**Figure 30B**). These genes and their ontology are concordant traditionally defined pathophysiology of PE (hypoxia-driven), represented in our cohort by cluster 2 preeclamptic placentas (canonical PE).

A few modules were noticeable because of the large difference in their expression between diagnostic groups, suggesting that expression of these modules is what differentiates one diagnostic group from another. The purple module showed this enrichment pattern, with high expression in immunological PE samples (within transcriptional cluster 3), compared to healthy samples from the same cluster, and importantly, when compared to canonical PE samples (within transcriptional cluster 2) (**Figure 29A**). Gene ontology analysis of the purple module genes revealed overwhelming enrichment for functions related to immunity and leukocyte response (**Figure 31A**). Interestingly, *FGL2* was found in this purple module, indicating its involvement in a gene set that discriminates between clinically significant diagnostic groups. Network representation of this module showed *FGL2* not to be a hub gene itself, but to have 8 direct neighbors: *CD86, CTSS, DOCK10, EVI2B, GPR65, PTPRC, SAMSN1,* and *TLR2* (**Figure**

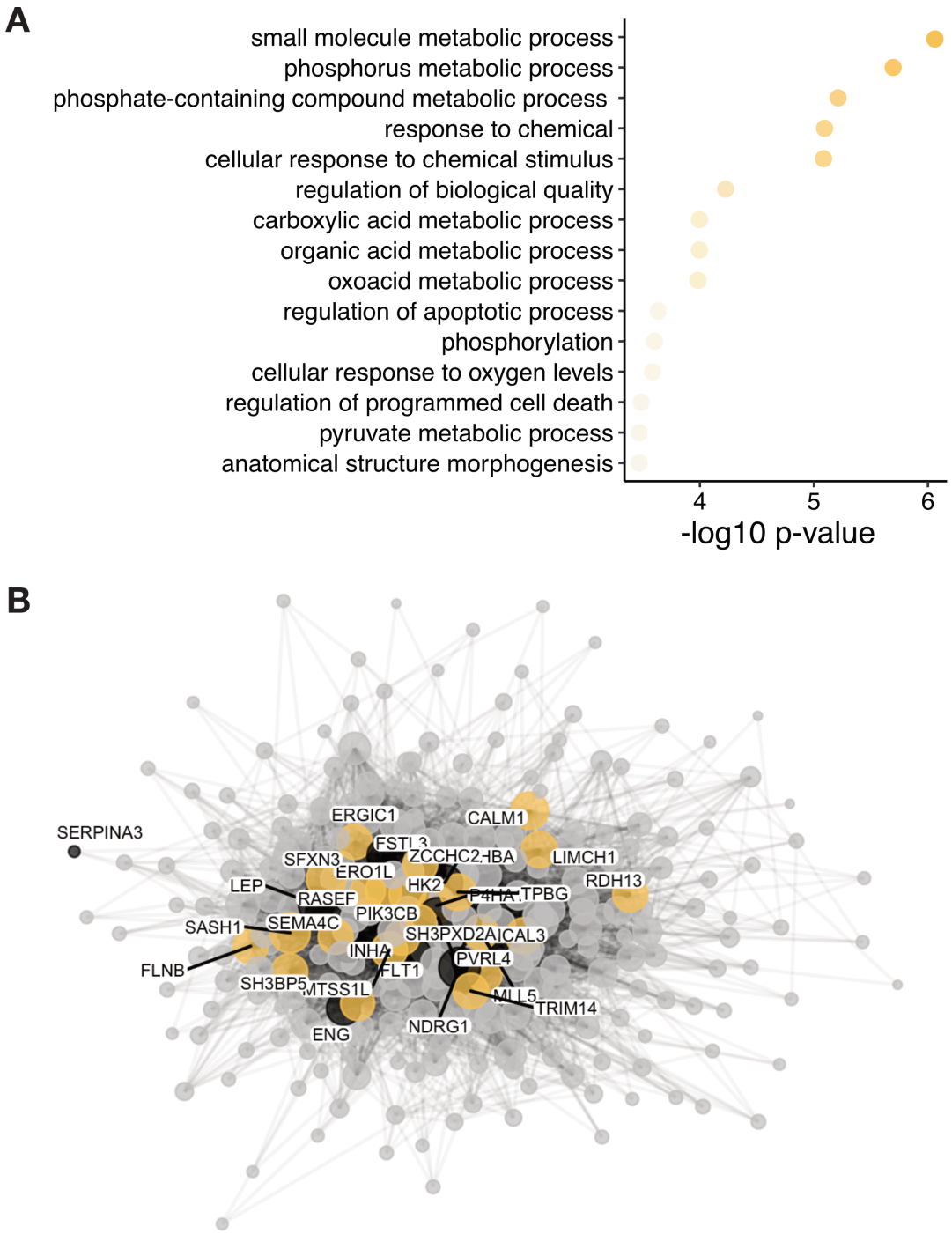

Figure 30: Hypoxia and metabolism-related genes known as traditional PE markers emerge as yellow module. A) Most significantly enriched GO terms in genes from yellow module. Yellow module genes relate to metabolic changes and response to hypoxia. **B)** Yellow module (942 genes) comprises a panel of previously investigated PE biomarkers, labeled and shown in black. Module hub genes (degree>30) are labeled and shown in yellow.

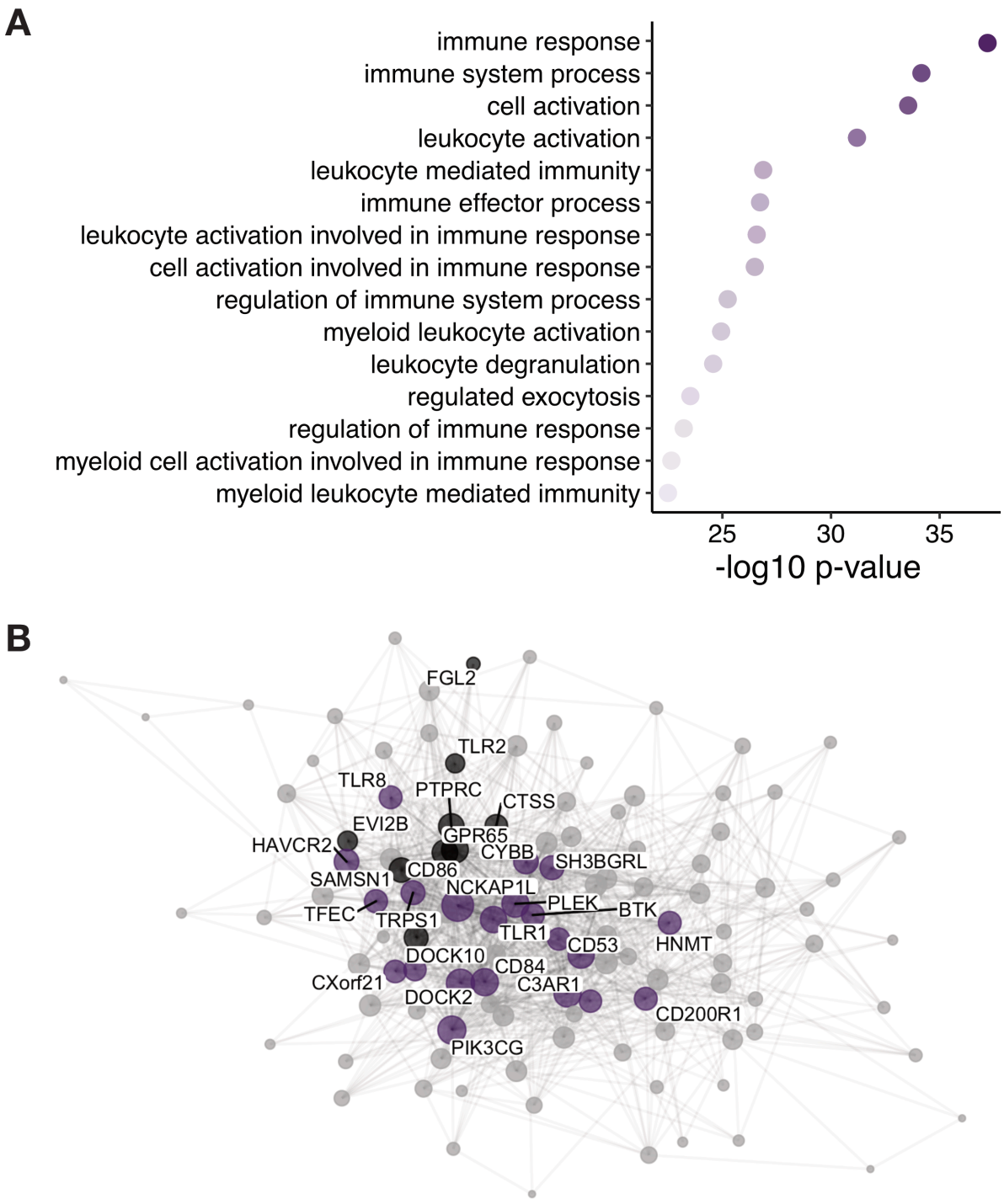

Figure 31: Immune response and leukocyte activation-related genes emerge as purple module. A) Most significantly enriched GO terms in genes from purple module. Purple module genes relate to immune response and leukocyte function. **B)** Purple module (268 genes) comprises *FGL2* and 8 direct neighbors, labeled and shown in black. Module hub genes are labeled and shown in purple.

31B). Several of these direct neighbors were hub genes of the network, suggesting that while *FGL2* itself may not be a core regulator of the gene set, its expression is closely related to those that are.

5.4. Placental *FGL2* expression poorly associates with pregnancy outcome parameters

5.4.1. Placental FGL2 expression poorly associates with maternal characteristics and PE symptoms

Previously, our group performed a correlative analysis between clinical demographic variables and transcriptional cluster membership[75]. Because of the observed differences in *FGL2* expression among gene expression clusters, we assessed the correlation between *FGL2* expression and the severity of maternal and fetal clinical phenotypes for all cases of diagnosed PE in our dataset. We found poor associations between placental *FGL2* expression and maternal characteristics at the time of pregnancy: maternal age (Pearson r = 0.0612, p = 0.6046) and maternal body mass index (BMI; Pearson r = -0.0343, p = 0.7984) (**Figure 32A-B**). *FGL2* was also a poor predictor of the severity of maternal PE symptoms: HELLP syndrome (p = 0.1373), maternal mean arterial pressure (MAP; Pearson r = -0,1124, p = 0.1894) and urinary protein, measured by dipstick score (Spearman rho = -0.0346, p = 0.7814) (**Figure 33A-C**).

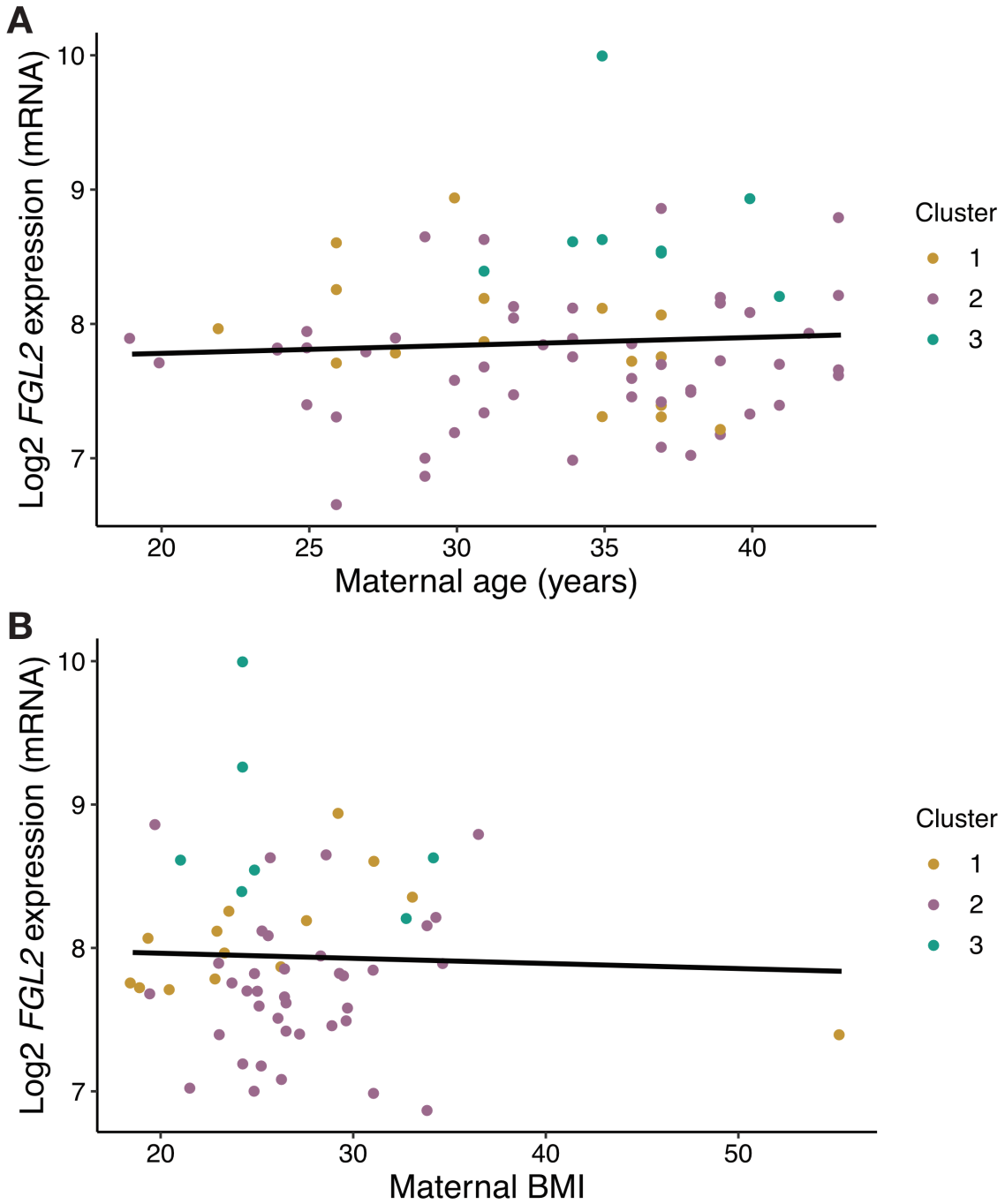

Figure 32: Placental FGL2 expression does not correlate with maternal characteristics in preeclamptic pregnancies. A) FGL2 expression does not correlate with maternal age (Pearson r=0.0612, p=0.6046) or **B)** maternal BMI (Pearson r=-0.0343, p=0.7984).

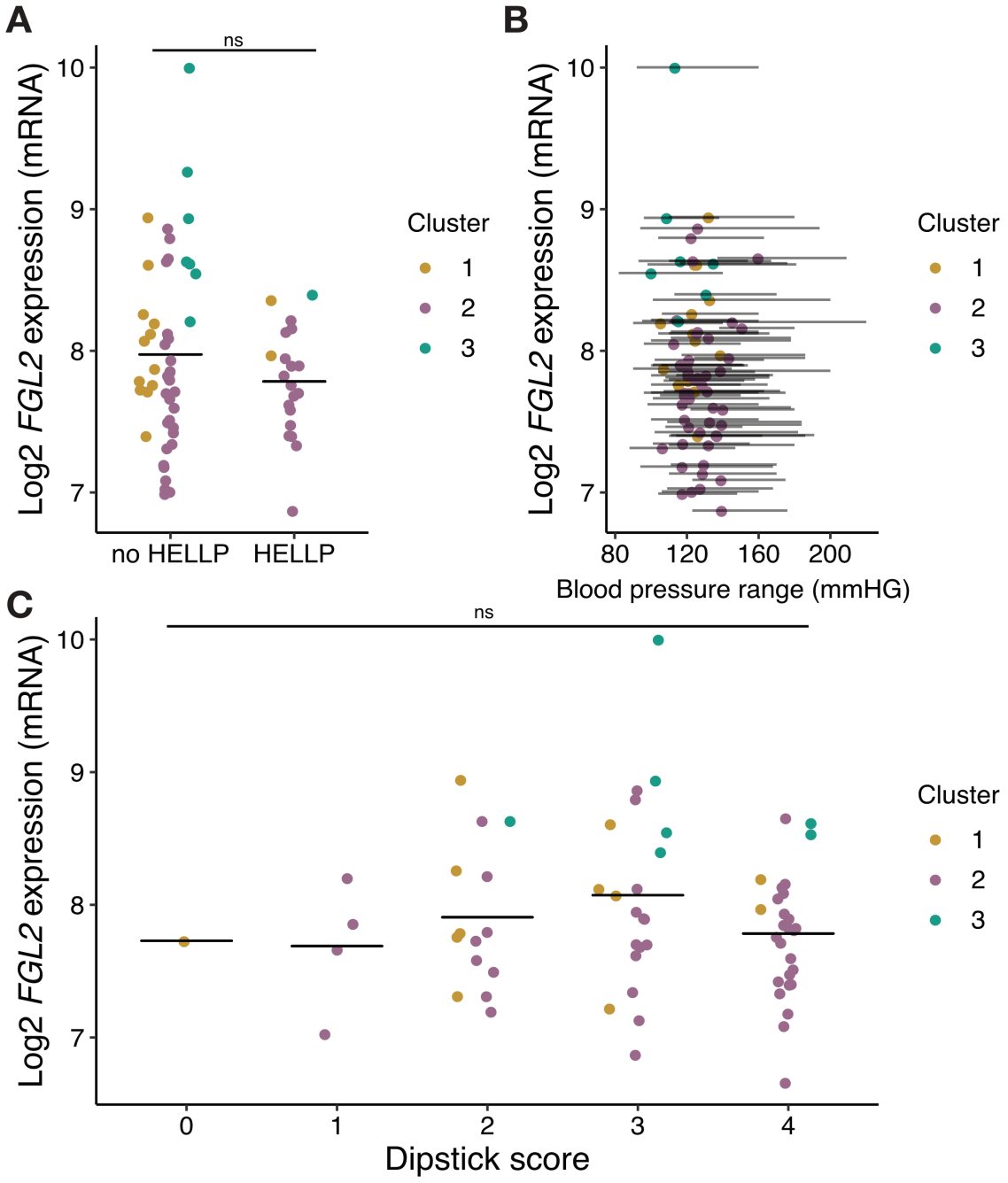

Figure 33: Placental *FGL2* expression does not correlate with maternal PE symptoms. A) *FGL2* expression is not different in pregnancies affected and unaffected by HELLP syndrome (p=0.1373; Welch's t-test). **B)** *FGL2* expression does not correlate with maternal MAP (Pearson r=-0.1124, p=0.1894) or **C)** maternal dipstick score (Spearman rho=-0.0346, p=0.7814).

5.4.2. Placental FGL2 expression poorly associates with fetal health outcomes

We found a weak but significant positive association between *FGL2* and gestational age at delivery—a proxy of disease severity (Pearson r = 0.2504, p = 0.0303) (**Figure 34A**). We found no association between *FGL2* and infant birthweight centile (Pearson r = -0.1770, p = 0.1519), but interestingly, samples found at both extremes of *FGL2* expression (high and low) demonstrate the lowest birthweight centile. This is indicative of poor fetal outcomes both in samples where placental *FGL2* is abnormally low and where it is abnormally high (**Figure 34B**). Concurrently, placental *FGL2* expression was not correlated with small for gestational age (SGA)/average for gestational age (AGA) categorization (p = 0.5288), fetal sex (p = 0.6610) or mode of delivery (p = 0.1600) (**Figure 35A-C**). Overall, we note that aberrantly low or high *FGL2* proves a poor predictor of the majority of maternal or fetal pregnancy outcomes, when tissue samples from all gene expression clusters are considered.

5.5. *FGL2* expression is associated with cluster-specific histopathological lesions of the placenta

We next sought to determine the relationship between placental *FGL2* expression and placental histopathology findings, from a blinded, semi-quantitative evaluation by a perinatal pathologist, across all placentas in our cohort[81]. For each lesion scored, we calculated an association score to *FGL2*, using the difference in mean placental *FGL2* expression between placentas with (score >= 1) and without (score = 0) this lesion. The lesions were subsequently

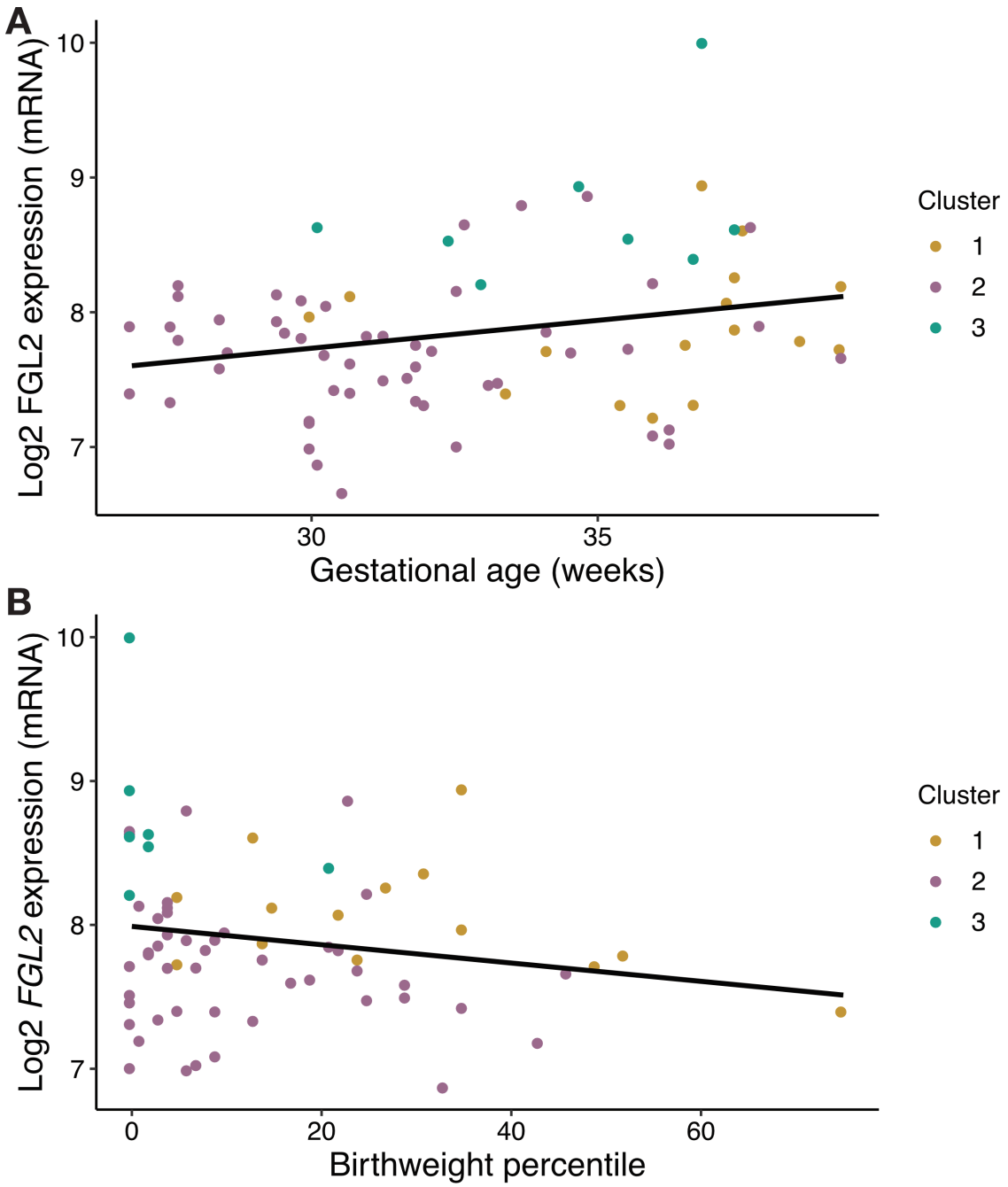

Figure 34: Placental *FGL2* expression correlates with gestational age, but not birthweight percentile in preeclamptic pregnancies. A) *FGL2* expression weakly correlates with gestational age at birth (Pearson r=0.2504, p=0.0303). **B)** *FGL2* expression does not correlate with infant birthweight percentile (Pearson r=-0.1770, p=0.1519).

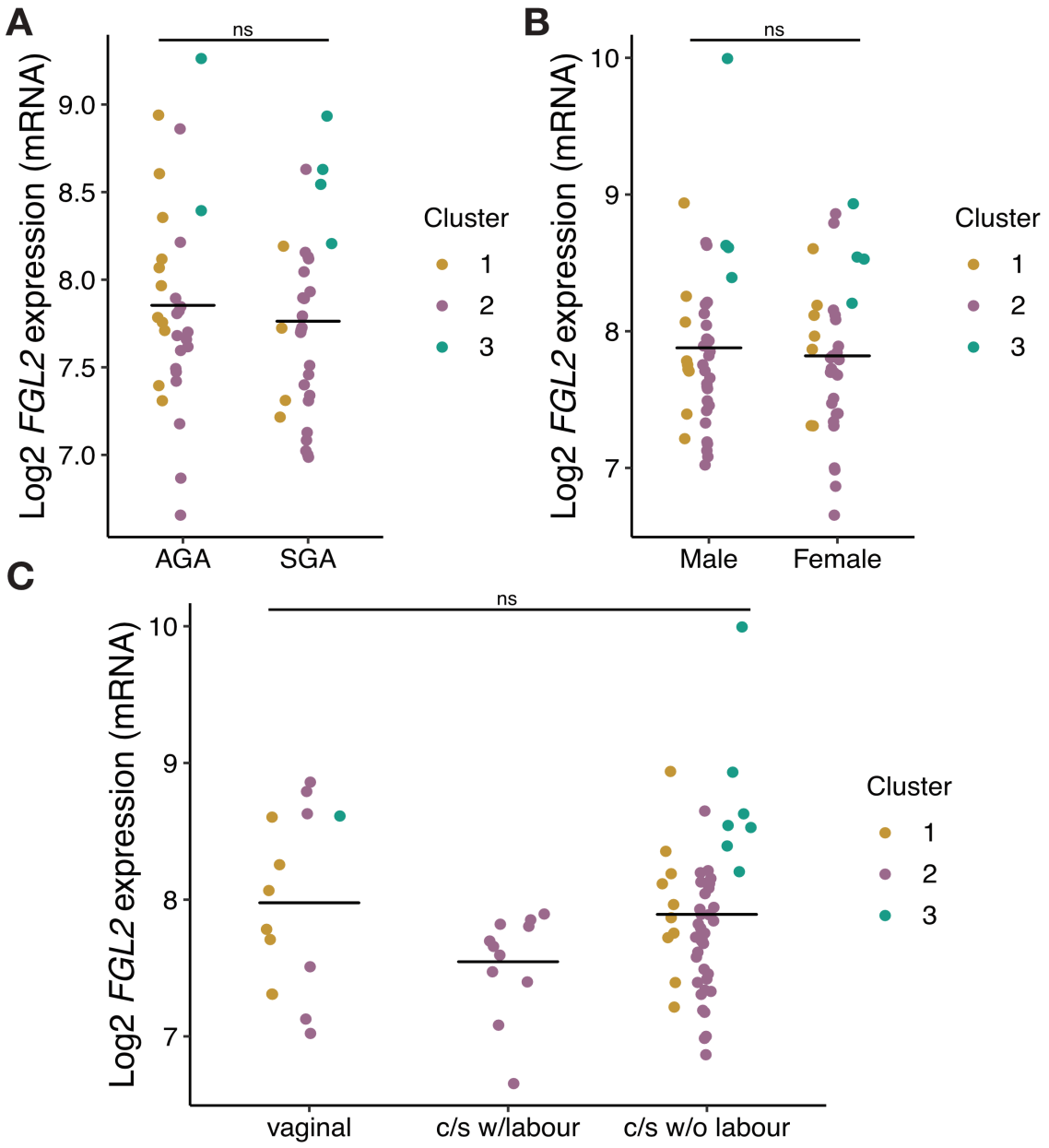

Figure 35: Placental *FGL2* expression des not correlate with fetal clinical features in preeclamptic pregnancies. A) *FGL2* expression is not different in pregnancies with AGA and SGA infants (p=0.5288; Welch's t-test), **B)** with male and female infants (Welch's t-test p=0.6610), or **C)** in pregnancies with any delivery type (p=0.1600; Kruskal-Wallis, Dunn's post-hoc test).

ranked from highest to lowest score, revealing which lesions have the strongest positive and negative associations with placental *FGL2* expression (**Figure 36A**).

5.5.1. *FGL2* expression associates positively with chronic inflammatory lesions

The lesions that most positively associated with placental *FGL2* expression were villitis of unknown etiology (VUE), delayed villous maturity, chronic deciduitis, maternal inflammation, avascular fibrotic villi, fetal inflammation and massive perivillous fibrin deposition (MPFD) (**Figure 36 and Figure 37A-D**). The majority of these lesions are representative of chronic inflammatory insults within the placenta, suggesting a role for excess *FGL2* in immune dysregulation within the placenta. VUE, chronic deciduitis and chronic intervillositis are chronic placental inflammation lesions, while MPFD is categorized as a maternal-fetal interface disturbance lesion that often co-occurs with chronic inflammation lesions[81,132,133]. Previously, these lesions were also shown to be prevalent in the immunological PE subclass placentas of our cohort. Based on those associations and on *FGL2*'s known role as an immunoregulator and as a prothrombinase, we chose to further investigate those four lesions (**Figure 37A-D**).

5.5.2. *FGL2* expression associates negatively with maternal vascular malperfusion (MVM) lesions

The lesions that most negatively associated with placental *FGL2* expression were distal villous hypoplasia (DVH), placental infarctions, advanced

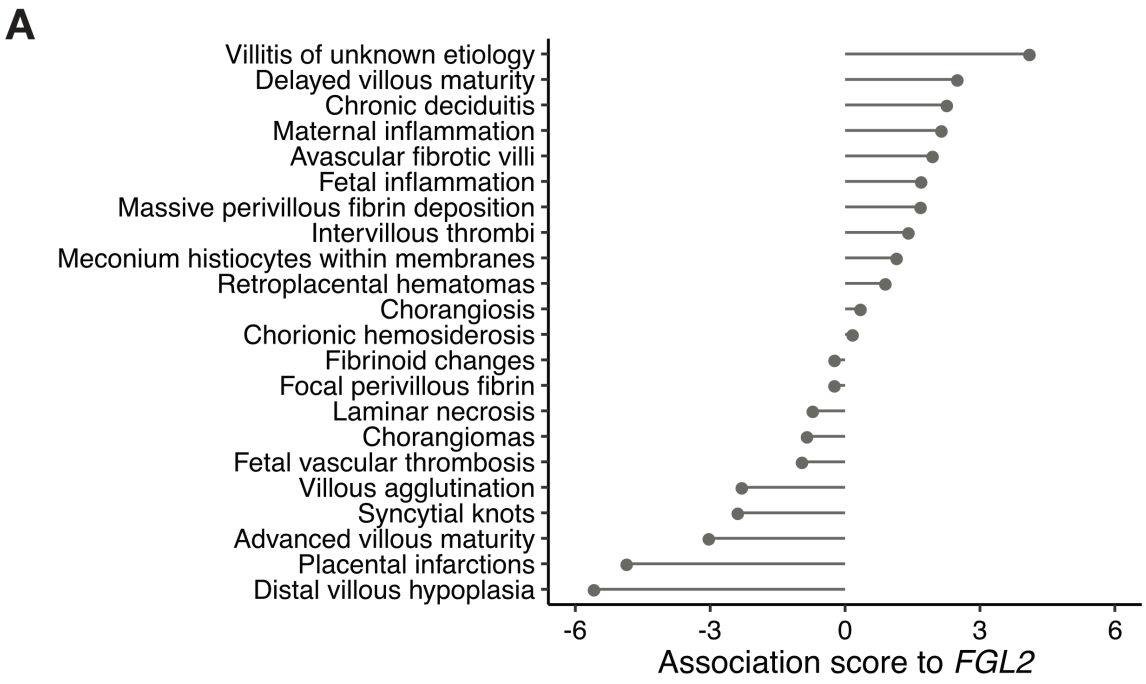

Figure 36: *FGL2* expression associates with cluster-specific histopathological lesions. A) Common placental histopathological lesions ranked by association score (t-value: difference in *FGL2* expression, relative to data variation, between affected and non-affected placentas).

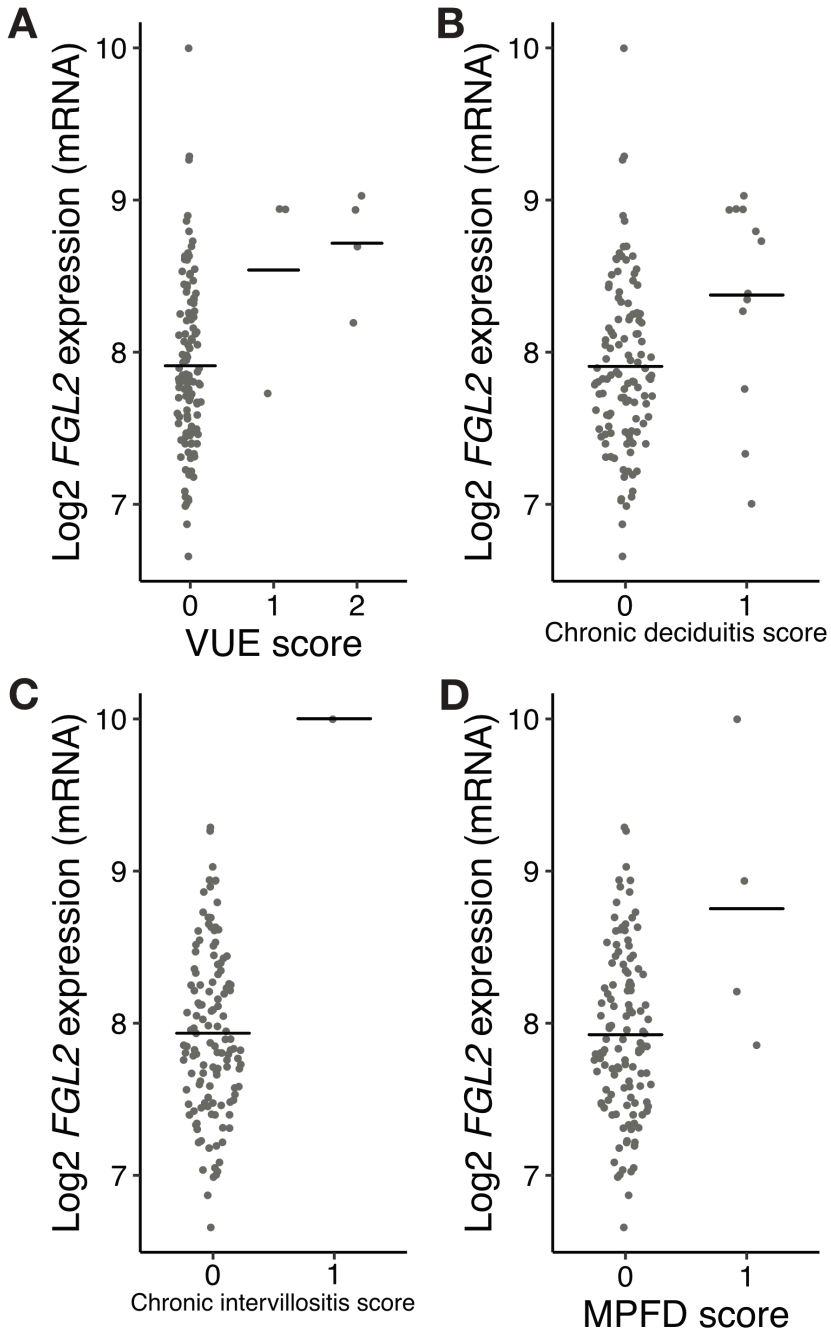

Figure 37: *FGL2* expression associates positively with chronic inflammation lesions. *FGL2* expression in placentas with (score of >=1) or without (score of 0) specific lesions: **A)** villitis of unknown etiology (VUE), **B)** chronic deciduitis, **C)** chronic intervillositis and **D)** massive perivillous fibrin deposition (MPFD). Horizontal bars represent group means.

villous maturity, and syncytial knots (**Figure 36A and Figure 38A-D**). All of these lesions, with the addition of villous agglutination, are representative evidence of MVM, a category of lesions found to be strongly associated with canonical PE placentas (hypoxia-driven), which have low *FGL2* expression[81].

5.5.3. High placental *FGL2* expression and widespread perivillous fibrin tend to co-occur in cluster 3 placentas

Because *FGL2* has known prothrombinase activity and has been shown to promote fibrin deposition in other tissues, and because MPFD only represents extreme cases, we chose to investigate more closely the relationship between *FGL2* expression and perivillous fibrin deposition. A semi-quantitative scoring of the total area of the villi occupied by perivillous fibrin was conducted by a perinatal pathologist. We first observed that the majority of transcriptional cluster 3/immunological PE samples, which have high *FGL2*, were attributed a fibrin score of 2 or 3 (**Figure 39A-B**). In fact, the samples with the highest degree of perivillous fibrin deposition (score of 3) also had the highest *FGL2* expression and belonged to transcriptional cluster 3. Overall, this suggests that placentas with high *FGL2* expression exhibit lesions consistent with chronic inflammatory insults and significant perivillous fibrin deposition.

5.6. *FGL2*-associated transcriptional profiles of histopathological lesions

We next sought to assess the global transcriptional changes associated with visible changes in the placenta, as evidenced by histopathological lesions.

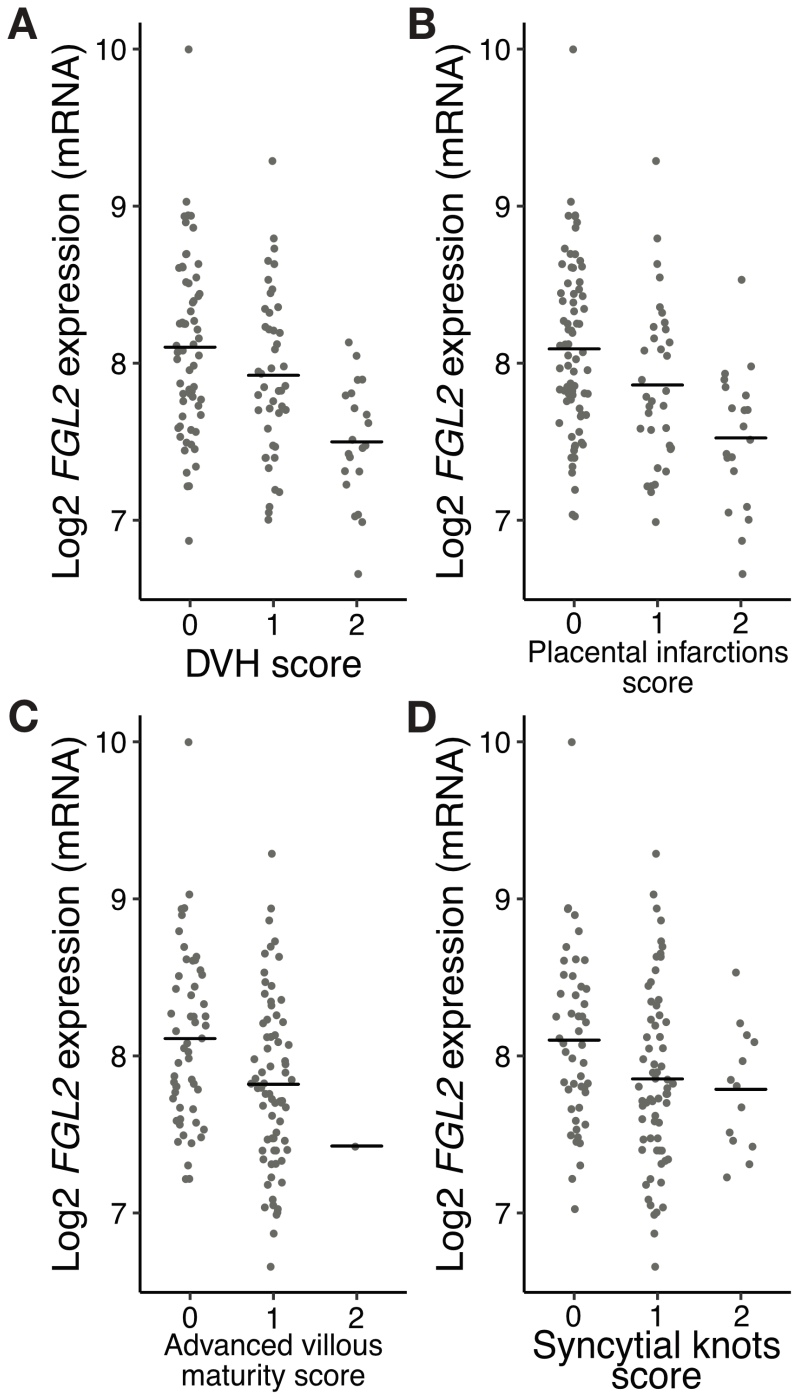

Figure 38: *FGL2* expression associates negatively with maternal vascular malperfusion lesions. *FGL2* expression in placentas with (score of >=1) or without (score of 0) specific lesions: **A)** distal villous hypoplasia (DVH), **B)** placental infarctions, **C)** advanced villous maturity **D)** and syncytial knots. Horizontal bars represent group means.

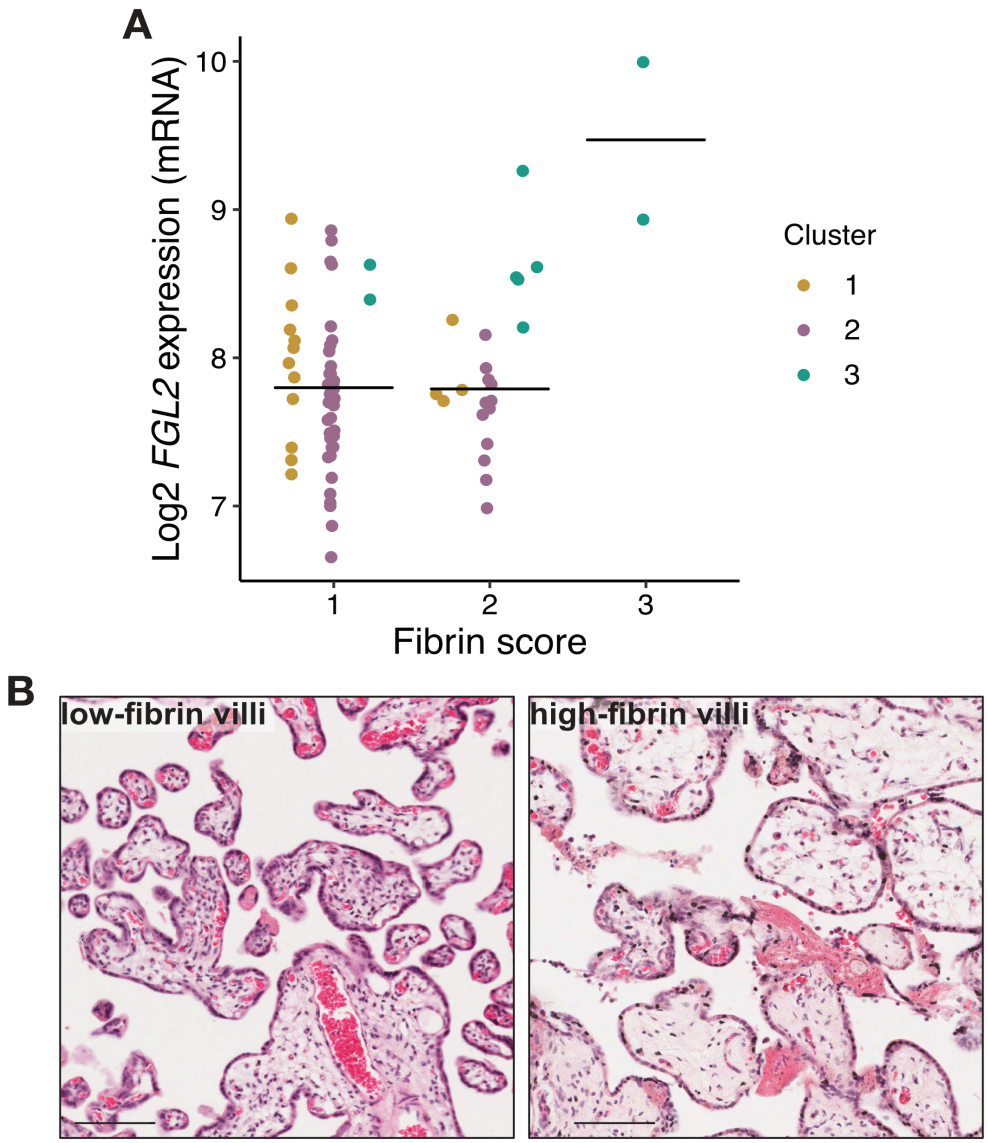

Figure 39: High placental *FGL2* and high fibrin deposition score tend to co-occur in cluster 3 placentas. A) Samples with highest fibrin score tend to have higher *FGL2* expression. Semi-quantitative examination of total villi area occupied by perivillous fibrin determined scores: 0 = 0%, 1 = <5%, 2 = 5-30%, 3 = 30-50%. **B)** Representative pictures of tissue samples with a score of 1 (left) and of 3 (right). Scale bars=100µm.

For all lesions, we conducted differential gene expression analysis between placentas with a histopathology score of 1 or over (lesion present), and those with a score of 0 (lesion absent).

5.6.1. Similarity of transcriptional profiles of MVM lesions

We first examined genes found to be differentially expressed in placentas affected by MVM lesions, as they were negatively associated with placental *FGL2* expression. Among upregulated genes was a panel of genes previously reported as biomarkers of PE, identified in the yellow module of our network analysis: *FLT1, ENG, INHA/INHBA, FSTL3, PVRL4, NDRG1, SERPINA3, LEP, TREM1* (**Figure 40A-D**). *FGL2* consistently fell within the downregulated group of genes, as did most genes from the purple module and other immune modules. As transcriptional profiles of these four lesions were very similar, we determined gene ontology reflective of an MVM transcriptional phenotype by using genes that were consistently upregulated across all four lesions. Most enriched terms were related to metabolism, proliferation, migration, and negative regulation of immune processes (**Figure 40E**).

5.6.2. *FGL2*-associated transcriptional profiles of chronic inflammation lesions

We then examined transcriptional changes in the chronic inflammation lesions that were positively associated with *FGL2* expression: VUE, chronic deciduitis, and MPFD. As only one sample from our cohort was affected by chronic intervillositis, we did not include it in our analysis. We examined

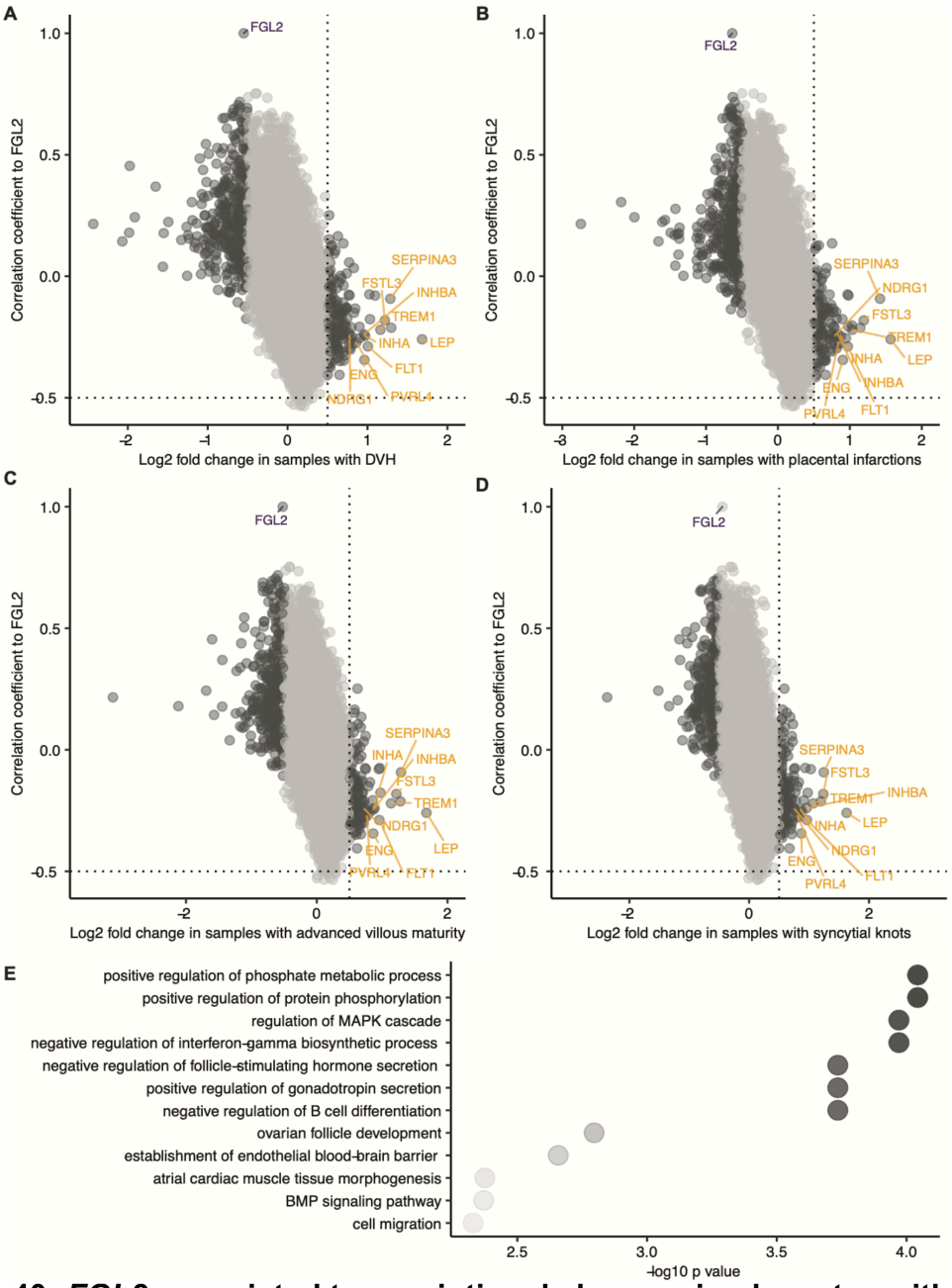

Figure 40: *FGL2*-associated transcriptional changes in placentas with MVM lesions. Differentially expressed genes in placentas with **A)** DVH, **B)** placental infarctions, **C)** advanced villous maturity and **D)** syncytial knots (correlation coefficient to *FGL2* as a function of log2 fold-change in affected placentas). The position of the fold change (0.5) and correlation coefficient (0.5) cutoffs are indicated on panels. Genes of interest are labelled. **E)** GO terms for genes commonly upregulated in all four MVM lesions indicate a role in metabolic processes and hormonal regulation.

upregulated genes, with emphasis on those with strong correlative expression to *FGL2*, as this suggests contribution to common biological processes. We noticed significant overlap between upregulated genes in VUE, chronic deciduitis and MPFD, suggestive of a common chronic inflammation transcriptional phenotype as a basis for several related, but distinct, histopathological lesions (**Figure 41A-C**). The majority of upregulated genes belonged to either the purple or the tan modules—both immune-specific modules identified in our network analysis. Broadly, gene ontology revealed roles in immune response and leukocyte function (**Figure 41A-C**). Among the top upregulated genes in all three lesions, an interesting group of IFNγ-induced genes were prominent: *CXCL9, CXCL10, CXCL11, CXCL13*, *GBP4*, *GBP5*, *RSAD2* and *IFNG* itself. Numerous leukocyte or lymphocyte activation or recruitment factors were present: *ICOS, CD38, CD48, TRAT1, CCL2, CCL5, CCL8* and *VCAM1*, as well as many genes specific to histiocyte activation or function: *CD74, MSR1, CD86* and *LYZ*. The genes that were found to be direct neighbors of *FGL2* by network analysis were consistently upregulated in placentas with VUE, chronic deciduitis and MPFD: *CD86, CTSS, DOCK10, EVI2B, GPR65, PTPRC, SAMSN1* and *TLR2.* The majority of these genes showed strong correlation to *FGL2*, suggesting its contribution to immune cell-specific, IFNγ-dependent processes that lead to the development of these lesions. Interestingly, the panel of genes previously reported as biomarkers of PE, identified in the yellow module of our network analysis (*FLT1, ENG, INHA/INHBA, FSTL3, PVRL4, NDRG1, SERPINA3, LEP, TREM1*), was found to be downregulated in placentas with VUE or chronic deciduitis (**Figure 41A-B**),

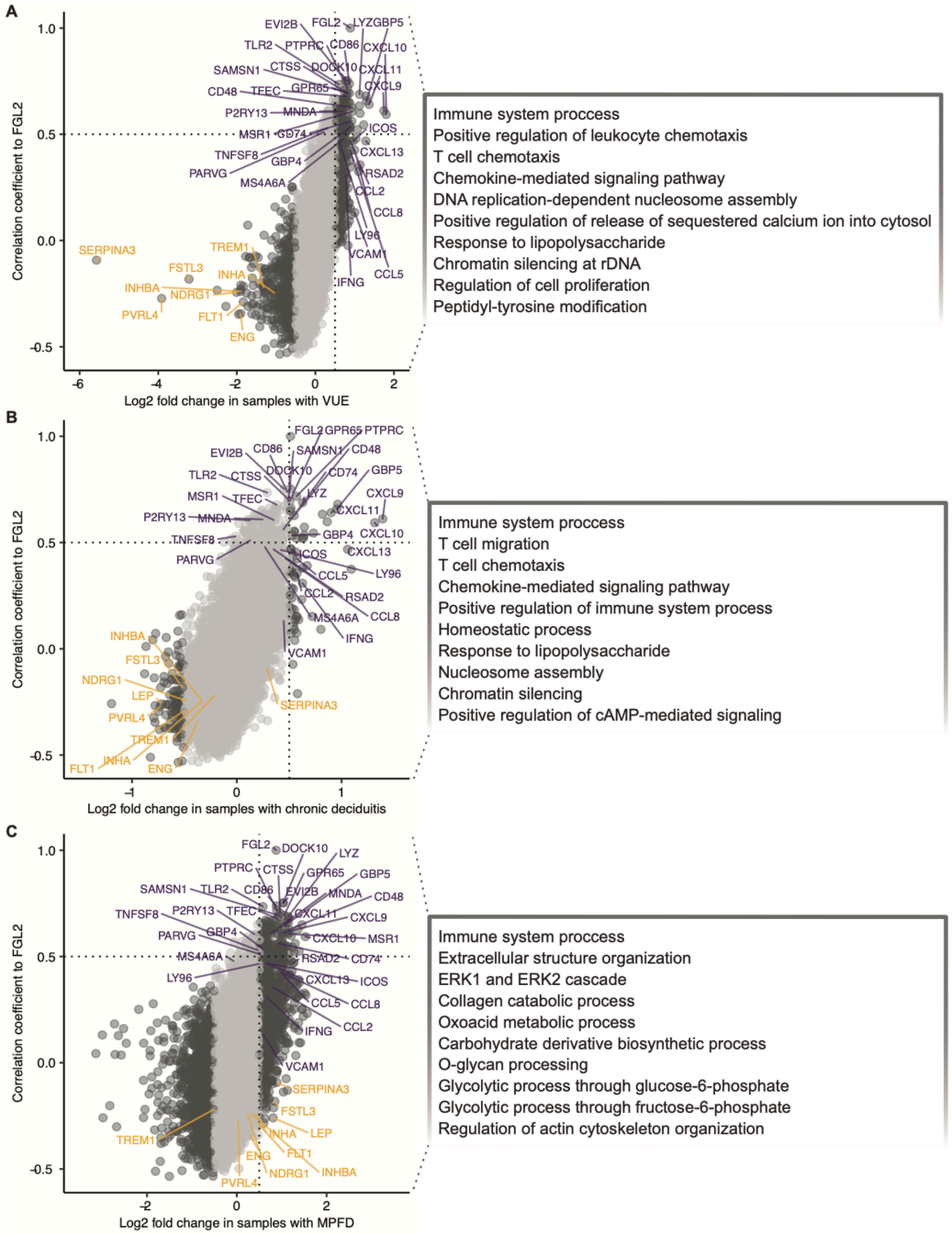

Figure 41: *FGL2*-associated transcriptional changes in placentas with chronic inflammation lesions. Differentially expressed genes in placentas with **A)** VUE, **B)** chronic deciduitis and **C)** MPFD (correlation coefficient to *FGL2* as a function of log2 fold-change in affected placentas). Genes of interest are labeled. For each lesion, GO terms presented are those significantly enriched in upregulated genes, listed from highest to lowest statistical significance.

suggesting they would be ineffective at identifying preeclamptic patients with these types of placental lesions/pathophysiology.

The transcriptional profile of placentas with MPFD was intriguing. Genes from the purple and tan modules, including IFNγ-induced genes and leukocyte and lymphocyte activation factors were upregulated. Similarly to the VUE and chronic deciduitis profiles, the majority of these genes correlated well with *FGL2* (**Figure 41C**), suggesting its contribution to fibrin deposition. Surprisingly, genes of the yellow module, including previously reported biomarkers of PE, were not downregulated, but upregulated or unchanged, as in placentas with MVM lesions, demonstrating that placentas with MPFD exhibit transcriptional characteristics of both chronic inflammation and MVM lesions. Gene ontology for genes upregulated in MPFD reflected this, with terms related to immune response but also to metabolic changes, similar to the terms enriched in yellow module genes (**Figure 41C**).

CHAPTER 6: DISCUSSION

6.1. Evolution and challenges of FGL2 detection and function

6.1.1. Challenges in FGL2 expression detection throughout the literature

When our work on FGL2 began, following its identification as a potential target of chromatin remodeller SNF2L[110], several commercially available antibodies were acquired, and their use optimized for detection by western blot or immunohistochemistry. We quickly noticed that they yielded wildly different results based on the target species (human or mouse), despite predicted cross-reactivity. We validated the species specificity of those antibodies by overexpressing human or mouse FGL2 in cell lines from the other species, and consequently used appropriate antibodies depending on the experiment and application. We eventually questioned the target specificity of our antibodies, starting with the one we used for all human tissues and cell lines. The single band appearing on the blot and the striking difference in intensity between HTR-8 and BeWo (**Figures 19, 20**) suggested optimized, reliable detection of the FGL2 protein. We also experienced reliability issues with primers for the detection of *FGL2* mRNA, but eventually designed pairs which were able to validate high efficiency and specificity. We soon noticed a striking difference between mRNA and protein expression of FGL2. While some amount of variation can normally be attributed to cell regulation of mRNA processing and degradation, or translation rate and protein stability, we had puzzling cases where no *FGL2* mRNA could be detected, but a strong, single band would be observed by western blot. These significant issues led to several years of unusable data, for example, in the case of an attempted *FGL2* knockout in the BeWo and

HTR-8/SVneo cell lines, where data was seemingly negative but knockout lines might have been successfully generated at some point.

Similarly, another FGL2 antibody routinely used for detection in mouse tissues or cell lines was doubtful. Despite testing many tissues, no clear negative control could be identified with this antibody. Serious doubts arose when we acquired *Fgl2*$^{ko/ko}$ mice, and their tissues appeared positive for FGL2, according to this antibody. Tissues from *Fgl2*$^{ko/tg}$ mice, however, displayed a strong increase in band intensity. We eventually confirmed knockout in these animals by making use of the insertion of the B-galactosidase gene into the first exon of *Fgl2* (**Figure 1**), showing that this antibody likely recognizes another unknown protein, as well as FGL2. Overall, our work led to the conclusion that most commercially available FGL2 antibodies are species and application-specific, if even detecting FGL2 at all.

The *Fgl2* gene and its transcription and translation products were characterized in the mouse, the rat and the human. For our species of interest, the mouse and the human, the resulting cDNA sequences are 82% homologous [84,134]. The proteins share 78% amino acid sequence identity, with high conservation of glycosylation and serine protease sites and fibrinogen-related domains, which suggests similar structure and function[84,87]. Despite these similarities, tissues that were deemed positive by northern blot or qPCR, in the literature, are not necessarily consistent between species. In the tissues where cell type specificity was assessed by *in situ* hybridization or immunohistochemistry, results also vary. We have not used northern blotting or *in situ* hybridization in our work on *Fgl2*, and therefore cannot prove or disprove them, but we remain skeptical of mRNA expression data

from earlier publications, considering our own difficulties with specificity. Tools developed in recent years, such as atlases of bulk or single-cell expression obtained by transcriptomics or proteomics, could help resolve these doubts. Meta-analyses and online tools based on them, such as Expression Atlas, which standardizes transcriptomics and proteomics data to present cell type, tissue and species-specific expression on their web tool, could also provide useful comparison of cell type, tissue and species specificity or commonality[135].

In any case, the specificity of all FGL2 detection methods should, in future studies involving this protein, be scrutinously validated before any conclusion is drawn. Any study based on published FGL2 literature should replicate data in-house, with validated methods, before basing any hypothesis on them.

6.1.2. Conflicting phenotypes of FGL2 function models

Importantly, numerous studies on the prothrombinase and immunosuppressive role of FGL2 were based on the phenotype resulting from *Fgl2* knockout in mice. Relevant to our studies, the original authors state a 40% reduction in $Fgl2^{ko/ko}$ pups from $Fgl2^{wt/ko}$ x $Fgl2^{wt/ko}$ mating pairs. A hemorrhage at the feto-maternal interface, observed at e7.5, is stated as the cause of embryo loss, which occurred at e8.5. While we did observe a significant subfertility in our $Fgl2^{ko/ko}$ colony (**Figure 2**), our study was done on $Fgl2^{ko/ko}$ x $Fgl2^{ko/ko}$ mating pairs, and as all offspring were homozygous, we did not conclude on preferential loss of embryos. We did not specifically assess conceptus morphology at e7.5, but we determined that the number of implantation sites at e5.5 and the number of fetuses at e18.5 are

similar, which contradicts the possibility of embryo loss due to placental hemorrhage, at e7.5. Examination of *Fgl2*$^{ko/ko}$ placentas at e18.5 did not show signs of hemorrhage either. Also in heterozygous matings, a subsequent paper from the same group reported neonatal deaths (also preferential to *Fgl2*$^{ko/ko}$ pups), in which mild cardiac dysfunction was observed, but no clear cause could be determined[98,99].

Interestingly, these findings of embryo or pup loss and their speculated causes are inconsistent throughout breeding cohorts of *Fgl2*$^{ko/ko}$ mice by the laboratory that generated them, and between laboratories[136]. Moreover, another laboratory generated *Fgl2*$^{ko/ko}$ mice and reported pups born at expected Mendalian ratios, as well as intact type 1 immunity and fibrin generation mechanisms[100]. These inconsistencies could reflect differences in knockout method, mouse background, breeding practices or analysis methods of fertility data. In any case, they are concerning for the hypotheses and research projects that were based on these data. Therefore, for our own studies, we ensured all experiments were done on the same mouse cohort and chose to apply regression analysis to remove as much as possible the effects of our lab's specific breeding protocols and experimental designs.

6.2. Ovarian FGL2 expression promotes luteal angiogenesis

Mammalian reproduction is a finely engineered machine made up of several moving parts that are sometimes individually, sometimes collectively regulated. The immune system carefully regulates immune cell populations in every reproductive tissue, contributing essential functional signals. Examples of this include the

modulation of Treg numbers in the ovary, in conjunction with fluctuating hormones throughout the menstrual cycle, the creation of an immunotolerant oviductal environment and importantly, crosstalk between maternal immune cells and trophoblast at the early maternal-fetal interface[34,137-139]. As FGL2 is a known immunomodulator, we aimed to determine which stage of the reproductive process is defective in mice that aberrantly express *Fgl2*.

The expression of FGL2 in ovarian stroma and theca cells and importantly, acquired in cumulus granulosa cells, first invoked the possibility of a role for FGL2 in the regulation of ovulation (**Figures 3 and 4**). Our investigation revealed that ovulation, induced or natural, was unaffected by lack or excess *Fgl2*, and we therefore turned to another possible role for theca cell expression of FGL2. Luteal angiogenesis originates in the theca cell layer, and macrophages polarized to an M2 phenotype accumulate there before migrating into the developing CL, secreting pro-angiogenic signals[13,15]. The rationale for essential involvement of FGL2 in luteal angiogenesis combines its immunomodulator (macrophage-polarizing) function with evidence that it promotes angiogenesis[96,109]. Dysfunctional corpora lutea, due to deficient vascularization, could explain the lower number of implantations detected at e5.5, in *Fgl2*$^{ko/ko}$ mice (**Figure 13A**)[4,14]. *Fgl2* knockout did not lead to a decrease in either M2 macrophage or vasculature density, as our hypothesis predicted (**Figures 8 and 10**). *Fgl2* overexpression, however, led to an increase in the density of both, hinting that our hypothesized angiogenesis regulation mechanism involving FGL2 is validated (**Figures 8 and 10**). This corresponds to the “luteal development” branch of the model for immune regulation of luteal angiogenesis put forward by

Shirasuna & Miyamoto[16] (see **1.1.1.**). While we did not directly show that neutrophils and M1 macrophages-secreted cytokines upregulate ovarian FGL2, as per the "luteal regression" branch, IFNγ and TNFα have been shown to do so in several other systems[86,90,91]. This is reminiscent of the mechanism we propose for the involvement of FGL2 in balancing the immune environment of the human placenta villous space: it is upregulated in response to inflammation (TNFα, IFNγ) and exerts immunosuppressive effects, which in this case, promotes angiogenesis. The lack of phenotype in *Fgl2*$^{ko/ko}$ CLs has several potential explanations. The number of CD206-positive cells in our ovary sections is very low even in *Fgl2*$^{wt/wt}$, potentially masking a difference in counts that could only be resolved by a higher sample size. There are also many known macrophage-independent regulation mechanisms of luteal angiogenesis. The initial signal, the LH surge, triggers directly or indirectly factors such as VEGFA, FGF2, fibronectin, PDGFB or Il-8, secreted from neutrophils as well as M2 macrophages[4]. Overall, this suggests that while FGL2 does contribute to promoting angiogenesis in the developing CL, its absence does not preclude it. It certainly would not be the only example, in reproductive biology, of mechanistic redundance.

6.3. Lack of FGL2 may diminish immunotolerance of the oviductal environment

Fluctuation of FGL2 levels through the estrous cycle suggests the possibility that ovarian steroid hormones directly regulate its expression. The oviductal epithelium, which expresses FGL2, also expresses ER and PR, which are mainly involved in oocyte transport[140,141]. Our preliminary experiments suggested this to be

true, but findings were difficult to confirm and interpret. We first attempted *ex vivo* culture of sections of the mouse oviduct, cultured for 0-48h with E2 or P4 at physiological concentrations, to mimic oviductal epithelium exposure to hormones. While immunohistochemistry results suggested stronger staining in the E2-treated sections, and weaker staining in the P4-treated sections, cell death and morphology changes due to culture conditions were too important for us to draw meaningful conclusions. In oviduct sections from mice that underwent long-term E2 exposure, stronger FGL2 staining was observed, but this result was confounded by the significant hyperplastic effect of E2 on the oviductal epithelium[142]. Lastly, we used OVE4, a primary mouse oviductal cell line, to determine the direct effect of E2 and P4 treatment on FGL2 expression and secretion. As our available antibodies for western blot do not reliably detect mouse FGL2, we assessed this by ELISA. Resulting media concentrations were above zero but below the detection limit that would confidently discriminate it from background. As the ciliated vs secretory features and markers of this cell line has not been fully characterized, we concluded that either the oviductal epithelium expresses and secretes too little FGL2 for detection, and neither E2 nor P4 significantly alters this, either OVE4 are too poor a model of the oviductal epithelium to reflect the *in vivo* situation. With the lack of an appropriate model, and therefore lack of evidence for direct regulation of FGL2 levels by either E2 nor P4, we turned to a functional characterization of lack or excess of FGL2 in the oviduct.

The reduction, in *Fgl2*$^{ko/ko}$ animals, of fertilization efficiency, is of notable interest from an immune regulation point of view. Oviductal fluid protein content

originates from both the vascular supply to the oviduct and secretory cell production. Composition fluctuates throughout the estrous cycle, regulated by hormones and immunity[34,138]. Interestingly, the presence of sperm, which carry antigens foreign to the maternal immune system, contributes to a shift in the immune component of the fluid, towards immunotolerance[23,143-145]. FGL2 has direct effects on activation status, apoptosis or cytokine secretion of several immune cell populations (see **1.2.1.**). While we have not investigated this mechanism yet, we hypothesize that in *Fgl2*$^{ko/ko}$ mice, lack of the immunosuppressive effect of FGL2 shifts the cytokine profile of the oviductal fluid, making the fertilization environment less tolerant to the presence of paternal antigens. As a result, fertilization efficiency is reduced.

6.4. Excess FGL2 contributes to fetal growth restriction through insufficient placental glycogen stores

Slightly reduced fetal to placental weight ratios in *Fgl2*$^{ko/tg}$ mice led us to investigate whether a placental lesion, defect or insufficiency contributed to the pups' low birthweight. A reduced ratio is commonly associated with placental insufficiency in both mice and humans[116,146-148]. The use of this ratio however has limitations, for example in the situation where both fetal and placental weights are low or high. Commonly, it is a measure of placental efficiency, meaning that placental growth reflects the metabolic needs of the fetus at all stages of pregnancy. A pregnancy with a low ratio will often present, upon placental examination, histological signs of an over-mature placenta.

Several placenta anatomical causes have been investigated for placental insufficiency, defined by a reduced capacity of the placenta to deliver oxygen and nutrients to the fetus, leading to fetal growth restriction[146]. Commonly, a decrease in volume of the syncytiotrophoblast subcompartment is observed, which results in a smaller total volume area for gas and nutrient exchange, as this syncytium forms the maternal-fetal interface. In this study, we did not examine labyrinth subcompartment volumes and volume ratios. A reduction in total Synl or Synll total volume, determined with markers specific to each layer, could provide an explanation to fetal growth restriction congruent with the literature.

Our stereological analysis of those placentas did not show altered compartment volume ratios but did however reveal a reduced volume of glycogen cells (GlyT) in *Fgl2*$^{ko/tg}$ placentas. Interestingly, a reduction of GlyT is often associated with fetal growth restriction, as shown in several mouse models[116,117]. It is thought that the mouse placenta stores glycogen as a source of glucose that can easily be mobilized, in periods of high fetal energy demands, although more evidence is needed to support this[117,149,150]. While offspring are viable when placentas are depleted of GlyT, they exhibit a growth restriction of 15-20%[151,152].

In our case, however, reduced numbers of junctional zone GlyT could be explained by their enhanced migration to the decidua. As the mouse pregnancy approaches term, massive migration of glycogen cells occurs from the junctional zone into the decidua. As our stereology analysis was done on e18.5 placentas, it's possible that the reduced proportion of GlyT found in the junctional zone is a proxy of their migration efficiency, which could be enhanced in *Fgl2*$^{ko/tg}$. Albeit in a very

different model system, the HTR-8/SVneo cell line, we have however shown that *FGL2* overexpression leads to decreased, not increased, migration (**Figure 21**). Additional staining could confirm volumes and volume ratios of glycogen cells found within the decidua. Examining placentas between e14.5 and e16.5, which have attained their definitive morphology but have not undergone massive trophoblast migration to the decidua or staining for markers of migratory vs. non-migratory GlyT, would allow us to conclude if this is an important factor or not, in this phenotype[153].

6.5. FGL2 mediates inflammation at the maternal-fetal interface

6.5.1. Interplay of inflammation and coagulation at the early maternal-fetal interface: a role for FGL2

The immune and hemostatic systems present significant overlap; induction of the coagulation cascade by inflammation has long been established, and in return, some components of clotting affect immune cells, by chemoattraction or physical interaction[154]. This relationship is particularly important when it comes to the question of success or failure of the establishment of pregnancy. While embryo loss can have a myriad of causes, and the condition of recurrent miscarriage is often idiopathic, coagulation almost always plays a role in the resorption of tissues. Coagulation dysfunction or overactivation has, additionally, often been studied in the context of pregnancy complications such as preeclampsia.

Tissue factor and other components of the coagulation cascade are necessary, at some level, to the establishment and successful completion of

pregnancy, but elevated levels were shown to have important negative consequences[155]. This concept of 'necessary in moderation' also applies to several immune cell types and inflammatory cytokines, whose presence at the maternal-fetal interface is essential to the establishment of pregnancy, but whose excess causes failure. It is therefore not surprising that the activation of those two systems, inflammatory and coagulatory, often co-occurs. FGL2 represents an interesting player on that field, since its prothrombinase role has been shown to be activated by inflammation. As an immunosuppressant, it also directly affects the level of inflammation, its own trigger, features that make it a prime regulatory candidate. Treating peritoneal macrophages with MHV-3, a coronavirus that can cause liver failure, upregulates an initially unidentified prothrombinase, leading to the discovery of *Fgl2*[89,90]*.* It was later determined that this upregulation also occurs in macrophages and endothelial cells of the liver, spleen and lung. Other inflammatory inducers of FGL2 include TNFα and IFNγ, which take on particular importance in the context of pregnancy and placental development.

In the initial papers concerned with the TNFα/ IFNγ-FGL2-fibrin axis in spontaneous abortion or preeclampsia, correlative expression of TNFα and FGL2 is shown in the decidua and possibly in the trophoblast. TNFα and IFNγ in synergy caused a strong upregulation of *Fgl2* mRNA. A clinical trial was even proposed, using an anti-FGL2 antibody to block the generation of fibrin, which would lift the hypothetical inhibition of trophoblast migration and invasion, preventing preeclampsia[90]. These initial data are dependent on the specificity and sensitivity of FGL2 detection methods, be it mRNA probes for *in situ* hybridization on tissues,

cDNA for northern blotting, primers for qPCR, or antibodies for western blotting or immunohistochemistry. We have discussed above why these data provide a good base for further investigation but should be interpreted with healthy skepticism.

6.5.2. Modelling the role of FGL2 in the establishment of pregnancy

As the aforementioned data suggest a major role of this inflammation-coagulation axis in success or failure of the establishment of pregnancy, we aimed to design experimental systems to delineate the precise contribution of FGL2 to this axis. In light of the discovery of *Fgl2* expression by trophoblast, we first planned to conduct embryo transfer experiments to determine if different effects were caused by an excess of FGL2 from fetal vs. maternal sources. We hypothesized, for example, that transferred *Fgl2*-overexpressing blastocysts to a pseudopregnant *Fgl2*$^{ko/ko}$ recipient mother would fail to implant or invade due to the immunosuppressive effect of FGL2 on immune populations of the maternal decidua. An FGL2-overexpressing mouse was not generated until 2015, at which point the bulk of FGL2 literature focused not on its role in spontaneous miscarriage, but in transplant tolerance/rejection or immunomodulation for cancer therapies[103,156]. It is not overly surprising, knowing its biochemical function, that a ubiquitous FGL2 overexpression was lethal due to massive thrombosis[101]. To circumvent this problem, the group that generated the model introduced a mutation at Ser89, the known serine protease of murine *Fgl2*, and therefore ubiquitously overexpressed a prothrombinase-null form of the FGL2 protein, and bred these on a *Fgl2*$^{ko/ko}$ background, to eliminate any endogenous contribution of FGL2 to coagulation.

Using these embryos in our transplant experiments would therefore ignore the fibrin deposition element of inflammation-induced miscarriage, and the biological significance of this experiment would be diminished.

We next attempted trophectoderm-specific overexpression of endogenous FGL2, directly in blastocysts[157-159]. We generated a full-length mouse *Fgl2* lentiviral expression vector, and successfully infected mouse cell lines, but encountered major technical difficulties when attempting to infect blastocysts and abandoned this experiment. This experiment could have helped answer the question of different effects of fetal or maternal FGL2 excess, but as we left intact the prothrombinase site of *Fgl2*, it could equally have resulted in failure of implantation due to thrombosis.

We resorted to using *Fgl2*$^{ko/tg}$ mice to examine the effect of its excess on the conceptus and the mature placenta. The caveat remains that any observed fibrin deposition cannot be attributed to excess FGL2. We determined, however, that FGL2 is expressed, in the mouse placenta, by various TGC lineages, and by circulating maternal leukocytes. In the human placenta, expression was evident in the cytotrophoblast, syncytiotrophoblast and again, in maternal circulating leukocytes. Overall, this suggests that FGL2 expression can be induced by inflammation in both the maternal and the fetal compartments. The prevalent expression by the syncytiotrophoblast, in the human placenta, led us to directly investigate the effect on FGL2 of inflammatory cytokines involved in the pathology of preeclampsia.

6.5.3. Effect of inflammation on mature placental function

The evidence for involvement of inflammatory cytokines TNFα and IFNγ in the pathology of preeclampsia precedes our own group's data involving them specifically in an immunological disease subclass. Several studies state the upregulation of TNFα in PE (serum or placental tissue), at least partly through activation of NF-KB[160-163].

It is sometimes stated as a direct cause of endothelial and trophoblast dysfunction, by decreasing migration/invasion[164]. In our group's identification of disease subclasses, in a gene expression dataset of preeclamptic and non-preeclamptic samples, *TNF* expression was enriched in preeclamptic samples of cluster 3 compared to preeclamptic samples of clusters 1 and 2[74]. IFNγ is also known to be upregulated in PE, although it is important to note that it is also present in healthy pregnancies[165-168]. In general, the studies that consider both cytokines conclude that their expression correlates. Their synergistic effects have been examined in some studies. TNFα and IFNγ are of course not the only inflammatory cytokines that could be at cause in trophoblast/endothelial cell dysfunction in preeclampsia. Although they are not the focus of this study, examples of such cytokines, some of which interplay with TNFα and IFNγ include IL-1, IL-6, IL-8, IL-12, TGF-B[161,167,169-171]. These findings, along with the correlative relationship between the cytokines and FGL2 previously observed in murine reproductive tissues enticed us to investigate it in human trophoblast cell lines.

In HTR-8/SVneo, we did not find that either IFNγ or TNFα reliably induced *FGL2* expression. Both cytokines did induce *FGL2* expression in BeWo, but the magnitude of this change was relatively small. Both cytokines have also been determined to inhibit syncytialization *in vivo*, and our own data supports this, although the strength of evidence varies with different markers of syncytialization. However, we found that an excess of FGL2 could rescue this inhibition, as shown by the induction of syncytium-specific genes. The transformed cell line nature of BeWo is likely a factor in the strength and consistency of this phenotype. Therefore, combining this *in vitro* evidence with our analysis of *in vivo* gene expression in the term placenta led us to propose a function for FGL2 in the villous space: increasing FGL2 in the syncytiotrophoblast is a protective physiological mechanism attempting to re-establish immune equilibrium. FGL2 is induced by inflammation and exerts immunosuppressive effects to try and decrease this inflammation at the maternal (immune)-fetal (trophoblast) interface. In the future, further mechanistic studies could firmly establish causes and effects in this immunoregulation cycle. The use of primary human trophoblast, explants, organoids or trophoblast stem cells could be warranted, to better reflect *in vivo* villous space biology.

6.6. *FGL2*-associated transcriptional and histopathological features of immunological preeclampsia

6.6.1. *FGL2* is differentially expressed between transcriptional clusters

The clinical presentation and placental pathology observed in cases of PE exhibit notable heterogeneity. Increasingly, it is becoming apparent that no one paradigm for the pathogenesis of PE can explain all cases, and no one biomarker can identify them all. Our group has proposed this is due to the existence of disease subtypes with divergent underlying placental pathophysiology, as supported by the identification of distinct patient clusters with high clinical, transcriptional, and histopathological similarities[74,75,81]**.** Investigation of cluster-specific expression patterns of genes and gene networks will help tease apart these distinct physiological processes and importantly, point to potential unique, subtype-specific biomarkers and/or therapeutic targets.

In our cohort, placental *FGL2* expression could not discriminate between clinical groups based on diagnosis, but was different among previously described transcriptional clusters, particularly high in cluster 3/immunological PE. Immunological PE represents a newly described disease subtype with a pathology that likely diverges from the traditional paradigm of PE. It has a transcriptional profile consistent with profound immune activation, and a histological profile indicative of maternal-fetal interface disturbances and chronic inflammation[74,75,81]. The known prothrombinase activity of FGL2 suggests that its excess in affected placentas could contribute to increased fibrin deposition, consistent with findings of MPFD in cluster 3/immunological PE placentas, while its immunomodulatory function could contribute to, or be elevated as a result of the activation of immune pathways[90,96,101].

Considering this, investigation into the role of FGL2 in pathogenesis in this group of patients is warranted.

6.6.2. *FGL2* is part of a gene module differentially enriched between PE disease subtypes

To better situate the molecular role of FGL2 within the PE subtypes, we applied network analysis, a common method to identify, without bias, functionally relevant groups of genes based on their co-expression across samples[112]. Our approach of module enrichment in diagnostic groups identified gene sets that drive the distinct placental phenotypes observed. The structure of module clustering revealed that immune-focused modules represent the gene sets with the largest difference in enrichment across diagnostic groups. This analysis indicated that *FGL2* is situated within a highly discriminating module, the purple module. Hub genes from the purple module and the other immune-focused modules are likely drivers of the inflammatory phenotype observed in the preeclamptic samples of transcriptional cluster 3 (immunological PE). *FGL2* was found on the periphery of the purple module network rather than centrally and highly connected, suggesting that inflammatory pathways driven by these hub genes converge on the observed upregulation of *FGL2.* While this analysis does not constitute evidence of a cause-and-effect relationship between *FGL2* and important immune mediators, this network structure and the identification of *FGL2*'s closest correlation neighbors provide the basis for future, more mechanistic studies of the involvement of *FGL2* in the distinct pathogenesis of immunological PE.

Anti-angiogenic factors sFLT and sENG have long been suggested as potential biomarkers of PE and were determined to be highly and consistently upregulated in our canonical PE samples[68,74]. Several other candidate biomarkers have been proposed over the years, and a panel of such genes was found within the yellow module of our network analysis. GO terms enriched in the yellow module mostly related to metabolism and response to hypoxia, which is consistent with the traditional paradigm for the pathology of preeclampsia and with previously conducted gene set enrichment analysis on the clusters of this cohort[75]. The lack of enrichment of this particular module in immunological PE samples, coupled with strong enrichment of immune-specific ones, further supports the hypothesis that women affected by different PE subtypes cannot be identified by the same biomarkers.

6.6.3. *FGL2* poorly associates with pregnancy outcome parameters in PE pregnancies

Severity of pregnancy outcomes varies across clusters-maternal symptoms tend to be more severe in canonical while several fetal outcomes are worse in immunological PE. The overall trend for a single parameter is driven by the largest group, canonical PE samples, while the pattern of *FGL2* expression is opposite between subtypes. We believe this opposition explains the poor correlations we observed between placental *FGL2* and parameters of pregnancy outcomes.

6.6.4. *FGL2*, chronic inflammatory lesions and the maternal rejection response

A recent study from our group has shown overall concordance between transcriptional and histological clustering of samples, suggesting that diagnostic group-specific gene expression patterns, described here, translate to visible changes in placental pathology[81]. MVM lesions are commonly associated with a diagnosis of PE[132,172]. In our cohort, many of them, including DVH, placental infarctions, advanced villous maturity and syncytial knots, were determined to be prevalent in cluster 2/canonical PE placentas[75,81]. The transcriptional profiles that we obtained for placentas affected by these lesions were consistent with the anti-angiogenic/hypoxic paradigm for the pathology of the disease. Further, a panel of previously investigated biomarkers of PE (including *FLT1* and *ENG*), observed in the yellow module of our network analysis, was consistently upregulated while *FGL2* was consistently downregulated in MVM-affected placentas.

Chronic inflammatory lesions of the placenta are distinct from acute, infectious lesions in that the cause of the immune insult is often unknown[132,133]. In our assessment, these include villitis of unknown etiology (VUE), chronic deciduitis, and chronic intervillositis. VUE is relatively common (5-15%), moderately recurrent (25-50%), and is associated with IUGR and intra-uterine/neonatal morbidity or mortality[132,133,173,174]. The hypothesis that VUE is the manifestation of maternal immune rejection of the fetoplacental unit is currently favored in the literature: it is characterized by infiltration of maternal T lymphocytes (CD3+, CD4+, CD8+ and/or Tregs) within the villous stroma, expansion of the fetal Hofbauer cells (intravillous fetal histiocytes), increased maternal monocytes/macrophages within the villous

space and a skewed Th1/Th2 cytokine profile[174-176]. Importantly, in affected placentas, expression of MHC class ll (HLA) molecules has been observed in the syncytiotrophoblast, which is normally devoid of it. This abnormal expression can be induced by excessive IFNγ[175-177]. A number of hub genes from highly discriminating immune modules were upregulated in VUE placentas, where we also observed several IFNγ-induced genes and several *HLA* genes, which exhibited remarkable correlation to *FGL2*. These findings are suggestive of an IFNγ-mediated maternal rejection response in placentas affected by VUE, and suggest that *FGL2* is involved in this response. Chronic deciduitis is characterized by lymphocytic infiltrates (largely plasma cells) within the decidua, and is associated with preterm labor. It sometimes co-occurs with VUE, and transcriptional and immune cell profiles of placentas with these lesions present a significant overlap[133,175,178]. Our data aligns with these reports, as generally, the *FGL2*-associated transcriptional changes seen in VUE, indicative of a maternal rejection phenotype, were also observed in chronic deciduitis. Strikingly, the transcriptional profiles of both chronic inflammation lesions investigated revealed that in addition to upregulated *FGL2* and maternal rejection-related genes, a panel of previously investigated PE biomarkers was downregulated. Since this type of lesions is more prevalent in PE subtype 3/immunological PE, this suggest that the clinical use of any of these known markers would lead to the omission of patients affected by immunological PE.

Chronic inflammation lesions are often associated with increased perivillous fibrin deposition, sometimes severe enough to warrant a diagnosis of MPFD. It's been hypothesized that immune insult in MPFD leads to syncytial injury and repair

through fibrin deposition. This loss of integrity of the syncytial layer may be at cause in allowing for villous infiltration of maternal T lymphocytes, in placentas affected by chronic inflammation lesions, which would provide a physiopathological link between the two types of lesions[133,174,179]. Along with the immunological basis for the pathogenesis of MPFD, a theory of imbalance between angiogenic and antiangiogenic factors exists[71]. Our data, interestingly, supports both the immune dysfunction and the angiogenic imbalance hypotheses for this pathology. While *FGL2* and several correlated immune genes were upregulated in the MPFD profile, the panel of previously investigated PE biomarkers was upregulated or unchanged in affected placentas, contrarily to the VUE/chronic deciduitis profile. The maternal rejection response towards the fetoplacental unit, present in chronic inflammation lesions, could also be at cause in the upregulation of *FGL2,* given the known role of *FGL2* in promoting allograft tolerance. The prothrombinase activity of FGL2 has been observed in several studies, where an increase in FGL2 caused increased fibrin deposition in systems like joints and microvasculature, in response to inflammatory stimulation[104,180]. We therefore propose that *FGL2* upregulation collaterally promotes fibrin deposition within the villous space.

6.7. Conclusion

The female reproductive tract is the theater of several immune adaptations to ensure the possibility of the establishment of a pregnancy. Previous literature on prothrombinase and immunomodulator Fibrinogen-like protein 2 (FGL2) suggested its involvement in a number of these adaptations.

We first demonstrated its patterns of expression in the ovary and oviduct, through the mouse estrous cycle. Although neither lack (knockout) or excess (overexpression) affected ovulation capacity, we have shown that it contributes to efficient luteal angiogenesis, in support of pregnancy establishment. Lack of FGL2 diminishes fertilization efficiency, likely through lack of immunosuppression in the oviduct, at the time of gamete presence. In the mouse placenta, an excess of FGL2 results in lower abundance of glycogen trophoblast, possibly contributing to lower placental efficiency and smaller fetuses.

In the human placenta, the localization of FGL2 expression to the cytotrophoblast and syncytiotrophoblast warranted our investigation of its function and role. In other systems, *FGL2* can be upregulated by pro-inflammatory cytokines TNFα and IFNγ, which we have shown are at high levels in an immunological subtype of preeclampsia and its associated lesions. We propose that this upstream signal upregulates FGL2 in the cytotrophoblast/syncytiotrophoblast, as a physiological attempt at re-establishing an appropriate immune equilibrium. Our evidence that overexpressed *FGL2* in forskolin-induced BeWo can rescue the deleterious effect of inflammatory cytokines supports this. It is therefore likely that, considering its immunosuppressive capacity, high *FGL2* expression dampens the immune response and contributes to pregnancy maintenance, even in unfavorable, inflammatory conditions. Our finding that previously investigated PE biomarkers would be poorly predictive of the presence of chronic inflammation lesions, common in immunological PE, highlights the need for subtype-specific biomarkers. *FGL2*-associated transcriptional evidence of a maternal rejection phenotype in these

lesions indicate that, as a subtype-discriminating secreted factor, FGL2 is a promising candidate.

REFERENCES

1. Usadi, R. S. *et al.* Endometrial development and function in experimentally induced luteal phase deficiency. *The Journal of Clinical Endocrinology & Metabolism* **93,** 4058–4064 (2008).
2. Cha, J., Sun, X. & Dey, S. K. Mechanisms of implantation: strategies for successful pregnancy. *Nat Med* **18,** 1754–1767 (2012).
3. Davis, J. S. & LaVoie, H. A. in *The Ovary* 237–253 (Elsevier, 2019). doi:10.1016/B978-0-12-813209-8.00015-7
4. Robinson, R. S. & Woad, K. J. in *The Life Cycle of the Corpus Luteum* 1–21 (Springer, Cham, 2017). doi:10.1007/978-3-319-43238-0_1
5. Duffy, D. M., Ko, C., Jo, M., Brannstrom, M. & Curry, T. E. Ovulation: Parallels with Inflammatory Processes. *Endocr. Rev.* **40,** 369–416 (2019).
6. Gilbert, I., Robert, C., Dieleman, S., Blondin, P. & Sirard, M.-A. Transcriptional effect of the LH surge in bovine granulosa cells during the peri-ovulation period. *Reproduction* **141,** 193–205 (2011).
7. Wissing, M. L. *et al.* Identification of new ovulation-related genes in humans by comparing the transcriptome of granulosa cells before and after ovulation triggering in the same controlled ovarian stimulation cycle. *Human Reproduction* **29,** 997–1010 (2014).
8. Brannstrom, M. & Enskog, A. Leukocyte networks and ovulation. *Journal of Reproductive Immunology* **57,** 47–60 (2002).
9. Acosta, T. J. & Miyamoto, A. Vascular control of ovarian function: ovulation, corpus luteum formation and regression. *Anim. Reprod. Sci.* **82-83,** 127–140 (2004).
10. Kim, J., Bagchi, I. C. & Bagchi, M. K. Signaling by hypoxia-inducible factors is critical for ovulation in mice. *Endocrinology* **150,** 3392–3400 (2009).
11. Ozerdem, U. & Stallcup, W. B. Early contribution of pericytes to angiogenic sprouting and tube formation. *Angiogenesis* **6,** 241–249 (2003).
12. Robinson, R. S. *et al.* Angiogenesis and vascular function in the ovary. *Reproduction* **138,** 869–881 (2009).
13. Turner, E. C. *et al.* Conditional ablation of macrophages disrupts ovarian vasculature. *Reproduction* **141,** 821–831 (2011).
14. Care, A. S. *et al.* Macrophages regulate corpus luteum development during embryo implantation in mice. *J. Clin. Invest.* **123,** 3472–3487 (2013).
15. Woad, K. J. & Robinson, R. S. Luteal angiogenesis and its control. *Theriogenology* **86,** 221–228 (2016).
16. Shirasuna, K. & Miyamoto, A. in *The Life Cycle of the Corpus Luteum* (ed. Meidan, R.) **31,** 99–116 (Springer, Cham, 2017).

17. Leese, H. J. *et al.* Female reproductive tract fluids: composition, mechanism of formation and potential role in the developmental origins of health and disease. *Reprod. Fertil. Dev.* **20,** 1–8 (2007).
18. Ulbrich, S. E., Kettler, A. & Einspanier, R. Expression and localization of estrogen receptor α, estrogen receptor β and progesterone receptor in the bovine oviduct in vivo and in vitro. *J. Steroid Biochem. Mol. Biol.* **84,** 279–289 (2003).
19. Ghosh, A., Syed, S. M. & Tanwar, P. S. In vivogenetic cell lineage tracing reveals that oviductal secretory cells self-renew and give rise to ciliated cells. *Development* **144,** 3031–3041 (2017).
20. Barton, B. E. *et al.* Roles of steroid hormones in oviductal function. *Reproduction* **159,** 125–137 (2019).
21. Tone, A. A. *et al.* Gene expression profiles of luteal phase fallopian tube epithelium from BRCA mutation carriers resemble high-grade serous carcinoma. *Clin Cancer Res* **14,** 4067–4078 (2008).
22. Pérez-Cerezales, S. *et al.* The oviduct: from sperm selection to the epigenetic landscape of the embryo. *Biology of Reproduction* **98,** 262–276 (2018).
23. Hess, A. P. *et al.* The human oviduct transcriptome reveals an anti-inflammatory, anti-angiogenic, secretory and matrix-stable environment during embryo transit. *Reproductive BioMedicine Online* **27,** 423–435 (2013).
24. Yousef, M. S. *et al.* Sperm Binding to Oviduct Epithelial Cells Enhances TGFB1 and IL10 Expressions in Epithelial Cells as Well as Neutrophils In Vitro: Prostaglandin E2 As a Main Regulator of Anti-Inflammatory Response in the Bovine Oviduct. *PLoS ONE* **11,** 1–19 (2016).
25. Maillo, V. *et al.* Oviductal response to gametes and early embryos in mammals. *Reproduction* **152,** R127–R141 (2016).
26. Sakkas, D., Ramalingam, M., Garrido, N. & Barratt, C. L. R. Sperm selection in natural conception: what can we learn from Mother Nature to improve assisted reproduction outcomes? *Human Reproduction Update* **21,** 711–726 (2015).
27. Parada-Bustamante, A. *et al.* The role of mating in oviduct biology. *Mol. Reprod. Dev.* **83,** 875–883 (2016).
28. Muro, Y. *et al.* Behavior of Mouse Spermatozoa in the Female Reproductive Tract from Soon after Mating to the Beginning of Fertilization1. *Biology of Reproduction* **94,** 1–7 (2016).
29. Suarez, S. S. Mammalian sperm interactions with the female reproductive tract. *Cell Tissue Res.* **363,** 185–194 (2016).

30. Robertson, S. A. Seminal plasma and male factor signalling in the female reproductive tract. *Cell Tissue Res.* **322,** 43–52 (2005).
31. Tremellen, K. P., Seamark, R. F. & Robertson, S. A. Seminal Transforming Growth Factor β1, Stimulates Granulocyte-Macrophage Colony-Stimulating Factor Production and Inflammatory Cell Recruitment in the Murine Uterus1. *Biology of Reproduction* **58,** 1217–1225 (1998).
32. Robertson, S. A., Guerin, L. R., Moldenhauer, L. M. & Hayball, J. D. Activating T regulatory cells for tolerance in early pregnancy — the contribution of seminal fluid. *Journal of Reproductive Immunology* **83,** 109–116 (2009).
33. Bromfield, J. J. *et al.* Maternal tract factors contribute to paternal seminal fluid impact on metabolic phenotype in offspring. *Proc. Natl. Acad. Sci. U.S.A.* **111,** 2200–2205 (2014).
34. Marey, M. A. *et al.* Local immune system in oviduct physiology and pathophysiology: attack or tolerance? *Domest. Anim. Endocrinol.* **56,** 204–211 (2016).
35. Gamage, T. K., Chamley, L. W. & James, J. L. Stem cell insights into human trophoblast lineage differentiation. *Human Reproduction Update* **23,** 77–103 (2016).
36. Knöfler, M. *et al.* Human placenta and trophoblast development: key molecular mechanisms and model systems. *Cellular and Molecular Life Sciences* **94,** 1–18 (2019).
37. Burton, G. J., Jauniaux, E. & Watson, A. L. Maternal arterial connections to the placental intervillous space during the first trimester of human pregnancy: The Boyd Collection revisited. *The American Journal of Obstetrics & Gynecology* **181,** 718–724 (1999).
38. Burton, G. J., Watson, A. L., Hempstock, J., Skepper, J. N. & Jauniaux, E. Uterine glands provide histiotrophic nutrition for the human fetus during the first trimester of pregnancy. *The Journal of Clinical Endocrinology & Metabolism* **87,** 2954–2959 (2002).
39. Kaufmann, P., Benirschke, K. & Baergen, R. N. *Pathology of the Human Placenta*. 1–1069 (2006).
40. Foidart, J.-M., Hustin, J.-M., Dubois, M. & Schaaps, J.-P. The Human Placenta Becomes Haemochorial at the 13th Week of Pregnancy. *Int. J. Dev. Biol.* **36,** (1992).
41. Pijnenborg, R., Vercruysse, L., Placenta, M. H. The uterine spiral arteries in human pregnancy: facts and controversies. *Elsevier (*2006)

42. Bevilacqua, E., Lorenzon, A. R., Bandeira, C. L. & Hoshida, M. S. *Biology of the Ectoplacental Cone*. *The Guide to Investigation of Mouse Pregnancy* 113–124 (Elsevier, 2014). doi:10.1016/B978-0-12-394445-0.00010-2
43. Hemberger, M., Hanna, C. W. & Dean, W. Mechanisms of early placental development in mouse and humans. *Nat. Rev. Genet.* **204,** 193 (2019).
44. Simmons, D. G. *12 – Postimplantation Development of the Chorioallantoic Placenta*. *The Guide to Investigation of Mouse Pregnancy* 143–161 (Elsevier, 2014). doi:10.1016/B978-0-12-394445-0.00012-6
45. Carter, A. M. Animal models of human pregnancy and placentation: alternatives to the mouse. *Reproduction* **160,** R129–R143 (2020).
46. Zhou, Y. *et al.* Human cytotrophoblasts adopt a vascular phenotype as they differentiate. A strategy for successful endovascular invasion? *J. Clin. Invest.* **99,** 2139–2151 (1997).
47. Expression and Activity of Matrix Metalloproteinase 2 and 9 in Human Trophoblasts. *Placenta* **24,** 53–64 (2003).
48. Loke, Y. W. & King, A. Immunology of human implantation: an evolutionary perspective. *Human Reproduction* **11,** 283–286 (1996).
49. van Mourik, M. S. M., Macklon, N. S. & Heijnen, C. J. Embryonic implantation: cytokines, adhesion molecules, and immune cells in establishing an implantation environment. *J Leukoc Biol* **85,** 4–19 (2009).
50. Lash, G. E., Robson, S. C. & Bulmer, J. N. Review: Functional role of uterine natural killer (uNK) cells in human early pregnancy decidua. *Placenta* **31,** S87–S92 (2010).
51. Robson, A. *et al.* Uterine natural killer cells initiate spiral artery remodeling in human pregnancy. *The FASEB Journal* **26,** 4876–4885 (2012).
52. Chakraborty, C., Gleeson, L. M., McKinnon, T. & Lala, P. K. Regulation of human trophoblast migration and invasiveness. *Can. J. Physiol. Pharmacol.* **80,** 116–124 (2002).
53. Hanna, J. *et al.* Decidual NK cells regulate key developmental processes at the human fetal-maternal interface. *Nat Med* **12,** 1065–1074 (2006).
54. Mi, S. *et al.* Syncytin is a captive retroviral envelope protein involved in human placental morphogenesis. *Nature* **403,** 785–789 (2000).
55. Evain-Brion, D. & Malassine, A. Human placenta as an endocrine organ. *Growth Hormone & IGF Research* **13,** S34–S37 (2003).
56. Shi, Q. J., Lei, Z. M., Rao, C. V., Endocrinology, J. L.1993. Novel role of human chorionic gonadotropin in differentiation of human cytotrophoblasts. *academic.oup.com*

57. Mayhew, T. M. Turnover of human villous trophoblast in normal pregnancy: what do we know and what do we need to know? *Placenta* **35,** 229–240 (2014).
58. Burton, G. J. & Jones, C. J. P. Syncytial Knots, Sprouts, Apoptosis, and Trophoblast Deportation from the Human Placenta. *Taiwanese Journal of Obstetrics and Gynecology* **48,** 28–37 (2009).
59. Smith, S. D., Dunk, C. E., Aplin, J. D., of, L. H. T. A. J.2009. Evidence for immune cell involvement in decidual spiral arteriole remodeling in early human pregnancy. *Elsevier*
60. Gauster, M., Moser, G., Orendi, K. & Huppertz, B. Factors Involved in Regulating Trophoblast Fusion: Potential Role in the Development of Preeclampsia. *Placenta* **30,** 49–54 (2009).
61. Dunk, C. E. *et al.* The Molecular Role of Connexin 43 in Human Trophoblast Cell Fusion. *Biology of Reproduction* **86,** 115–115 (2012).
62. Holder, B. S., Tower, C. L., Abrahams, V. M. & Aplin, J. D. Syncytin 1 in the human placenta. *Placenta* **33,** 460–466 (2012).
63. Parks, W. T. in *Pathology of the Placenta* **7,** 131–137 (Springer, Cham, 2019).
64. Task Force on Hypertension in Pregnancy. *Hypertension in Pregnancy*. 1–100 (2014).
65. Ness, R. B. & Roberts, J. M. Heterogeneous causes constituting the single syndrome of preeclampsia: A hypothesis and its implications. *The American Journal of Obstetrics & Gynecology* **175,** 1365–1370 (1996).
66. Steegers, E. A., Dadelszen, Von, P., Duvekot, J. J. & Pijnenborg, R. Pre-eclampsia. *The Lancet* **376,** 631–644 (2010).
67. Eastabrook, G., Brown, M. & Sargent, I. The origins and end-organ consequence of pre-eclampsia. *Best Practice & Research Clinical Obstetrics & Gynaecology* **25,** 435–447 (2011).
68. Levine, R. J. *et al.* Circulating Angiogenic Factors and the Risk of Preeclampsia. *The New England Journal of Medicine* **350,** 672–683 (2009).
69. Staff, A. C. *et al.* Redefining preeclampsia using placenta-derived biomarkers. *Hypertension* **61,** 932–942 (2013).
70. Maynard, S. E. *et al.* Excess placental soluble fms-like tyrosine kinase 1 (sFlt1) may contribute to endothelial dysfunction, hypertension, and proteinuria in preeclampsia. *J. Clin. Invest.* **111,** 649–658 (2003).
71. Whitten, A. E. *et al.* Evidence of an imbalance of angiogenic/antiangiogenic factors in massive perivillous fibrin deposition (maternal floor infarction): a placental lesion associated with recurrent miscarriage and fetal death.

American Journal of Obstetrics and Gynecology **208,** 310.e1–310.e11 (2013).

72. Romero, R. *et al.* Maternal Floor Infarction/Massive Perivillous Fibrin Deposition: A Manifestation of Maternal Antifetal Rejection? *Am J Reprod Immunol* **70,** 285–298 (2013).
73. Zhou, Y. *et al.* Vascular Endothelial Growth Factor Ligands and Receptors That Regulate Human Cytotrophoblast Survival Are Dysregulated in Severe Preeclampsia and Hemolysis, Elevated Liver Enzymes, and Low Platelets Syndrome. *The American Journal of Pathology* **160,** 1405–1423 (2002).
74. Leavey, K., Bainbridge, S. A. & Cox, B. J. Large Scale Aggregate Microarray Analysis Reveals Three Distinct Molecular Subclasses of Human Preeclampsia. *PLoS ONE* **10,** 1–21 (2015).
75. Leavey, K. *et al.* Unsupervised Placental Gene Expression Profiling Identifies Clinically Relevant Subclasses of Human Preeclampsia. *Hypertension* **68,** 137–147 (2016).
76. Roberts, J. M. & Hubel, C. A. The two stage model of preeclampsia: variations on the theme. *Placenta* **30 Suppl A,** S32–7 (2009).
77. Staff, A. C. The two-stage placental model of preeclampsia: An update. *Journal of Reproductive Immunology* **134-135,** 1–10 (2019).
78. Rana, S., Lemoine, E., Granger, J. P. & Karumanchi, S. A. Compendium on the Pathophysiology and Treatment of Hypertension Preeclampsia. *Circulation Research* 1094–1112 (2019).
79. Tan, M. Y. *et al.* Screening for pre-eclampsia by maternal factors and biomarkers at 11-13 weeks' gestation. *Ultrasound Obstet Gynecol* **52,** 186–195 (2018).
80. Stepan, H., Hund, M. & Andraczek, T. Combining Biomarkers to Predict Pregnancy Complications and Redefine Preeclampsia. *Hypertension* **75,** 918–926 (2020).
81. Benton, S. J., Leavey, K., Grynspan, D., Cox, B. J. & Bainbridge, S. A. The clinical heterogeneity of preeclampsia is related to both placental gene expression and placental histopathology. *American Journal of Obstetrics and Gynecology* **219,** 604.e1–604.e25 (2018).
82. Parr, R. L. *et al.* Association of mouse fibrinogen-like protein with murine hepatitis virus-induced prothrombinase activity. *Journal of Virology* **69,** 5033–5038 (1995).
83. Koyama, T., Hall, L. R., Haser, W. G., Tonegawa, S. & Saito, H. Structure of a cytotoxic T-lymphocyte-specific gene shows a strong homology to fibrinogen beta and gamma chains. *Proceedings of the National Academy of Sciences* **84,** 1609–1613 (1987).

84. Yuwaraj, S., Ding, J., Liu, M., Marsden, P. A. & Levy, G. A. Genomic Characterization, Localization, and Functional Expression of FGL2, the Human Gene Encoding Fibroleukin: A Novel Human Procoagulant. *Genomics* **71,** 330–338 (2001).
85. Rüegg, C. & Pytela, R. Sequence of a human transcript expressed in T-lymphocytes and encoding a fibrinogen-like protein. *Gene* **160,** 257–262 (1995).
86. Marazzi, S. *et al.* Characterization of Human Fibroleukin, a Fibrinogen-Like Protein Secreted by T Lymphocytes. *J Immunol* **161,** 138–147 (1998).
87. Levy, G. A. *et al.* Molecular and Functional Analysis of the Human Prothrombinase Gene (HFGL2) and Its Role in Viral Hepatitis. *The American Journal of Pathology* **156,** 1217–1225 (2000).
88. Liu, H. *et al.* Characterization of fibrinogen-like protein 2 (FGL2): Monomeric FGL2 has enhanced immunosuppressive activity in comparison to oligomeric FGL2. *International Journal of Biochemistry and Cell Biology* **45,** 408–418 (2013).
89. Ding, J. W. *et al.* Fulminant hepatic failure in murine hepatitis virus strain 3 infection: tissue-specific expression of a novel fgl2 prothrombinase. *Journal of Virology* **71,** 9223–9230 (1997).
90. Knackstedt, M. *et al.* Activation of the Novel Prothrombinase, fgl2, as a Basis for the Pregnancy Complications Spontaneous Abortion and Pre-eclampsia. *Am J Reprod Immunol* **46,** 196–210 (2001).
91. Clark, D. A. *et al.* The Emerging Role of Immunoregulation of Fibrinogen-Related Procoagulant Fg12. *Am J Reprod Immunol* **52,** 37–43 (1999).
92. Clark, D. A., Ding, J. W., Yu, G., Levy, G. A. & Gorczynski, R. M. Fgl2 prothrombinase expression in mouse trophoblast and decidua triggers abortion but may be countered by OX-2. *Molecular Human Reproduction* **7,** 185–194 (2001).
93. Chan, C. W. Y. *et al.* Kinetic Analysis of a Unique Direct Prothrombinase, fgl2, and Identification of a Serine Residue Critical for the Prothrombinase Activity. *J Immunol* **168,** 5170–5177 (2002).
94. Chan, C. W. Y. *et al.* Soluble fibrinogen-like protein 2/fibroleukin exhibits immunosuppressive properties: suppressing T cell proliferation and inhibiting maturation of bone marrow-derived dendritic cells. *J Immunol* **170,** 4036–4044 (2003).
95. Knackstedt, M. *et al.* Th1 Cytokines and the Prothrombinase fgl2 in Stress-triggered and Inflammatory Abortion. 1–11 (2003).

96. Shalev, I. *et al.* Targeted Deletion of fgl2 leads to impaired regulatory T cell activity and development of autoimmune glomerulonephritis. *J Immunol* **180,** 249–260 (2008).
97. Marsden, P. A. *et al.* The Fgl2/fibroleukin prothrombinase contributes to immunologically mediated thrombosis in experimental and human viral hepatitis. *J. Clin. Invest.* **112,** 58–66 (2003).
98. Clark, D. A. *et al.* The fgl2 prothrombinase/fibroleukin gene is required for lipopolysaccharide-triggered abortions and for normal mouse reproduction. *Molecular Human Reproduction* **10,** 99–108 (2004).
99. Mu, J. *et al.* Fgl2 deficiency causes neonatal death and cardiac dysfunction during embryonic and postnatal development in mice. *Physiological Genomics* **31,** 53–62 (2007).
100. Hancock, W. W. *et al.* Intact type 1 immunity and immune-associated coagulative responses in mice lacking IFN-inducible fibrinogen-like protein 2. *Proceedings of the National Academy of Sciences* **101,** 3005–3010 (2004).
101. Bartczak, A. *et al.* Overexpression of Fibrinogen-Like Protein 2 Promotes Tolerance in a Fully Mismatched Murine Model of Heart Transplantation. *Am. J. Transplant.* **16,** 1739–1750 (2016).
102. Liu, H. *et al.* The FGL2-FcγRIIB pathway: A novel mechanism leading to immunosuppression. *Eur. J. Immunol.* **38,** 3114–3126 (2008).
103. Yang, G. & Hooper, W. C. Physiological functions and clinical implications of fibrinogen-like 2: a review. *World J Clin Infect Dis* **3,** 37–46 (2013).
104. Melnyk, M. C. *et al.* The prothrombinase activity of FGL2 contributes to the pathogenesis of experimental arthritis. *Scand. J. Rheumatol.* **40,** 269–278 (2011).
105. Bézie, S. *et al.* Immunosuppressive role of fibrinogen-like protein 2 (FGL2) in CD8. *J Transl Med* **9,** O5 (2011).
106. Bézie, S. *et al.* Fibrinogen-Like Protein 2/Fibroleukin Induces Long-Term Allograft Survival in a Rat Model through Regulatory B Cells. *PLoS ONE* **10,** e0119686 (2015).
107. Pan, G. *et al.* Soluble fibrinogen-like protein 2 ameliorates acute rejection of liver transplantation in rat via inducing Kupffer cells M2 polarization. *Cancer Med* **7,** 3168–3177 (2018).
108. Liu, Y. *et al.* Downregulation of FGL2/prothrombinase delays HCCLM6 xenograft tumour growth and decreases tumour angiogenesis. *Liver Int* **32,** 1585–1595 (2012).
109. Rabizadeh, E. *et al.* The cell-membrane prothrombinase, fibrinogen-like protein 2, promotes angiogenesis and tumor development. *Thrombosis Research* **136,** 118–124 (2015).

110. Pépin, D. *et al.* The Imitation Switch ATPase Snf2l Is Required for Superovulation and Regulates Fgl2 in Differentiating Mouse Granulosa Cells. *Biology of Reproduction* **88,** 1–9 (2013).
111. Veras, M. M., Costa, N. S. X. & Mayhew, T. in *The Guide to Investigation of Mouse Pregnancy* 545–556 (Academic Press, 2014).
112. Langfelder, P. & Horvath, S. WGCNA: an R package for weighted correlation network analysis. *BMC Bioinformatics* **9,** 559 (2008).
113. Reimand, J. *et al.* g:Profiler—a web server for functional interpretation of gene lists (2016 update). *Nucleic Acids Research* **44,** W83–W89 (2016).
114. Stein, M., Keshav, S., Harris, N. & Gordon, S. Interleukin 4 potently enhances murine macrophage mannose receptor activity: a marker of alternative immunologic macrophage activation. *J Exp Med* **176,** 287–292 (1992).
115. Mosser, D. M. & Edwards, J. P. Exploring the full spectrum of macrophage activation. *Nat. Rev. Immunol.* **8,** 958–969 (2008).
116. Woods, L., Perez-Garcia, V. & Hemberger, M. Regulation of Placental Development and Its Impact on Fetal Growth-New Insights From Mouse Models. *Front Endocrinol (Lausanne)* **9,** 570 (2018).
117. Tunster, S. J., Watson, E. D., Fowden, A. L. & Burton, G. J. Placental glycogen stores and fetal growth: insights from genetic mouse models. *Reproduction* **159,** R213–R235 (2020).
118. Graham, C. H. *et al.* Establishment and characterization of first trimester human trophoblast cells with extended lifespan. *Exp. Cell Res.* **206,** 204–211 (1993).
119. Pattillo, R. A. & Gey, G. O. The establishment of a cell line of human hormone-synthesizing trophoblastic cells in vitro. *Cancer Res.* **28,** 1231–1236 (1968).
120. Leisser, C. *et al.* Tumour necrosis factor-alpha impairs chorionic gonadotrophin beta-subunit expression and cell fusion of human villous cytotrophoblast. *Molecular Human Reproduction* **12,** 601–609 (2006).
121. Zani, A. *et al.* Interferon-induced transmembrane proteins inhibit cell fusion mediated by trophoblast syncytins. *J. Biol. Chem.* **294,** 19844–19851 (2019).
122. Orendi, K., Gauster, M., Moser, G. & Meiri, H. *The choriocarcinoma cell line BeWo: syncytial fusion and expression of syncytium-specific proteins*. (Reproduction, 2010).
123. Redman, C. W. & Sargent, I. L. Latest advances in understanding preeclampsia. *Science* **308,** 1592–1594 (2005).
124. Lim, R., Barker, G. & Lappas, M. TREM-1 Expression Is Increased in Human Placentas From Severe Early-Onset Preeclamptic Pregnancies Where It

May Be Involved in Syncytialization. *Reproductive Sciences* **21,** 562–572 (2014).
125. Ito, M. *et al.* Potential role for nectin-4 in the pathogenesis of pre-eclampsia: a molecular genetic study. *BMC Med Genet* **19,** 1–9 (2018).
126. Taylor, B. D. *et al.* Serum Leptin Measured in Early Pregnancy Is Higher in Women With Preeclampsia Compared With Normotensive Pregnant Women. *Hypertension* **65,** 594–599 (2015).
127. Fu, Y., Wei, J., Dai, X. & Ye, Y. Increased NDRG1 expression attenuate trophoblast invasion through ERK/MMP-9 pathway in preeclampsia. *Placenta* **51,** 76–81 (2017).
128. Guo, J. *et al.* Alterations of maternal serum and placental follistatin-like 3 and myostatin in pre-eclampsia. *Journal of Obstetrics and Gynaecology Research* **38,** 988–996 (2012).
129. Chelbi, S. T. *et al.* Expressional and Epigenetic Alterations of Placental Serine Protease Inhibitors: SERPINA3 Is a Potential Marker of Preeclampsia. *Hypertension* **49,** 76–83 (2006).
130. Aquilina, J., Barnett, A., Thompson, O. & Harrington, K. Second-trimester maternal serum inhibin A concentration as an early marker for preeclampsia. *The American Journal of Obstetrics & Gynecology* **181,** 131–136 (1999).
131. When Is Hub Gene Selection Better than Standard Meta- Analysis? 1–16 (2013).
132. Redline, R. W. Classification of placental lesions. *The American Journal of Obstetrics & Gynecology* **213,** S21–S28 (2015).
133. Katzman, P. J. Chronic inflammatory lesions of the placenta. *Seminars in Perinatology* **39,** 20–26 (2015).
134. Rychlik, D. F., Chien, E. K., Wolff, D., Phillippe, S. & Phillippe, M. Cloning and tissue expression of the tissue prothrombinase Fgl-2 in the Sprague-Dawley rat. *J. Soc. Gynecol. Investig.* **10,** 67–73 (2003).
135. Papatheodorou, I. *et al.* Expression Atlas: gene and protein expression across multiple studies and organisms. *Nucleic Acids Research* **46,** 246–251 (2018).
136. Foerster, K. *et al.* LPS-Induced Occult Loss in Mice Requires FGL2. *Am J Reprod Immunol* **58,** 524–529 (2007).
137. Arruvito, L., Sanz, M., Banham, A. H. & Fainboim, L. Expansion of CD4+CD25+and FOXP3+ regulatory T cells during the follicular phase of the menstrual cycle: implications for human reproduction. *J Immunol* **178,** 2572–2578 (2007).
138. Seavey, M. M. & Mosmann, T. R. Immunoregulation of fetal and anti-paternal immune responses. *Immunol Res* **40,** 97–113 (2008).

139. Vigano, P., Mangioni, S., Pompei, F. & Chiodo, I. Maternal-conceptus Cross Talk—A Review. *Placenta* **24,** 56–61 (2003).
140. Akison, L. K. & Robker, R. L. The critical roles of progesterone receptor (PGR) in ovulation, oocyte developmental competence and oviductal transport in mammalian reproduction. *Reprod. Domest. Anim.* **47,** 288–296 (2012).
141. Li, S. *et al.* Estrogen receptor α is required for oviductal transport of embryos. *FASEB J.* **31,** 1595–1607 (2017).
142. Vuong, N. H. *et al.* Single-cell RNA-sequencing reveals transcriptional dynamics of estrogen-induced dysplasia in the ovarian surface epithelium. *PLoS Genet* **14,** e1007788–22 (2018).
143. Fazeli, A. & Pewsey, E. Maternal communication with gametes and embryos: a complex interactome. *Briefings in Functional Genomics* **7,** 111–118 (2008).
144. Georgiou, A. S. *et al.* Gametes alter the oviductal secretory proteome. *Mol Cell Proteomics* **4,** 1785–1796 (2005).
145. Rickard, J. P., Pool, K. R., Druart, X. & de Graaf, S. P. The fate of spermatozoa in the female reproductive tract: A comparative review. *Theriogenology* **137,** 104–112 (2019).
146. Hayward, C. E. *et al.* Placental Adaptation: What Can We Learn from Birthweight:Placental Weight Ratio? *Front. Physiol.* **7,** 1–13 (2016).
147. Christians, J. K., Grynspan, D., Greenwood, S. L. & Dilworth, M. R. The problem with using the birthweight:placental weight ratio as a measure of placental efficiency. *Placenta* **68,** 52–58 (2018).
148. Aplin, J. D., Myers, J. E., Timms, K. & Westwood, M. Tracking placental development in health and disease. *Nat Rev Endocrinol* **16,** 479–494 (2020).
149. Coan, P. M., Conroy, N., Burton, G. J. & Ferguson-Smith, A. C. Origin and characteristics of glycogen cells in the developing murine placenta. *Dev. Dyn.* **235,** 3280–3294 (2006).
150. Sferruzzi-Perri, A. N., Macpherson, A. M., Roberts, C. T. & Robertson, S. A. Csf2 null mutation alters placental gene expression and trophoblast glycogen cell and giant cell abundance in mice. *Biology of Reproduction* **81,** 207–221 (2009).
151. Oh-McGinnis, R., Bogutz, A. B. & Lefebvre, L. Partial loss of Ascl2 function affects all three layers of the mature placenta and causes intrauterine growth restriction. *Developmental Biology* **351,** 277–286 (2011).
152. Bogutz, A. B. *et al.* Transcription factor ASCL2 is required for development of the glycogen trophoblast cell lineage. *PLoS Genet* **14,** e1007587 (2018).

153. Simmons, D. G., Fortier, A. L. & Cross, J. C. Diverse subtypes and developmental origins of trophoblast giant cells in the mouse placenta. *Developmental Biology* **304,** 567–578 (2007).
154. Smith, S. A., Travers, R. J. & Morrissey, J. H. How it all starts: Initiation of the clotting cascade. *Critical Reviews in Biochemistry and Molecular Biology* **50,** 326–336 (2015).
155. Girardi, G. Role of tissue factor in feto-maternal development: a xiphos. *J Thromb Haemost* **9,** 250–256 (2011).
156. Hu, J. *et al.* The Duality of Fgl2 - Secreted Immune Checkpoint Regulator Versus Membrane-Associated Procoagulant: Therapeutic Potential and Implications. *Int. Rev. Immunol.* **35,** 325–339 (2016).
157. Okada, Y. *et al.* Complementation of placental defects and embryonic lethality by trophoblast-specific lentiviral gene transfer. *Nat Biotechnol* **25,** 233–237 (2007).
158. Kaufman, M. R. *et al.* Important aspects of placental-specific gene transfer. *Theriogenology* **82,** 1043–1048 (2014).
159. Fan, X. & Nayak, N. R. in *The Guide to Investigation of Mouse Pregnancy* 331–339 (Academic Press, 2014). doi:10.1016/B978-0-12-394445-0.00028-X
160. Xie, C., Yao, M. Z., Liu, J. B. & Xiong, L. K. A meta-analysis of tumor necrosis factor-alpha, interleukin-6, and interleukin-10 in preeclampsia. *Cytokine* **56,** 550–559 (2011).
161. Rahardjo, B., Widjajanto, E., Sujuti, H. & Keman, K. Different levels of IL-1α, IL-6, TNF-α, NF-κB and PPAR-γ in monocyte cultures exposed by plasma preeclampsia and normotensive pregnancy. *Pregnancy Hypertens* **4,** 187–193 (2014).
162. Weel, I. C. *et al.* Association between Placental Lesions, Cytokines and Angiogenic Factors in Pregnant Women with Preeclampsia. *PLoS ONE* **11,** 1–15 (2016).
163. Kim, J. *et al.* Aspirin prevents TNF-α-induced endothelial cell dysfunction by regulating the NF-κB-dependent miR-155/eNOS pathway: Role of a miR-155/eNOS axis in preeclampsia. *Free Radic. Biol. Med.* **104,** 185–198 (2017).
164. Xu, B., Nakhla, S., Makris, A. & Hennessy, A. TNF-α inhibits trophoblast integration into endothelial cellular networks. *Placenta* **32,** 241–246 (2011).
165. Matthiesen, L. *et al.* Immunology of Preeclampsia. *Immunology of Pregnancy* **89,** 49–61 (2005).
166. Murphy, S. P. *et al.* Interferon Gamma in Successful Pregnancies. *Biology of Reproduction* **80,** 848–859 (2009).

167. Ozkan, Z. S. *et al.* Plasma IL-17, IL-35, interferon-γ, SOCS3 and TGF-β levels in pregnant women with preeclampsia, and their relation with severity of disease. *J. Matern. Fetal. Neonatal. Med.* **27,** 1513–1517 (2014).
168. Yang, Y., Su, X., Xu, W. & Zhou, R. Interleukin-18 and interferon gamma levels in preeclampsia: a systematic review and meta-analysis. *Am J Reprod Immunol* **72,** 504–514 (2014).
169. Pober, J. S. & Cotran, R. S. Cytokines and endothelial cell biology. *Physiological Reviews* **70,** 427–451 (1990).
170. Conrad, K. P. & Benyo, D. F. Placental cytokines and the pathogenesis of preeclampsia. *Am J Reprod Immunol* **37,** 240–249 (1997).
171. Shaw, J. *et al.* Inflammatory processes are specifically enhanced in endothelial cells by placental-derived TNF-α: Implications in preeclampsia (PE). *Placenta* **43,** 1–8 (2016).
172. Parks, W. T. Placental hypoxia: The lesions of maternal malperfusion. *Seminars in Perinatology* **39,** 9–19 (2015).
173. Redline, R. W. & Patterson, P. Villitis of Unknown Etiology Is Associated with Major Infiltration of Fetal Tissue by Maternal Inflammatory Cells. *The American Journal of Pathology* 1–7 (1993).
174. Chen, A. & Roberts, D. J. Placental pathologic lesions with a significant recurrence risk - what not to miss! *APMIS* **126,** 589–601 (2017).
175. Redline, R. W. Villitis of unknown etiology: noninfectious chronic villitis in the placenta. *Human Pathology* **38,** 1439–1446 (2007).
176. Tamblyn, J. A., Lissauer, D. M., Powell, R., Cox, P. & Kilby, M. D. The immunological basis of villitis of unknown etiology - Review. *Placenta* **34,** 846–855 (2013).
177. Labarrere, C. A. & Faulk, W. P. MHC Class ll Reactivity of Human Villous Trophoblast in Chronic Inflammation of Unestablished Etiology. *Transplantation* 1–5 (1990).
178. Raman, K. *et al.* Overlap Chronic Placental Inflammation Is Associated with a Unique Gene Expression Pattern. *PLoS ONE* **10,** e0133738–12 (2015).
179. Kanellopoulos-Langevin, C. Tolerance of the fetus by the maternal immune system: role of inflammatory mediators at the feto-maternal interface. *Reprod Biol* (2003).
180. Li, W.-Z. *et al.* FGL2 prothrombinase contributes to the early stage of coronary microvascular obstruction through a fibrin-dependent pathway. *International Journal of Cardiology* **274,** 1–8 (2018).